2 Tectonic Stress Fields and Karst

2.1 Generalities About the Tectonic Stress Fields

The notion for the *stress* from mechanical point of view was firstly introduced by Augustin Louis Cauchy (1789–1857). He defined the stress as *the average intensity of the strain applied on surface unit*. According to the general sense of the mechanics terminology the stress has to be understood as the integrity of the internal strains that appear when the material is submitted under loads or deformations. Every resulting deformation, no mater of its spatial dimensions, has to be analyzed in the context of the initialing strains. For estimating the state of stress of a given material, the vectors of the impacting stresses on every one of the infinite number of elementary surfaces dividing the material have to be evaluated. Six are the components forming the *stress tensor* inside the elementary volume of given material—three principal and three tangential (Fig. 2.1).

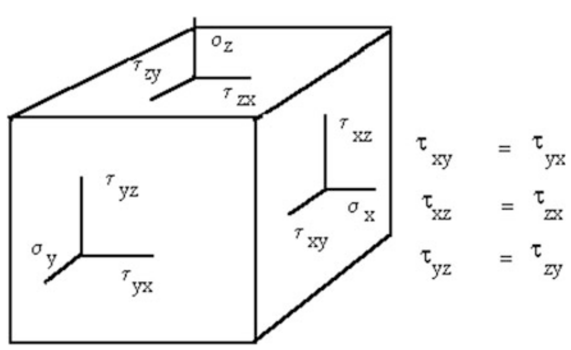

Fig. 2.1 Stress components impacting the elementary volume

No mater how complex could be the applied stresses they can be decomposed at three perpendicularly to each other *normal stresses*. If the values of the applied strains are known, it is possible to evaluate the values and the directions of these three principal stresses. The *stress tensor* defines completely the state of stress. Practically, it is sufficient to know the principal stresses for evaluating the state of stress of the studied material and to determine the values of the normal and tangential stresses on every other plane crossing it. For these purposes, the formulas and the circles of Moore can be used. The method is well described in every book on Engineering Geology and Rock Mechanics (we can suggest the books of Jaeger 1975 or Spenser 1981).

Trollop (1983) introduced the *differential definition of the stress* for expressing the basic conditions of the Theory of Elasticity as continuous mathematical function (Trollop 1983):

$$\sigma = \lim_{\delta_a \to 0} \frac{\delta f_n}{\delta a} = \frac{df}{da} \tag{2.1.1}$$

where f_n is the normal strain applied on the surface *a.*

This definition is valuable for ideal continuous medium. But for discrete and granulate materials (that are normally all geological bodies) this differential definition is not acceptable. As it was mentioned above, the total stress state is completely defined by the three principal stresses σ_1, σ_2, and σ_3, where:

$$\sigma_1 > \sigma_2 > \sigma_3. \tag{2.1.2}$$

The characterization of the state of stress in Tectonophysics is defined at least by three vectors of the principal stresses. If they are equal the state of stress

S. Shanov and K. Kostov, *Dynamic Tectonics and Karst*, Cave and Karst Systems of the World,
DOI: 10.1007/978-3-662-43992-0_2, © Springer-Verlag Berlin Heidelberg 2015

is defined as uniform; if not,the state of stress is no uniform. For the uniform state of stress, the values of the stresses are calculated by the values of the applied strains. For the no uniform state of stress the values of the stresses can not be calculate directly, but using the effect of their impact. Exactly, this approach is used for qualitative evaluation of the stress by the different Earth's sciences. The type of the stress field in Tectonophysics is determined by the space orientation of the principal stress axes and their relative rates. Practically, this approach has lead to the definition of the extensional stress (in spite the impossibility to accept this type of mechanical deformation inside the Earth's crust), the compression stress, the strike stress, etc.

Angelier (1994) comments that always when a reconstruction of the stress field is done, one of the reconstructed axes is subvertical. He explains this effect with the gravitational field and the free Earth's surface. The vertical stress is directly dependent from the weight of the rocks and the pore strain. Hence, the tectonic stress is acting, in the most of the cases, on subhorizontal plane. The reconstruction of the paleostresses from the analyses of the fault systems has shown that the deviation of the stress axis determined as a vertical one is surprising small—normally about 10° (Angelier 1994).

The strains creating the deformations in the rocks can be defined in the space by the ellipsoid, the three axes *A*, *B*, and *C* of which determine the maximum, the intermediate, and the minimum strain (Fig. 2.2). Generally, this ellipsoid is randomly space-oriented relatively to the geometric characteristics of the rocks before their deformation. The relationship between the strain ellipsoid and the stress ellipsoid (axes *X*, *Y* and *Z* in Fig. 2.2) is not direct, nor simple. The example in Fig. 2.2 (according to Aubouin et al. 1988) represents the ideal case of isotropic material. Both the two ellipsoids have the same orientation of the axes. The maximum deformation is corresponding to the maximum strain. The general case is the random orientation of the ellipsoids to each other. The field studies on the rock deformations define the orientation of the axes *X*, *Y*, and *Z*. It is not easy, nor simply to determine the principal stresses σ_1, σ_2, and σ_3. But in some conditions regarding the orientation of the principal strains before the deformation, the relationship between the two ellipsoids can be

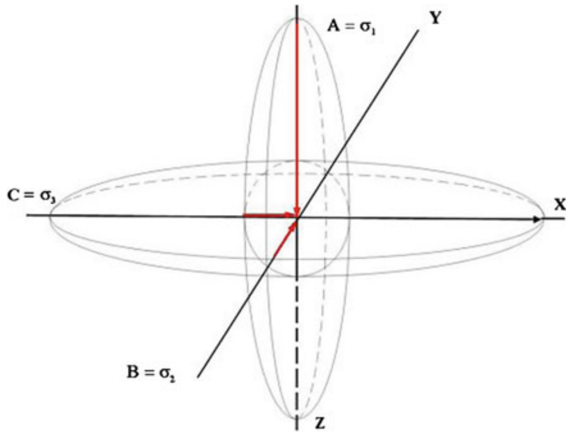

Fig. 2.2 Ellipsoid of the acting strain (*ABC*) and ellipsoid of the deformations (*XYZ*). *A*—maximum compression; *B*—intermediate compression; *C*—minimum compression; *X*—maximum deformation (lengthening); *Y*—intermediate deformation; *Z*—minimum deformation (shortening) (after Aubouin et al. 1988)

simplified. For the structural studies, a simplified acceptance for the relationship *tectonic strain* $\Longleftrightarrow$ *resulting deformations* in the rocks is applied.

It is well known that the strain and the stress relationship does not directly mean fractures formation, but however strain and stress are causes of fracturing. Hunt et al. (2011) described the principal causes of fracture–density variations (Table 2.1), but concluding immediately that this list of fracture-causing variables is much more extensive, and often unique to a particular fracture system.

As a result of the rock fracturing, different types of single or complex structures appear. The ranging and mutual relationship can be simplified to the scheme presented in Fig. 2.3, following Norsk Geologisk Tidsskrift 69 Supplement (Nystuen 1989).

A fracture is used as a more general term for all kinds of fracturing caused by mechanical stress in the rocks. The term is irrespective of whether dislocation has taken place along the fracture.

A joint is a fracture surface in the rock along which no displacement has occurred. A *joint system* is composed of intersecting joints assumed to have been formed during the same deformational event.

A fault is a fracture separating two bodies of rock, which have moved relatively to one another and it is the fundamental term for a fracture surface in the Earth's crust on which displacement has occurred.

Table 2.1 Causes of fracture-density variation (after Hunt et al. 2011)

Type	Parameter	Direction of correlation
Material property	Rock brittleness	Positive
	Grain size	Negative
	Porosity	Negative
	Bed thickness	Negative
In situ	Depth	Variable effect
	Pore pressure	May hold fractures open
Strain	Structural position	Positive with strain

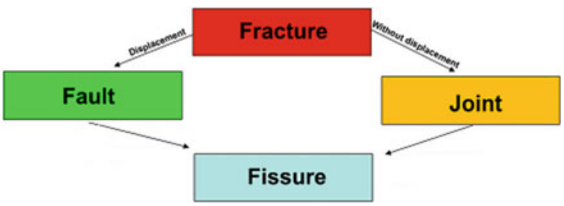

Fig. 2.3 Relationship between the terms fracture, fault, joint, and fissure (according to Norsk Geologisk Tidsskrift 69, Supplement 1989)

A fissure, commonly used term in karst studies, is an open joint or crack. Some fissures appear clearly to be open, but they could be subsequently filled with mineral growth, as well as eroded and enlarged by the water in karstified rocks.

Here a brief overview of the most popular theories of the shear joints formation will be presented, because the shear joint systems are widely used in our studies for reconstruction of the tectonic stress fields' main axes.

One of the most valid theories of failure of rock-like materials is this of Coulomb-Navier, widely accepted in the geotectonic practice. According to this theory, the shear strength consists of two components—cohesion shear strength τ_c and the frictional resistance on the corresponding plane $\tau_f = \mu\sigma_\theta$ (following Stoyanov 1970). The destruction appears when the tangential stress on the plane reaches the value of the strength:

$$\tau_\theta = \tau_c + \mu\sigma_\theta. \quad (2.1.3)$$

Here θ is the shear angle (the orientation of the shear plane toward the maximum normal stress σ_1) and μ is the coefficient of internal friction.

The orientation of the shear plane is defined by the equation:

$$tg2\theta = \frac{1}{\mu}. \quad (2.1.4)$$

It follows, that the shear angle θ is depending exclusively from the type of the material. The theory is considered to describe with sufficient accuracy, the destruction of rocks at low and moderate pressures (Brace 1960; Lundborg 1968).

From physical point of view, the Theory of Griffith published in 1921, was accepted as more justified, because it is based on the internal characteristics of the brittle material. This theory accepts that the real material contains a number of randomly oriented micro-joints. Under stress conditions in the material, at the ends of these joints, a stress concentration is present. The maximum stress concentration is along the direction φ. If a critical value of the stress is reached, the micro-joints with orientation φ will grow by secondary micro-fracturing, and finally a macro-fracturing shall be produced. Following this theory McClintock and Walsh (1962) proposed the so-called Modified Griffith's Theory. They have accepted that under a minimum pressure the micro-joints are closed. When differential stresses exist, on the walls of the joints reactive frictional stress appears, being proportional to the compression stress. The equation of destruction is:

$$\tau_\varphi = 2_K + \mu_e\sigma_\varphi. \quad (2.1.5)$$

Here τ_φ is the tangential stress acting on the plane oriented at the angle φ toward the maximum stress σ_1, K is the uniaxial tensile strength, μ_e is the frictional coefficient along the walls of the initial joints (i.e., it is a coefficient of external friction), and σ_φ is the normal stress on the critical planes (it is positive). Finally, the critical angle of the shear joints is:

$$tg2\varphi = \frac{1}{\mu_e}. \quad (2.1.6)$$

The difference between μ (from Eq. 2.1.4) and μ_e is that the physical meaning of μ is not well defined especially for real rock conditions, while μ_e is a real physical parameter (Stoyanov 1970).

The caves in karst terrains are a result of the water erosion along the most open fractures under given tectonic conditions. In this case, the normal faults and the tensional fractures (fissures) are most favorable for the karst network evolution. The study of the mechanism of formation of fractures in the rocks by Price (1959, 1966) lead to the conclusion, that the vertical tensional and shear fractures and faults are formed as a result of residual elastic stresses during the post-tectonic uplifting of compressed volumes. One very important statement in these works is that these types of structures can be formed only if horizontal tectonic extension exists.

If the Earth's crust is three-dimensionally analyzed, only in the state of the own weight of the rocks, and taking into account that the horizontal enlargement of given volume is not possible because of the environment conditions, σ_x, σ_y and σ_z will be the principal stress axes. It could be written that:

$$\sigma_x = \sigma_y = \frac{v}{1-v}\sigma_z. \quad (2.1.7)$$

In this case, we accept that the horizontal deformations along the horizontal axes X and Y, i.e., $\varepsilon_x = \varepsilon_y = 0$, and the axis Z is vertical. The coefficient of Poisson v is less than 0.5 and σ_z will be the *maximum stress = gravitational stress*.

Now it is necessary to add the stress from the tectonic strain. Let us say that the tectonic strain has only horizontal components and the stress effect in every point can be presented by two perpendicular stresses c_x and c_y. The equations of superposition of the horizontal and gravitational stresses will be (after Stoyanov 1970):

$$\begin{aligned} \sigma'_x &= \frac{v}{1-v}\sigma_z + c_x + vc_y \\ \sigma'_y &= \frac{v}{1-v}\sigma_z + c_y + vc_x \\ \sigma'_z &= \sigma_z. \end{aligned} \quad (2.1.8)$$

Our interest in the formation of suitable conditions for the karst evolution is directed to the formation of open fractures. If conditionally, the horizontal stress components $c_y > c_x$, than $\sigma_y > \sigma_x$. The formation of tensile fractures, as well as normal faults in larger scales, can be possible under the condition:

$$\sigma'_x < \sigma'_y < \sigma'_z. \quad (2.1.9)$$

Because the vertical stress is determined as $\sigma'_z = \sigma_z = \gamma h$, where γ is the bulk weight of the rock and h is the depth from the surface, it can be finally written for the formation of tensile fractures:

$$c_x < c_y < \frac{1-2v}{1-v}\gamma h - c_x. \quad (2.1.10)$$

Most of the quantitative studies of the tectonic stress field of the Earth reflect the ongoing contemporary processes, and for them direct or indirect data can be obtained depending of the chosen method of investigation. The presumption for heritability of the tendencies from the past geological times can be applied only for the Quaternary time, under some conditions it could be accepted also the heritability of the Neotectonic tendencies for specific regions. Every reconstruction of the tectonic stress field in older geological formations needs careful analysis of the studied parameters, taking into account the multiform responses of the inverse problem solutions.

When explaining the causes for existing of tectonic stresses and their evaluated rates, it is necessary to realize that the analyses cover only relatively narrow time window and they reflect the contemporary, "the moment" state (in geological sense) of the tectonic stress field. Hence, it is of critical importance to understand what is measured when applying instrumental in situ investigations for stress determination. The terminology used for describing in situ stresses is analyzed by Amadei (1983). More complete and hierarchically structured terminology is presented by Bielenstein and Barron (1971), and it described well the real situation for the near surface geological formations of the Earth's crust (Fig. 2.4).

When analyzing the processes of karst formation and evolution, it is clear that the tectonic factor is the principal controller of the fracturing in the rocks with specific brittleness at given structural position of the rock formations (see Table 2.1). Our experience gives reason to the assumption that the active tectonic

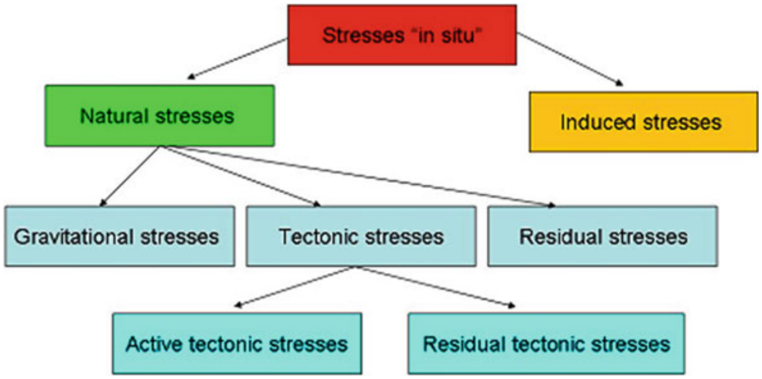

Fig. 2.4 Terminology for the measured in situ tectonic stress fields (following the hierarchy proposed by Bielenstein and Barron 1971)

stresses (Fig. 2.4) during the process of the evolution of the karst systems are the main factor for creating of fissures—tensional fractures or opening of the pre-existing shear joints, in this way facilitating the water circulation and formation of underground galleries with dominant directions.

2.2 Methods of Reconstruction and Analyses of the Tectonic Stress Fields

Among the methods for reconstruction of the spatial direction of the axes of tectonic stress paleo-fields these ones using the fracturing of the rocks in karst areas have shown valuable results. The studies of the striation on tectonic slickensides take a sizable place in the information collected through the years of study on different karst terrains. This type of reconstructions corresponds to the meso-level of the description of the structures, and where the kinematic characteristics of the movements between the rock blocks are used. Here only methods used in the practical works of the authors for analyses of the tectonic stress fields in relationship to the karst systems evolution will be described and discussed.

Another possibility is the analysis of the physical anisotropy when measuring in situ in karst terrains the electrical or the seismic characteristics of the rocks.

The information about the contemporary regional tectonic stress field can be also deduced on the base of the fault-plane solutions from earthquakes at the nearest vicinity of the studied karst terrains.

2.2.1 Striations on Tectonic Slickensides

In these studies, the kinematic characteristics of the movements between rock blocks are used. They could appear at the moment of forming of joints and faults or the orientation of older disruptions could favor the relative movement of adjacent blocks under the conditions of younger tectonic stress field. The orientation of the normal principal tectonic stresses could be reconstructed through meso-structural analysis, using the concept about the relation of movement along shear joints with tectonic stresses (Ramsay 1980; Gamond 1983). The basic working hypothesis, called by the name of Wallace-Both (Angelier 1994) is that if there is a movement and the system "stress $\Longleftrightarrow$ fracturing" is examined independently of environment, then the relative displacement should be parallel to and along the direction of the shearing stress. In Sect. 2.1 the basic relationships have been presented (Griffith's Theory).

The critics of this hypothesis point out as its main defect the fact that, due to the complicated real geometry and the interrelation of faults and joints, a considerable local deviation of the principal normal stresses always appears. The practical analytical results of a great number of conjugated disruption surfaces with movements along them show (Angelier 1994) that amazing constancy is kept and small angle error in the orientation of the shearing stresses τ. The digital modeling (Dupin et al. 1983—cited after Angelier 1994) has shown that the variances depend on the geometry of the intercrossing of the joints, but these variances are very small, within the limits of the error

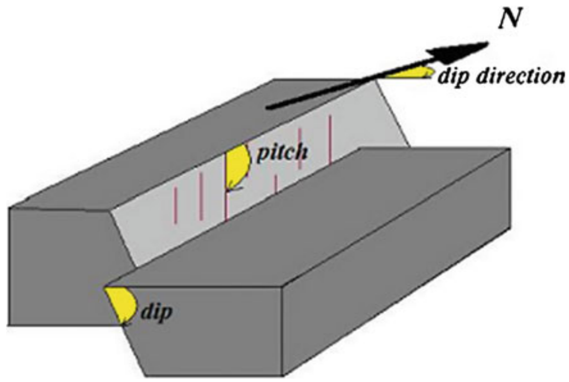

Fig. 2.5 Measured parameters as input datum for the Programme FAULT: dip direction, dip, pitch and sense of movement (*N*—normal, *I*—reverse, *D*—dextral, *S*—sinistral)

of measuring, and practically the movement is always parallel to the medium shearing stress. Thus, the practical usage of Wallace-Both' hypothesis has been confirmed. Numerous researchers created methods and computer programs for reconstructions of tectonic stress directions, using this very hypothesis (good analyses and practical references could be found in Sassi and Carey-Gailhardis 1987; Vergely et al. 1987).

The programme FAULT (Caputo 1989) uses three methods for reconstruction of the principal stress axes by measurements of spatially oriented striations on slickenside and the types of movement on them (Fig. 2.5).

2.2.1.1 Right Dihedron Method

The RDM (after Angelier and Mechler 1977) uses the main hypothesis that the material is preliminary fractured and the size of movement along every single surface is much smaller than the size of the studied rock body. The plane orthogonal to the striation on the disruption surface is defined as a complementary plane. Both planes divide the space around the disruption surface into four rectangular dihedrons (sectors). Every two conjugated dihedrons contain the axes σ_1 and σ_3, which could be presented into a stereographic projection. In a set of measurements, the sectors are defined as zones of action of σ_1 and σ_3 axes.

2.2.1.2 Method of Pressure (*P*) and Tension (*T*) Axes (*P*/*T*)

It is based on the assumption that in homogeneous and isotropic materials, the axis of maximum extension is under 45° toward the disruption surface and the movement direction. Correspondingly, the axis of maximum compression is at 90° toward it.

2.2.1.3 Method of the Smallest Squares

This method complements the procedures for evaluation of the spatial position of the principal axes of stress field, and through it the final result of data processing is formed. The reconstructed principal axes of tectonic stress should be orthogonal toward each other, but they might be dispersed around a center, depending on the data. Exactly, through the method of the smallest squares the position of this center is determined for every principal axis observing the condition for spatial orthogonality between them (Caputo and Caputo 1989).

The main problem that arises at work with striations on slickensides is that the registered movements along various surfaces, even very close (within one outcrop), could not reflect synphase movements. If within the rock volume there is a more than one tectonic impact provoking movement along joints and faults, it is obligatory during the field measurements to find out or at least to suspect the relative temporary sequence of the impacts. The accuracy of the final result is depending from the number of the measured surfaces with striations. It is represented by stereogram (lower hemisphere) with results from RDM and *P*/*T* methods (Fig. 2.6).

2.2.2 Shear Joint Systems

The tectonic fracturing of the rocks gives valuable information about the stress field that caused it and about the orientation of dynamic axes, although it is difficult to extract this information. In spite of the lack of kinematic indicators on most of the joints, they have great potential for reconstruction of the paleostress fields. Especially, this can be used when the joint sets keep consistent spatial orientation on wide areas (Dunne and Hancock 1994). Examples from a platform region were presented and discussed by Shanov (2005). Conjugated joint systems exist in all cases of spatial orientation of the principal axes of particular tectonic stress fields, which should be studied for the reconstruction of the paleo-stresses. In the most simple case, which is observed at preliminary undeformed rocks (as the young sediments are), there is a simple relation between the geometry

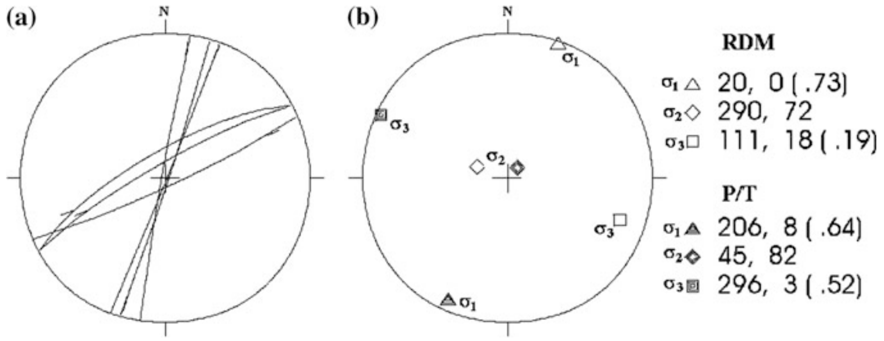

Fig. 2.6 Solution (lower hemisphere) on 6 data from the karst region of Lakatnik (Western Balkan Mountain—Bulgaria). **a** Input data; **b** Reconstruction of the principal stress axes. Close to the symbols for σ_1, σ_2 and σ_3 on the right of the stereonet the azimuth, the dip angles and the Last Square Error (in brackets) are plotted

of the conjugated joints and faults and the stress field, defined with its principal axes σ_1, σ_2, and σ_3 (Angelier 1994). Nikolaev (1977) developed a method for statistical processing and interpretation of joints with good opportunities at various practical structural studies. After analyzing important quantity of joint diagrams, he concluded that the joints' maximums are always distinguished by more or less expressed asymmetry and eccentricity. Accepting that the joints grouped into maximums have been formed at a constant regional tectonic stress field, he concluded that the angle between the conjugated joints changes in a particular way (Fig. 2.7) during the joints' formation.

This change is explained with the fact that the appearance of every new joint causes some change in the stress conditions in its close vicinity. The universal pressure changes and this leads to change in the shear angle θ, at which the next joints originate. Explanation can be easily found if we consider the relationship (2.1.4) from Sect. 2.1. The creation of a new joint leads to decreasing of μ (the coefficient of friction), and consequently the angle θ for every next discontinuity will grow, i.e., the dispersion of the joints will be oriented toward the minimum tectonic stress σ_3.

Similar conclusions were also made by Engelder (1994). According to him, when a pair of shear joints is developed, a torsion of the joint plane appears due to local changes in the stress field, which under particular conditions might lead to the forming of en-echelon segments. As a whole, an asymmetric distribution of frequencies is obtained in the joint sets (Fig. 2.7), which is expressed through the forming of eccentric fields of density on the density diagrams. As

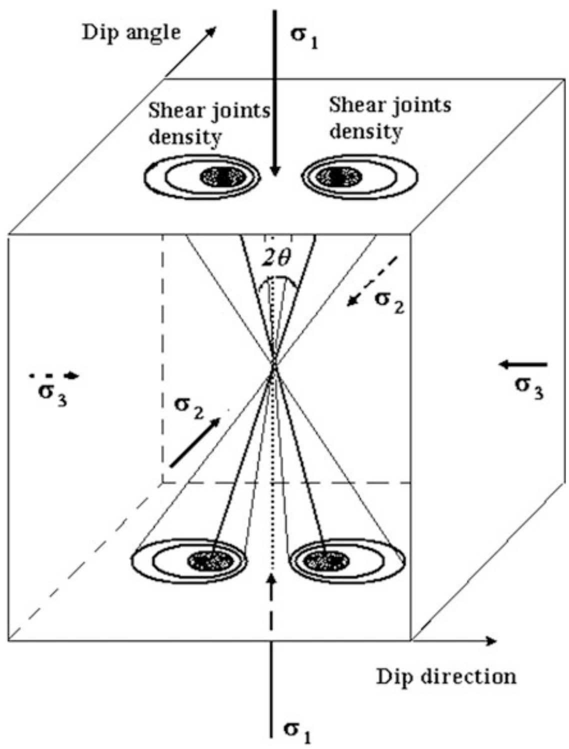

Fig. 2.7 Schematic 3D model of the shear joints' formation and their asymmetric dispersion (following the idea of Nikolaev 1977)

a rule, the extension of iso-areas disperses toward the axis of minimum stress σ_3.

From the Griffith theory (Griffith 1924), it is known that the joints are not distributed in their own plane, but concentrated toward a direction closer to σ_1. This tendency of deviation of the joints' own planes toward the direction of maximum stress is

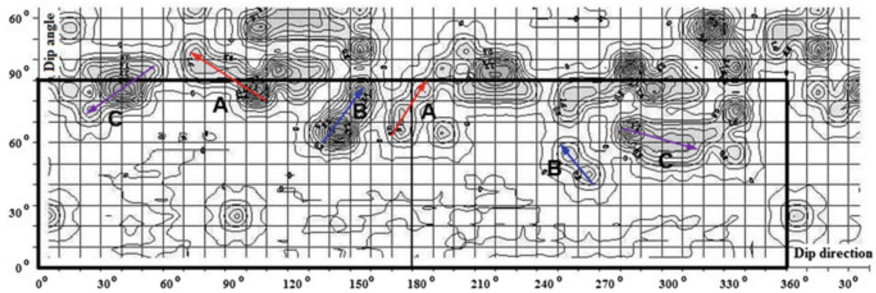

Fig. 2.8 A rectangular diagram of the shear's joints density in the karst area of Cherepish (Western Balkan Mountain—Bulgaria). The sense of dispersion of the pair groups of joints is indicated (*colored arrows*)

shown also experimentally. At conjugated brittle-plastic shear zones, the angle 2θ between them (Fig. 2.7) can vary from 40° to 130° toward σ_1 (Dunne and Hancock 1994). This is especially important for such rock types as dolomites, limestones (the dominant karstified rocks), or alternations of sandstones and more clayey rocks. The usage of joints sets dispersion toward the minimum tectonic stress protects from incorrect determinations of σ_1 and σ_3 axes.

A specific and substantial part of the method is the presentation of measurement data as a rectangular diagram of the joints' density. In a Cartesian coordinate system along one axis, the joints' dip angles are plotted and along the other axis, the azimuth angles of the dip direction are shown. Shanov and Stoyanov (1986) made an analysis and grounded the advantages of Nikolaev's method of presentation. It completely satisfies the conformity requirement regarding the most frequently observed joints: sub-vertical ones. Regardless of its "matrix" shape, this diagram should be examined also as the transformation of the spherical surface—its projection on unfolded cylindrical surface is tangent to the equator of the sphere.

Finally, the plotting of the centers and the ends of the conjugated joint groups on stereograph projection (Wulf's stereonet) gives the possibility to recognize the principal stress axes σ_1, σ_2, and σ_3. They should be orthogonal and the axis σ_3 is perpendicular to the favorable plane for formation of tensile fractures. Hence, the plane is containing the projection of the axes σ_1 and σ_2. Karst cave networks usually are formed by the water erosion on these planes.

Practically, during field works, it can be recommended to perform between 50 and 100 measurements of joints from the chosen outcrop without giving any priority to some of the existing joint systems. But it is very important to note the coupling of the systems, their spatial superposition, and if possible the relative time sequence. As an example, in Fig. 2.8 is plotted the rectangular diagram of the shear's joints density from the karst area of Cherepish (Western Balkan Mountain—Bulgaria). The interpretation of the results is presented in Fig. 2.9.

Comments

Stress field A: The direction of the maximum compression is NE–SW. It corresponds to the main compression direction during the Middle Laramian tectonic phase. The probability for appearance of open fractures and normal faults striking NE–SW and dipping to SE exists (the gray colored surface).

Stress field B: The maximum compression is directed NNE–SSW. This characteristic corresponds to the advance toward NNE of thrust sheet from South. The formation of new open fractures is of low probability, because their strike is close to the direction of the existing fractures from the previous tectonic impact.

Stress field C: The fracturing is due to the Neotectonic stress field. The deduced surface of normal faulting (in gray color) is corresponding to the geometry of the nearest regional fault. The dominant part of the galleries of the caves of the area follows this

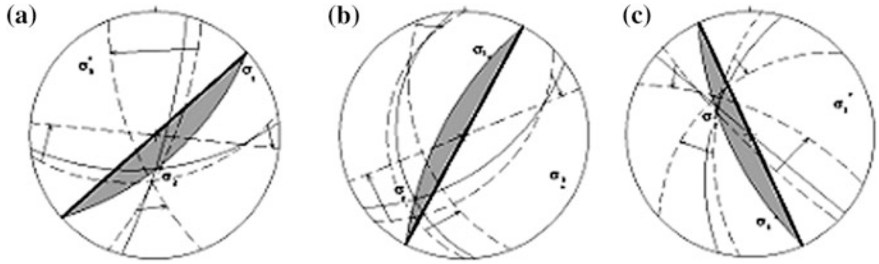

Fig. 2.9 Reconstructions of the tectonic stress fields (lower hemisphere) using the shear joints groups from Fig. 2.8. **a** Paleocene deformations (Middle Laramian tectonic phase). **b** Late Eocene deformations (Late Illyriyan tectonic phase). **c** Neotectonic deformations

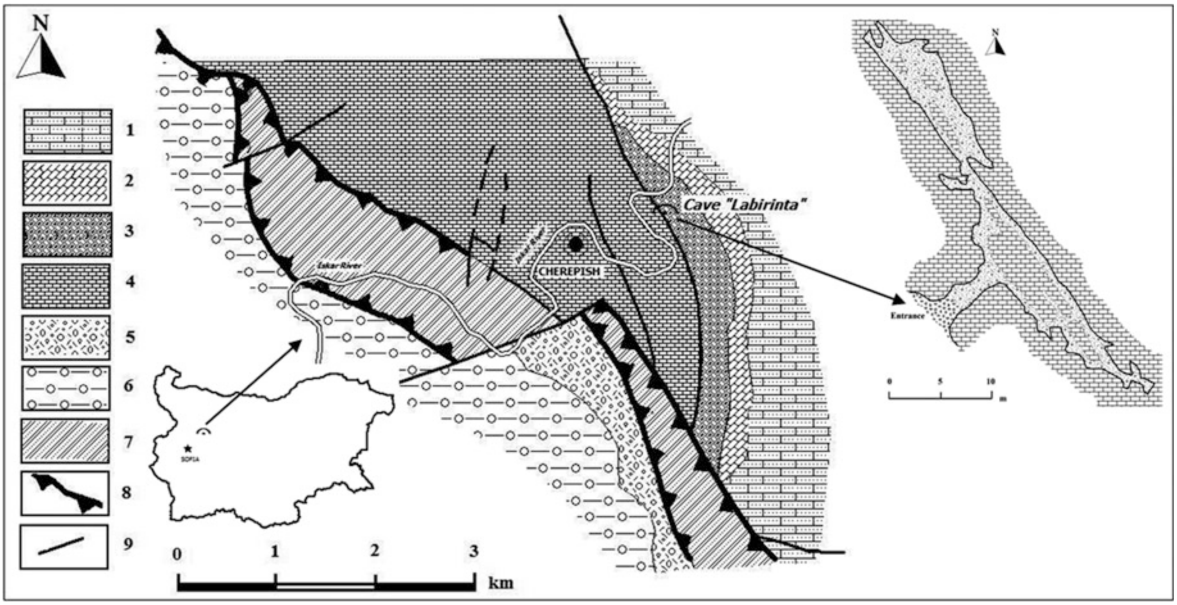

Fig. 2.10 Geological scheme of the karst area of Cherepish (from the Geological map of Bulgaria, Sheet "Vratsa" 1991). The position and the map of the Labirinta Cave are indicated. *Lower Cretaceous*: *1*—Lutibrod formation (oolitic and sandy limestones); *2*—Cherepish formation (massive organogenic limestones); *3*—Mramoren formation (marls with layers of clayey limestones and sandstones); *Jurassic—Lower Cretaceous: 4*—Slivnitsa formation (massive limestones); *Carboniferous—Permian*: *5*—Vrana formation (breccia-conglomerates, conglomerates); *6*—Buk formation (conglomerates, sandstones, siltstones, argillites); *Cambrian: 7*—Berkovitsa group (metamorphosed argillites, siltstones, marbles and sandstones); *Fault structures: 8*—overthrust; *9*—fault

direction. Especially, the cave "Labirinta" is one of the example of the tectonic control on the formation of preferentially oriented galleries that follow the trend of the open (tensional) fractures deduced from the reconstruction using the shear joints. Here, the impact of the youngest tectonic stress field is evident (Fig. 2.10).

2.2.3 Physical Anisotropy

The physical anisotropy of the rock massifs is the variance of its physical characteristics, depending on the direction of their measurement. The causes for the rock anisotropy can be summarized, as follows (after Uhov 1975):

1. Heterogeneity of the composition and the physical status, caused by the lithological changeability of the rocks in the massif, by the depositional character, by the folding and fracturing in various localities, including big faults, intrusions, fragmentation zones, weathering processes, and water influx.
2. Heterogeneity of the stress condition, caused by the natural stresses in the rock massifs.
3. Large-scale heterogeneity—varies by quality and quantity features of the rocks in studying different volumes from them.

The mineral composition of sedimentary rocks, particularly limestones and dolomites, plays a relatively insignificant role for the anisotropy at meso- and macro-level. The folded structures and the faults impact substantially the physical properties of the rocks, and the resulting rocks anisotropy depends to a great extent on the particular type of deformations and the position of the studied site relatively to these structures. The question about the "scale effect" is also a complex phenomenon and the conformity with it is an obligatory condition for realistic interpretations. For this reason, in geophysical practice, the term "apparent anisotropy" is used, instead of the term "anisotropy" applied mostly for the mineral characteristics (Sheriff 1984).

Two factors are extremely significant at all levels of the studies—the fracturing and the tectonic stresses. As the fracturing is predominantly a result of the impact of the consecutive acts during the geological time of tectonic stresses in the rocks, in fact every study of rock anisotropy in situ could be also presented as a study of the history of tectonic stresses for a particular site. The following working hypotheses should be kept in mind, while the results and analyses presented are obtained from sedimentary terrains predominantly:

1. The fracturing of sedimentary rocks is due to the tectonic stress fields, acting after the rocks lithification.
2. All changes in the direction of principal normal stress axes in space have been reflected in the rock massifs through formation of new joint systems. Our experience has shown that normally more than three sequences of tectonic impacts are difficult to be detected.
3. The anisotropy in the brittle rock varieties (limestones, dolomites, sandstones) is due mainly to the rupture joint system. There is a reason to suggest that after the first-joint system arises, every consecutive by time tectonic stress field will act on already disrupted medium, and will have a weaker deformation effect. The extensional fractures have a definite advantage in anisotropy forming, and their usage at paleotectonic stresses reconstruction is grounded from other authors as well (for example, Letouzey 1986; Caputo and Caputo 1988). Practically, these extensional fractures are presenting the preferential underground routes of the water. The knowledge of the anisotropy in karst areas can be used for determining the dominant direction of the underground karst galleries.
4. In clayey rocks, marls, non-lithified sediments as sands and their varieties, a well-expressed fracturing is not observed, or is missing at all. However, in such kind of materials a compaction along the direction of maximum stress (at regime of compression) or decompaction along the direction of minimum pressure (at regime of extension) is obtained. In both cases, the initial isotropy of the rock material is disturbed.

One of the approaches for anisotropy determination in rocks is to investigate the physical parameters, such as the electrical resistivity. Our experience has provided a number of successful implementation of this type of studies especially on karst terrains.

Some important basic principles are necessary to be presented here for understanding the relationship of the electrical anisotropy measurements and the anisotropic characteristics of the rocks. Theoretical and practical information can be found in many handbooks in different languages. We can suggest the textbook of Sharma (1997) presenting at comprehensible way the modern basis of the geoelectrical survey, including theoretical principles, field procedures and interpretation techniques.

The commonly used method for electrical measurements is to drive an electrical current through the ground and to measure the resulting potential differences on the surface. Electrically better or poorer conducting layers deflect the current and distort the normal potential. Thus, when measuring subsurface variations in electrical resistivity it us possible to detect the anomalous conditions and inhomogeneities within the ground. Different schema of field measurements and related specific methods of interpretations give the possibility to recognize the peculiarities of the electrical properties of the rocks at different depths and to build the corresponding geological model.

The prospection with direct current is widely applied and very useful for determination of the anisotropic characteristics of the rocks. The karstified rocks are, as rule, bad conductors of electricity. Geological processes as faulting, dissolution, shearing, jointing, weathering, and alteration can increase the fluid permeability of the rocks and contribute to the formation of patterns of lower electrical resistivity. In this case, the minerals of the karstified rocks are practically insulators and the electrical conduction is due to the electrolytes (groundwater, wet clayey substance, etc.) filling the pore space and the fissures. If the fractures or the underground karst galleries are without electrically conductive filling (air), these inhomogeneities will have higher (infinite) electrical resistivity relatively to the rock's matrix.

The measurements by direct electrical current can be performed using point or dipole sources. The disposition of the electrodes on the ground determines the geometrical type of the array. The most common disposition of the electrodes is shown in Fig. 2.11.

The aim is to measure the potential difference ΔU between the electrodes M and N when a direct current I is applied between the electrodes A and B. If the resistance between opposite faces of the conducting body with length L and uniform cross-sectional area S is R, the resistivity ρ in homogenous material from single point source is:

$$\rho = \frac{S \cdot R}{L}. \qquad (2.2.1)$$

The resistivity SI unit is *ohm meter* (Ωm).

When electrical current I is applied, and the measured potential difference is ΔU, then the relationship with the electrical resistance R is given by Ohm's law:

$$\Delta U = R \cdot I. \qquad (2.2.2)$$

Using Eq. (2.2.1) the above relationship can be written, as follows:

$$\rho = \frac{\Delta U}{I} \cdot \frac{S}{L}. \qquad (2.2.3)$$

At a distance r, away from the source electrode (A or B), the hemisphere has a surface area $S = 2\pi r^2$, so if $L = r$, and $\Delta U_{MN} = U_M - U_N$:

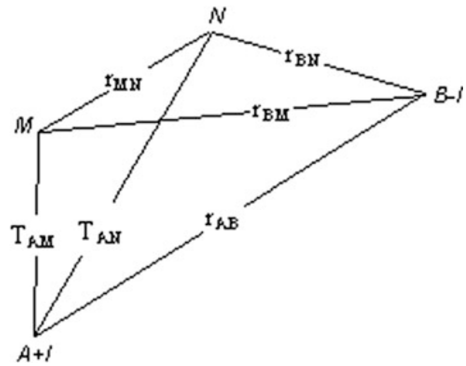

Fig. 2.11 Four electrodes array *AMNB*. *A* and *B* are the current electrodes (C_1 and C_2 in some textbooks), and *M* and *N* (respectively P_1 and P_2) are the electrodes measuring the potential difference

$$\rho = \frac{U_M - U_N}{I_{AB}} \cdot 2\pi r. \qquad (2.2.4)$$

The potentials in points M and N are the sums of the potentials from the current electrodes A and B, the electrical current being $+I$ and $-I$, respectively:

$$\begin{aligned} U_M &= U_M^A + U_M^B = \frac{\rho \cdot I}{2\pi}\frac{1}{r_{AM}} - \frac{\rho \cdot I}{2\pi}\frac{1}{r_{BM}} \\ U_N &= U_N^A + U_N^B = \frac{\rho \cdot I}{2\pi}\frac{1}{r_{AN}} - \frac{\rho \cdot I}{2\pi}\frac{1}{r_{BN}}. \end{aligned} \qquad (2.2.5)$$

So, the resistivity for uniform homogenous volume in the upper hemisphere is:

$$\rho = \frac{\Delta U_{MN}}{I_{AB}} \frac{2\pi}{\frac{1}{r_{AM}} - \frac{1}{r_{BM}} - \frac{1}{r_{AN}} + \frac{1}{r_{BN}}}. \qquad (2.2.6)$$

The relative disposition of the electrodes determine the so-called "coefficient of the array"—k:

$$k = \frac{2\pi}{\frac{1}{r_{AM}} - \frac{1}{r_{AN}} - \frac{1}{r_{BM}} + \frac{1}{r_{BN}}}. \qquad (2.2.7)$$

Practically, at meso- and macro-level, the rocks are neither uniform, nor homogenous. At given position between the electrodes, the electrical current passes trough composite rock material with imposed secondary brittle or ductile deformations. This fact argues the use of the term "apparent resistivity" ρ_a for the measured in situ resistivity. The final equitation becomes:

$$\rho_a = k\frac{\Delta U}{I}. \qquad (2.2.8)$$

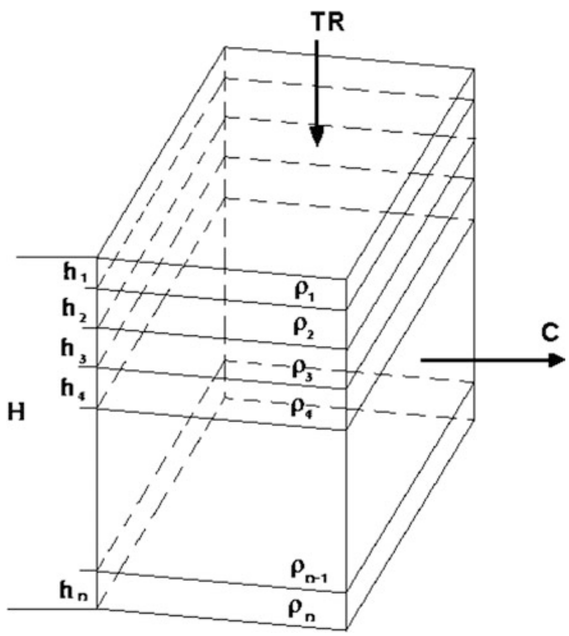

Fig. 2.12 Model of a sequence of horizontal layers

The apparent resistivity is a function of the specific electrical resistivity of the rocks, the thickness and the depth of the layers and other rock inhomogeneities as fractures and the type of their filling substance. Thus, the electrical field should be not symmetric in the space. Its configuration will depend on the superposition of the electrical conductivity of the studied "package" of layers and structures. The same is valid for the electrical resistivity.

Let us consider the simplest case, representing a package of horizontal layers with electrical resistivity of every layer $\rho_1, \rho_2, \rho_3, \ldots \rho_N$ (Fig. 2.12).

In this model $L = 1$. The thickness of the layers is $h_1, h_2, h_3, \ldots h_N$. From Eq. (2.2.1) is seen that the resistance R is:

$$R = \frac{\rho \cdot L}{S}. \qquad (2.2.9)$$

The parallel conductivity C_i when the electrical current is applied on the transversal walls of every layer i is:

$$C_i = \frac{1}{R_i} = \frac{h_i}{\rho_i}. \qquad (2.2.10)$$

The transversal resistance TR_i when the electrical current is applied from the top and the bottom of the layers' package is:

$$\mathrm{TR}_i = R_i = \rho_i h_i. \qquad (2.2.11)$$

From Eqs. (2.2.10) and (2.2.11) it can be determined that:

$$h_i = \sqrt{C_i \mathrm{TR}_i} \qquad \rho_i = \sqrt{\frac{\mathrm{TR}_i}{C_i}}. \qquad (2.2.12)$$

For the total thickness $H = \sum_{i=1}^{N} h_i$ the total parallel conductivity C and the total transversal resistance TR are:

$$C = \sum_{i=1}^{N} \frac{h_i}{\rho_i} \qquad \mathrm{TR} = \sum_{i=1}^{N} h_i \rho_i. \qquad (2.2.13)$$

The average parallel resistivity ρ_l and the average transversal resistivity ρ_t will be:

$$\rho_l = \frac{H}{C} \qquad \rho_t = \frac{\mathrm{TR}}{H}. \qquad (2.2.14)$$

It is proven that always the transversal resistivity ρ_t is higher than the parallel resistivity ρ_l (Hmelevskoy 1984).

Let us now consider a more complicated and close to the practice case, when the layers are dipping from the surface at angle α and the measurement of the electrical resistivity is executed using the symmetric four electrodes array Schlumberger (Fig. 2.13). The array can be oriented randomly on the surface, crossing the parallel layers at angle β.

Without entering in the theoretical details, it can be shown (Yakubovskiy 1973) that:

$$\rho_a = \frac{\rho_l \sqrt{\rho_t}}{\sqrt{\rho_l(\cos^2\beta + \sin^2\beta \cdot \cos^2\alpha) + \rho_t \sin^2\beta \cdot \sin^2\alpha}}. \qquad (2.2.15)$$

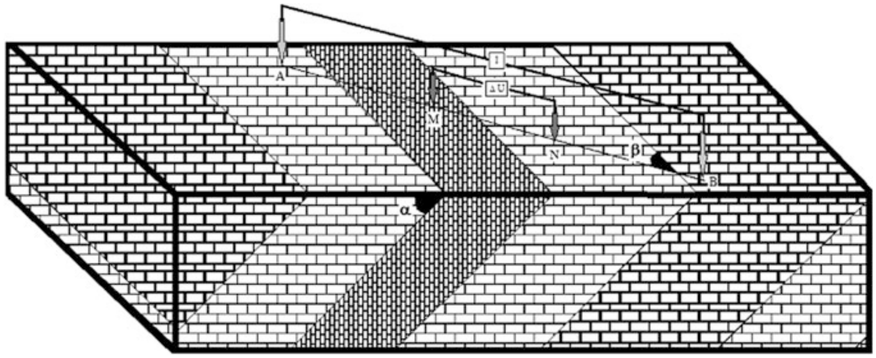

Fig. 2.13 Model of field measurement of the electrical resistivity of layered rocks

Two extreme case exist—when the array is parallel to the layering (or to the extension of the inhomogeneities), i.e., $\beta = 0$, and when the array is perpendicular to the layering ($\beta = \pi/2$). For the first case the maximum apparent resistivity will be measured, because:

$$\rho_a(0) = \sqrt{\rho_l \cdot \rho_t} = \rho_{\max}. \quad (2.2.16)$$

For the second case the apparent resistivity is lower

$$\rho_a(\pi/2) = \frac{\sqrt{\rho_l \rho_t}}{\sqrt{1 + (\lambda^2 - 1)\sin^2\alpha}} = \frac{\rho_{\max}}{\sqrt{1 + (\lambda^2 - 1)\sin^2\alpha}}. \quad (2.2.17)$$

Here λ is the coefficient of macro-anisotropy, because it characterizes the integral anisotropy of the studied rock volume and it is $\lambda > 1$:

$$\lambda = \sqrt{\frac{\rho_t}{\rho_l}}. \quad (2.2.18)$$

It is evident, that $\rho_a(0) > \rho_a(\pi/2)$. The measured apparent resistivity parallel to the elongation of the inhomogeneities is higher then perpendicularly to them. So, this is the "paradox of the anisotropy," because in reality the transversal resistivity ρ_t is higher than the parallel resistivity ρ_l.

In practice, using arrays with different azimuths around a given point and with different distance between the electrodes *A* and *B*, it is possible to obtain the electrical anisotropy ellipse for different depths (Azimuthal Vertical Electrical Sounding). For different depths (different stratigraphic layers), the ellipse of the electrical anisotropy can be obtained, which is closely related to the rock bedding and fracturing through the "paradox of anisotropy." In most of the practical cases, the longest axis of the electrical anisotropy in horizontal plane is coinciding with the dominant direction of the tensile fractures, normally controlling the general orientation of the karst galleries.

As example, a study in karst area in Bulgaria is presented here.

2.2.3.1 Rumiantsevo Region (Central North Bulgaria)

The investigation aimed to study the space position of 3 m high karst cavity crossed by an exploration well at a depth of 19.6 m below the surface. The studied area is located near the village of Rumiantsevo (North Bulgaria). This is a potential area for a future mining of limestones from Kailaka Formation. It is built of white, massif, and organic limestones with various biological inclusions. The age is considered to be Upper Maestrichtian. Limestones are easily karstified near the fractured zones and faults. The region of nearby Karlukovo village is known with its numerous surface negative karst forms and many caves (Fig. 2.14).

Above-mentioned modification of Vertical Electrical Sounding (VES) method was used to applying an azimuth scheme on the site where Well No.10 crossed an underground cave. An important data on the electric anisotropy of the rock at different depths and prevailing direction of the fractures could be obtained by using this scheme of measurements. VES 1 is coinciding with the wellhead. Knowing the real depth of the layers and the crossed cavity, the survey at this site was as a "parametric" VES, because the information from the well was used for calibration of the rock resistivity (Fig. 2.15). When fixing the known depths, it was possible to evaluate the real pseudo-resistivities of the cross-section. Nevertheless, the automatic interpretation of the curve by the

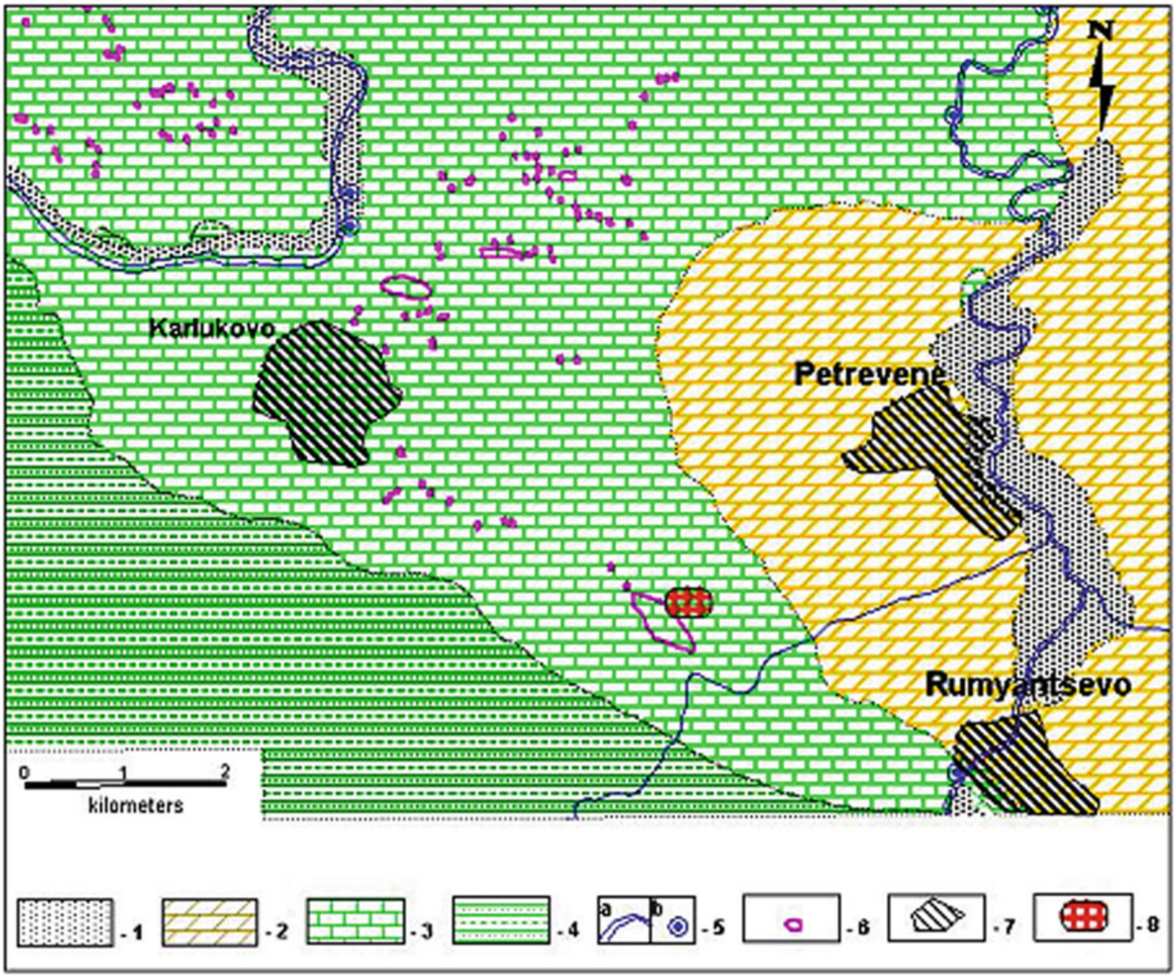

Fig. 2.14 Geological map of the studied area near the village of Rumyantsevo (according to Tsankov 1991): *1*. Alluvial deposits—sands, gravels, clays; *2*. Paleogene marls, sandstones, siltstones, clays; *3*. Upper Maestrichtian limestone; *4*. Lower Cretaceous sandstones, marls, siltstones; *5*. **a** rivers; **b** karstic springs; *6*. dolines; *7*. villages; *8*. studied area

program IPI2WIN gave the position of the cave between 22.5 and 29.9 m from the surface. The only point on the electrical curve showing the presence of the cave is at $AB/2 = 25$ m. This length of the electrical current supplying array was used for the Method of Dipole Profiling.

Two types of limestones (according to their electric properties) are present in the geological cross-section of the area. Limestones of comparatively high electric resistivity (1,000 Ωm) are defined near the surface, particularly in the northeastern part of the area. They could be identified with the third horizon of Kailaka Formation. Limestones of lower resistivity (400–600 Ωm) are disposed below them with a top at about 11–15 m depth from the surface. They could be identified with the second horizon of Kailaka Formation. Karst forms are found only in the horizon of lower resistivity. No available data exist for presence of such forms in the overlying limestones of higher resistivity. Electric resistivity of karst cavities is high (practically tends to infinity). According to VES curves, ρ_a is in the range of 4,000–5,000 Ωm.

Measurements at 4 azimuths (N 0, 45, 90, and 135°) were carried out near the wellhead. The result from the array $AB/2 = 25$ m is very important. It gave information from the depth of the karst cavity crossed by the well (Fig. 2.16). Abrupt changes of electric parameters (coefficient of anisotropy, eccentricity, direction of the long axis of the anisotropy ellipse and electrical resistivity) of the rocks were

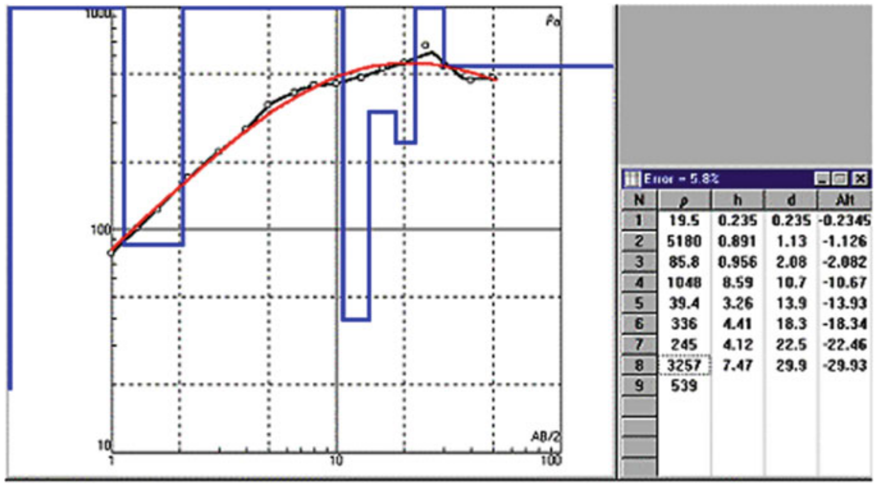

Fig. 2.15 Interpretation of VES 1 curve (Software IP2WIN). The thickness of the layers is according to the well log. The error of the approximation is 5.8 %

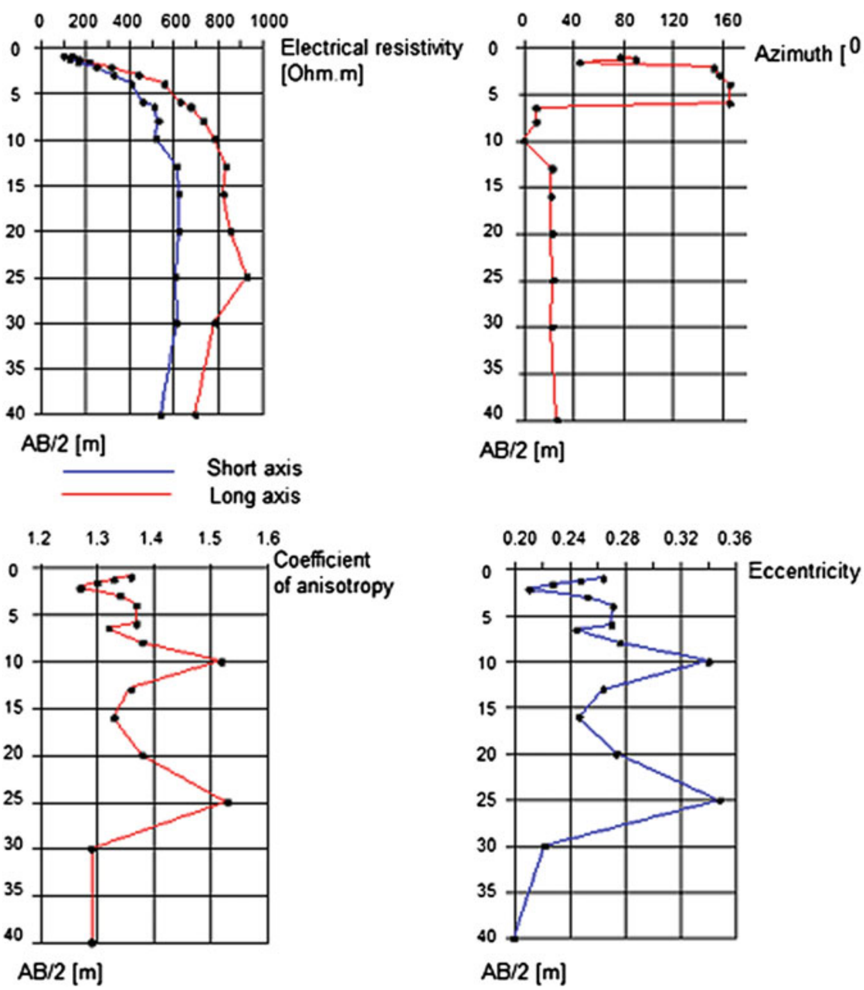

Fig. 2.16 Graphic characteristics of changing electric anisotropy in limestone layers with depth

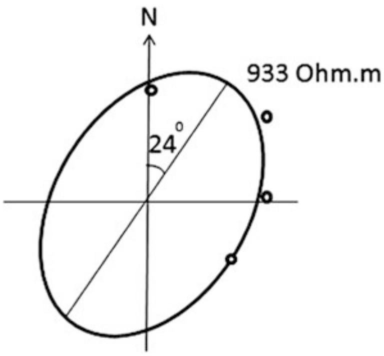

Fig. 2.17 Ellipse of anisotropy of the apparent resistivity values measured by array $AB/2 = 25$ m at 4 azimuths (Rumyantsevo, North Bulgaria). Direction of the long axis of anisotropy—N 24°; Coefficient of anisotropy—1.29; Eccentricity—0.348

detected at depths corresponding to arrays $AB/2 = 10$ m and $AB/2 = 25$ m.

Lithological alternation is the possible reason for the shallow level ($AB/2 = 10$ m), while for greater depth ($AB/2 = 25$ m), this could reflect only the presence of karst cavity elongated in NE–SW direction (Fig. 2.17).

Dipole profiling in 65 points located in the area using the scheme of Middle Gradients was applied with 50 m spacing between the current electrodes *A* and *B*. A map of apparent electric resistivity of the southern part of the studied area has been compiled (Fig. 2.18). It is evident, that the discovered by Well 10 karstic cavity is reflected by the elongated toward SW electrical anomaly with values higher then 850 Ωm. But the very high resistivities in the northern part of the studied area, probably related to near surface limestone forming the third horizon of Kailaka Formation, can mask any other existence of karst structures below these layers. The high electrical resistivity could be also related to karst structures in the upper part of the section, but this can be verified only by drilling. The practical conclusion is that the karst cavity zone intersected by the well is probably developing as underground gallery in southwest direction. It drains the system toward the open surface karst and underground forms at the southwest of the studied area.

2.2.4 Earthquake Fault-Plane Solutions

The knowledge of the processes inside the earthquakes foci at first look is not evidently related to the processes of karst formation and evolution. But a broader understanding of the contemporary Earth's dynamics and its direct impact on the faulting and fracturing of the rock volumes leads to the inevitable conclusion that these two phenomena are final results at different levels of the tectonic stresses. The mechanism in the focus of every earthquake is an informative source today about the regional (strong earthquakes) and local (weaker earthquakes) tectonic stress characteristics. It has been demonstrated in Sect. 2.2.2 how the tectonic stresses control the principal tendencies of the formation of the underground karst systems of galleries. Furthermore, if the karstified rocks are situated inside a tectonic province with contemporary expressed activity, the earthquakes could be the factor for secondary moment deformations of the speleosediments. This phenomena and its significance is discussed in Chap. 3. That is why some basic information on the mechanism of formation of the dislocation in the earthquake focus, and how it is recognized by "the fault plane solution" from the records of the seismic waves will be presented.

Reid (1911) presented his theory about the "elastic rebound" in his classic study on the dislocations along the fault system San Andreas after the earthquake in San Francisco in 1906. Reid formulated five principal statements in the theory (after Stacey 1972), as follows:

1. The rocks destruction causing tectonic earthquake comes as a result of accumulation of elastic deformation beyond the limit that rock can withstand. The deformation arises at relative movement of neighboring blocks in the Earth's crust.
2. The relative displacement of the blocks is not sudden at the moment of disruption, but it increases gradually for a longer or shorter periods of time.
3. The movement at the moment of earthquake consists only of "elastic rebound"—a sharp moving of the fault' walls up to the position, where the elastic deformations are missing. This movement is visual only to a few miles far from the fault.
4. The seismic waves originate out of the fault surface. First, the area of the surface where they arise out is very small, but after that it increases fast and becomes very large, but the velocity of its propagation does not exceed the shear wave's velocity of the rocks.

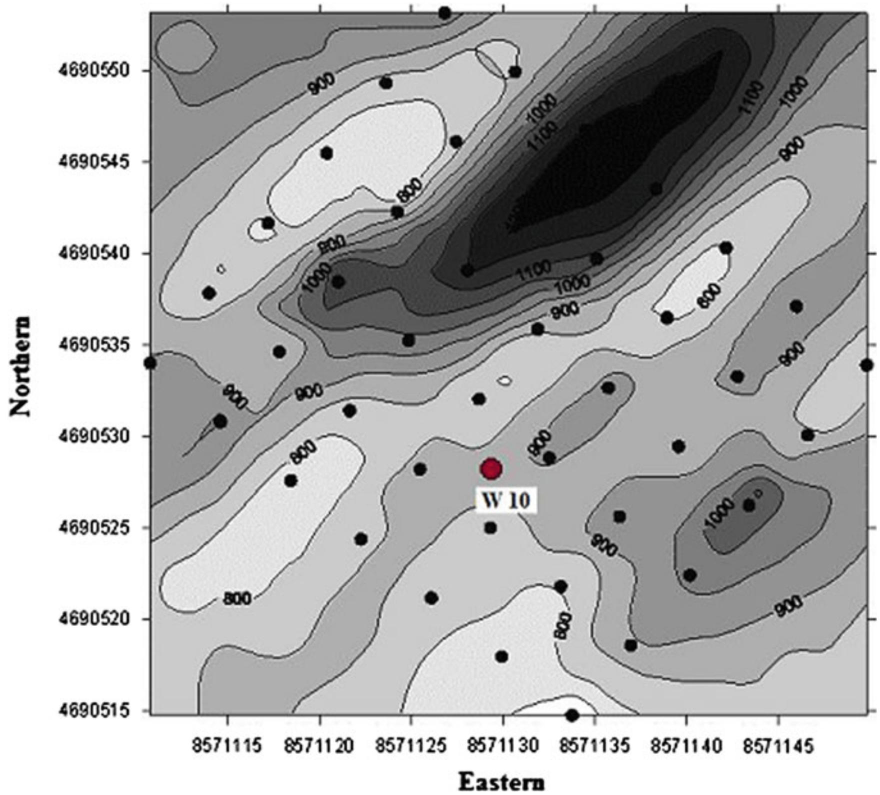

Fig. 2.18 Detailed map of the apparent electric resistivity anomaly zone around *Well 10*. The *dots* are the points of measuring of the apparent electrical resistivity

5. The energy released during the earthquake, immediately before the earthquake, is the energy of the elastic deformation of the rocks.

This theory also initiates the development of the Dislocation theory of earthquakes. Without any details upon the theory (very well shown in the works of Stacey 1972; Cox and Hart 1989, and others), it is important to note that this theory created the basis for explanation of the character of the emitted seismic waves, depending on the type of movement along the dislocation. The main idea is to present the final dislocation in the earthquake focus as an equivalent of a pair of stresses with or without moment. There is no united opinion about which of both cases describes more precisely the processes in the focal zone. In any case, the pair of stresses with moment describes better the arising of medium disruption, moving along it, and creation of waves of "contraction" and "dilatancy" (Fig. 2.19), which are registered with different polarity of their first breaks on the seismograms.

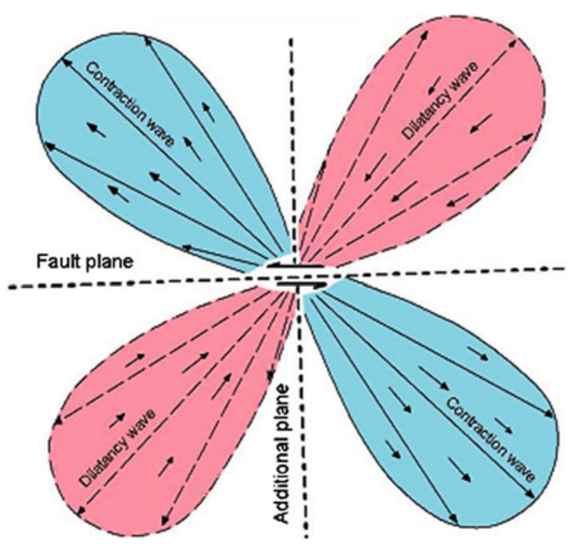

Fig. 2.19 Formation of waves of "contraction" and "dilatancy" in the earthquake focus (following Drumia and Shebalin 1985)

Usually, the study of the seismic source is through analysis of the seismic waves' records on seismic stations, outlying from the focal zone at a distance bigger than the size of the focus. It means, loss of a considerable quantity of information due to fading of the high frequencies with the distance. Nevertheless,

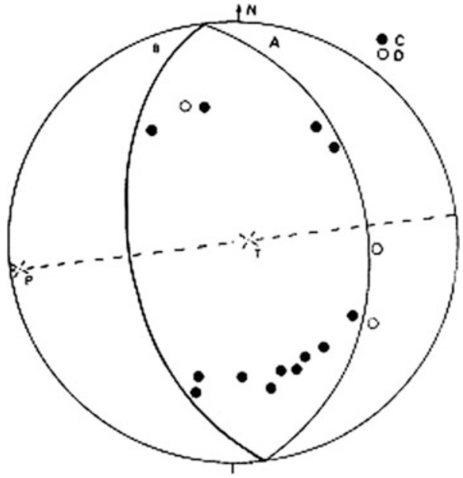

Fig. 2.20 Example of stereographic projection (lower hemisphere) with recorded first brakes of type "contraction" C and "dilatancy" D by the seismic stations from different azimuths around the earthquake focus (Georgiev and Shanov 1991—Reproduced by permission of *Bulgarian Geophysical Journal*). The nodal planes and the position of *P* and *T* axes are determined

the parameters of the focus and the processes in it are calculated, sufficiently, for the tectonic studies accuracy through these records. The regions of positive and negative first breaks (first arrival) of longitudinal waves enter on circle in Wolf' Projection, and both possible nodal planes are defined (Fig. 2.20).

The movement occurred along one of the nodal planes. The direction of tectonic compression (*P*) and tectonic tension (*T*) are situated at the two opposite bisectors of the angles defined by the nodal planes. The crossing of the nodal planes defines the intermediate axis B. These three axes are practically indirectly related to the principal axes of tectonic stresses within the rocks $\sigma_1(P)$, σ_2 (*B*) and $\sigma_3(T)$.

The interpretation of focal mechanisms for tectonic analysis has to make the distinction between the fault-plane and the auxiliary plane. The ambiguity of this interpretation is that it cannot be made from the focal mechanism itself and it must be based on comparison with the local geological structures. The main problem is connected with the synonymous determination of the nodal plane, along which the movement is performed, and it could be realized through additional tectonic and geophysical information only. The other uncertainty arises in attempting to relate the *P* and *T* axes with σ_1 and σ_3 axes of the tectonic stress field. Various inversion schemes have been developed (Gephard and Forsyth 1984; Michael 1987). The assumption of these methods is that the orientations of the principal stress axes are constant within the volume, which is being analyzed. Such dynamic interpretation of focal mechanism data is not always appropriate (Scholz 2002). For some areas, limited number of earthquakes has fault-plane solutions, for weaker earthquakes ($M < 4$) it could be expected determination of the focal mechanism only in the case of sufficient records from seismic stations around the epicentral area.

For the karst areas, the nearest earthquakes with determined fault-plane solutions can give useful information about the tendency of spatial orientation of the active (with water stream) galleries. These galleries, by their definition, have to be oriented approximately at along the same direction as the axis *P* (the compression) or perpendicularly to the axes *T* (tectonic extension).

2.2.5 Time Sequence of the Reconstructed Stress Fields

When working in karst areas, any collected information concerning the reconstructions of the stress fields can be of importance for ranging the tectonic impacts consecutively in the geological time scale, and to make the conclusions for the relationship between tectonics and karst evolution. Normally, a number of paleotectonic stress fields can be reconstructed. The first of evident bench marks for ranging them in the time is the age of the concerned karstified rocks. The first impact forming fractures had been obligatory manifested after the formation and lithification of the rocks, not earlier. The next steps are to find reconstructions of the stress field in the area in younger sediments than these containing the karst system. These sediments can provide information about the stress fields after their formation, but the deformations obligatory have impacted the older rock sequences. The last step is to compare the reconstructions of the stress field with the fault-plane solutions from nearest earthquakes, if available. These solutions give immediate information closely corresponding to today stress conditions and they can help the correct interpretation. The appropriate arrangement in time of the deformations can be successful only when using all available geological, geomorphological, hydrogeological, geophysical, and geodetic

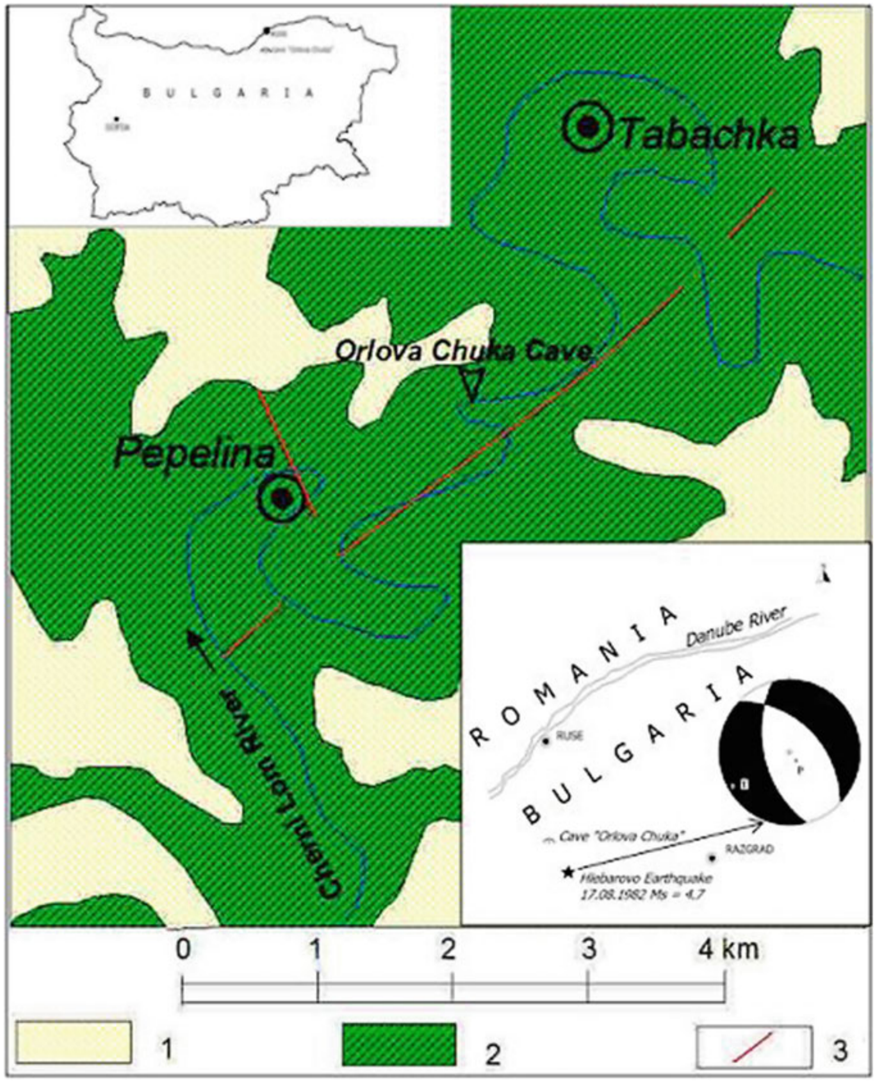

Fig. 2.21 Regional scheme, nearest earthquake fault-plane solution and geological background of the Orlova Chuka Cave area (North Bulgaria). The fault-plane solution for Hlebarovo Earthquake ($M_s = 4.7$) is based on the data published by Shanov et al. (1988). The geological map is based on Sheet "Byala" from the Geological Map of Bulgaria in scale 1:100 000 (Filipov 1992) *1*—Loess cover; *2*—Aptian limestones (Lower cretaceous); *3*—fault

information. The maps of the known karst galleries are necessary to make the most possible realistic conclusions for the features of the karst formation and evolution in the area concerned.

An example from the Moesian Platform (Northern Bulgaria) is presented below.

Orlova Chuka Cave, North Bulgaria

The cave *Orlova Chuka* (means Eagle rocky peak) is located on the left bank of Cherni Lom River (Fig. 2.21). The cave is a complex system of galleries, caves, and large and small halls. It is the second in Bulgaria by the total length of its galleries—13,437 m. The cave is formed in Cretaceous (Aptian-Urgonian) limestones and calcareous sandstones. According to Radulov (2002), the morphological features of the cave galleries suggest a phreatic origin. The cave system lies just below an old river terrace at elevation about 60 m above the present floodplain of Cherny Lom River, tributary of Danube River. Terrace at 60 m corresponds to an erosion surface formed in the southern margin of the so-called Dacian Basin during the Pliocene and Early Pleistocene. Erosional surface is cut 2.59 Ma BP, and the alluvium deposits over it extend to the beginning of loess formation in NE Bulgaria. The main phreatic stage of cave formation should be assigned to the same time span. Brunhes/Matuyama geomagnetic boundary (0.78 Ma BP) has been found

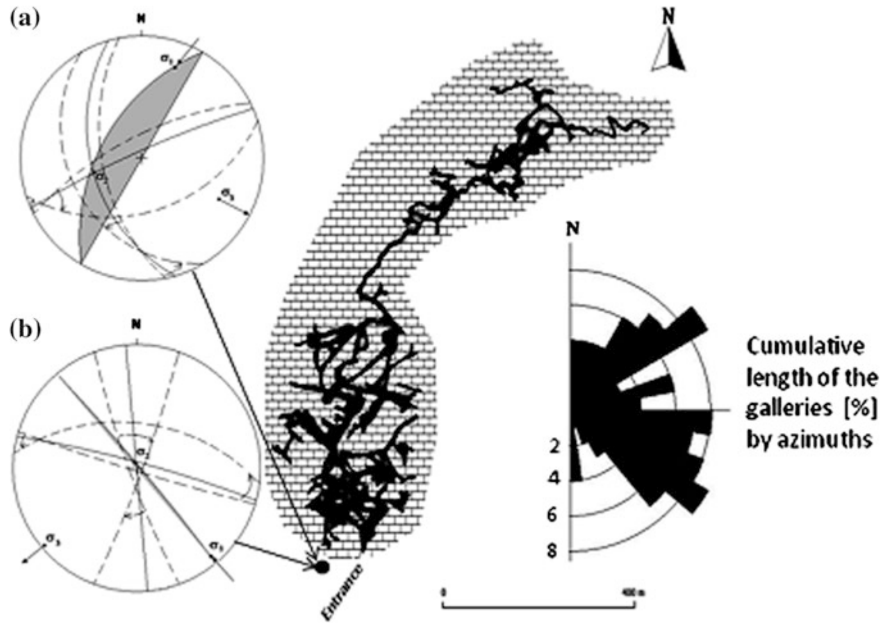

Fig. 2.22 Map of the Orlova Chuka Cave (North Bulgaria) with rose-diagram of the cumulative length (in %) of the galleries, compared to the directions of the open (tensile) fractures (in *gray* on diagrams *A* and *B*) generated by the tectonic stress fields in the Aptian limestones

at 1.20 m below the top of sedimentary sequence in an excavation in the cave (Evlogiev et al. 1997).

The reconstruction of the stress fields in the SE Moesian Platform in Bulgaria has been made by means of earthquake fault-plane solutions, tectonic fractures, and fold patterns (Shanov 2005) in rocks restricted stratigraphically from the Early Cretaceous up to the Late Pliocene. The philosophy of the study is that the recognition of the older stress fields for a given area can be successful if the characteristics of the youngest ones are known. The contemporary stress field is discussed using the fault-plane solutions from earthquakes and the kinematics of the activated faults. The reconstruction of the Post-Pliocene paleo-stress field was made by studies of conjugate shear joints systems in Upper Pliocene limestones, covering the area east of the location of the cave and containing traces from only one tectonic deformation (Post-Pliocene).

Measurements of elements of tectonic fractures were also performed in situ on more than 60 outcrops of rocks of Aptian age. A more complete study of the tectonic meso- and micro-structures has been performed on the Sarmatian sediments in the SE Moesian Platform. This study includes a description of the discovered folds, brittle tectonic analysis, and reconstruction of the Post-Sarmatian paleo-stress field. As a result, it was deduced that the compression after the Early Cretaceous period is NE-SW directed. The direction of compression since Sarmatian to Early Quaternary was NW-SE. A clockwise rotation of the main stress axes was established for a number of sites. The contemporary contraction is directed also NW-SE, according to the fault-plane solutions determined for crustal earthquakes in the region. This result is tested using the data from the GPS measurement recently performed in this part of the Balkan Peninsula (Shanov 2005).

Having in mind this regional analysis, it is easier to understand the results from the reconstruction of the tectonic stress fields using measurements of joints (106 joints) from an outcrop at the entrance of the Orlova Chuka Cave (Fig. 2.22).

At the first stage of its formation, the Post-Cretaceous fracturing (the age is not evaluated but the deformation happened before the end of Sarmatian time) probably had some role to predestine the NE–SW trend of the open fractures, able to form karstic galleries (solution *A* in Fig. 2.22). In any case the longest gallery in the cave is parallel to the regional fault striking NE–SW.

The second impact *B* was due to the more recent deformations, probably related to the Post-Sarmatian processes. The Post-Sarmatian (Late Neogene?) deformations marked a total change of the preferential direction of cave formation due to the interchange of the orientations of σ_1 and σ_3 tectonic stress axes. Since this time, because the tectonic regime as general tendencies has not changed till present, the main tectonic stress field axes keep their general orientation and the consecutive dominant NW-SE direction of the largest galleries in the cave. The main phreatic stage of cave formation and especially the formation of the large halls can be assigned to this period. The today stress field has not impacted the galleries trend, because the cave has been not active at least during the last 0.7 Ma.

The comparison of the reconstructed tectonic stress fields with the dominants directions of the galleries of the Orlova Chuka Cave confirms totally the tectonic control of the cave formation (Fig. 2.22).

2.3 Tectonic Stress Control on Karst Systems: Case Studies

The presented case studies are from different countries and different tectonic context had impacted the formation of the karst systems. Nevertheless, the tectonic control is always present and the contemporary processes of karst evolution show clear relationship with the youngest fracturing, i.e., with the recent tectonic stress field characteristics.

2.3.1 Albania: Tectonic Factor for Karst Formation in the Albanian Dinarides

2.3.1.1 Short Geological and Tectonic Characteristics

The structural complex characterizing the exceptionally complex geological structure of the not so large Albanian territory is named by Albanian geologists Albanides (Biçoku et al. 1978). Both basic megastructural units of the Albanides—North Albanides and South Albanides (related with the Helenides) are separated by the Shkodra - Pejio transversal zone representing an old paleogeographic province. The tectonic domains display different deformation styles. The External domain, where the presented studies were performed, including Paleogene and younger units of the Krasta–Çukali and other tectonic zones to the west, has been affected by compression, manifested in west-directed folds, thrust faults and oblique strike-slip fault systems (Dilek and Koçiu 2004). The karst of Albanian Dinarides (Albanian Alps zone according to some authors) is considered as continuation of the High Karst of Dinarides (Fig. 2.23).

The lower part of the geological section is represented by terrigenous sediments of Permian to Lower Triassic age. They are covered by carbonate sediments. Their accumulation began during the Middle Triassic. Bauxites were formed in the same time. A continuous sedimentation of neritic limestone followed to Maastrichtian time. Jurassic pelagic limestones with silicitic layers occur in the eastern part of the Albanian Dinarides. This part (called also Valbone Subzone) is considered as an independent transitional element of uplifted Vermosh flysh, which covers a period from Maastrichtian to Eocene.

At the end of the Eocene, the zone of the Albanian Dinarides was deformed and thrusted to the south over the zone Krasta-Çukali. From structural point of view, the Albanian Dinarides are a monocline dipping northwest. The large Valbone anticline is located to the northeast and the large Malesia-Madhe syncline is situated to the northwest.

The region in which the expeditions of the Bulgarian Speleological Federation worked during four consecutive years (beginning from 1990) is a part of the North Albanides. According to the age of the more intense folding, the region belongs to the areas deformed at the end of the Eocene. More detailed structural and tectonic investigations in 1994 have been carried out on the territory of the SE limb of Malesia-Madhe syncline, and especially near its axial part. The geology of this territory is represented mainly by carbonate complexes of Lower Jurassic up to Lower Cretaceous (Barremian-Aptian) age. The results of the structural-geological studies were published by Shanov (1999). Here, the tectonic control on the karst formation in the studied area is discussed following this publication.

Different-order faults determine the formation of the tectonic block structure of the limestone massif. They are long-term acting faults with quite explicitly manifested neotectonic activity affecting the relief and the karstic processes in the region. The recent activity of some of the faults is manifested by concentration of earthquake foci along them (Fig. 2.24). The fault Rapsh- Boçani is quite active during the recent tectonic stage (No. 4 in Figs. 2.24 and 2.25).

It is clear, that energy accumulation occurs along this fault, periodically being released by earthquakes

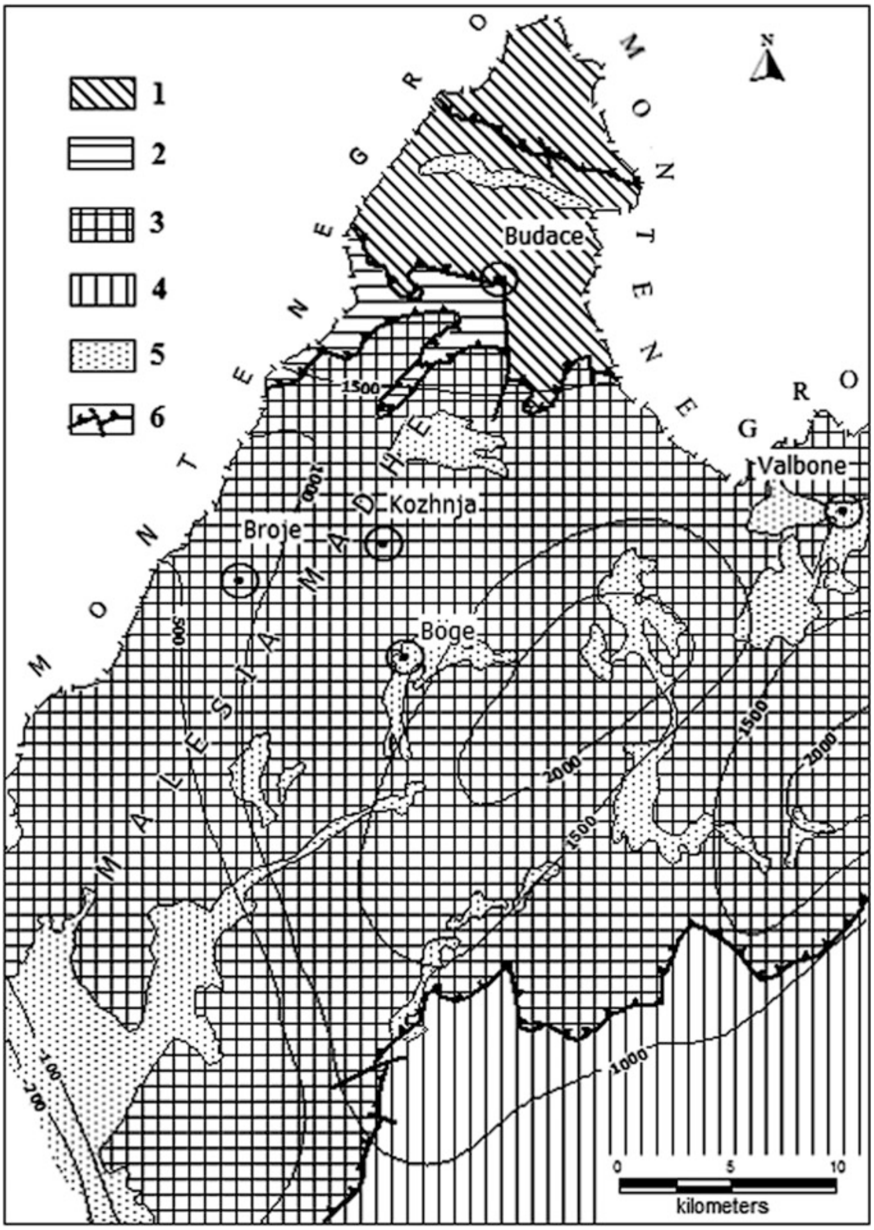

Fig. 2.23 Regional tectonic scheme of North Albania (after Biçoku and Aliaj 1973a, b and the Geological Map of Albania in scale 1:200 000—Harta Geologjike 1981). Isolines of the maximum uplift in metres during the Neotectonic stage are shown (Shanov 1999—Reproduced by permission of *Geologica Balcanica*) *1*—Zone Gashi, uplifted after Early Paleogene; *2*—Zone of the High Karst, uplifted after the end of early Paleogene; *3*—Zone of Albanian Dinarides (Albanian Alps), uplifted during the first half of the Paleogene; *4*—Zone Kras-Cukali, uplifted during the second half of the Paleogene; *5*—Neotectonic superimposed depressions; *6*—thrust front lines

in the zones of its crossings with other regional faults (e.g., with fault No. 1—Pjetroshan- Velicikut-Kozhnje, or with fault No. 3—Böge-Budace). Following the most general considerations reflected on the geological map of the region, it could be assumed that, in the contemporary tectonic stage, there is an uplift of the northern adjacent to the fault block and subsidence of the southern one. This is a continuation of the tendency of neotectonic development of the region, which has predestined the contemporary relief. The neotectonic stage is marked by intense uplift total amplitude in some parts more than 2,000 m.

2.3.1.2 Geological and Hydrogeological Conditions of Karst Formation

During the whole Mesozoic after Early Triassic time, the depositional settings, existing almost continuously up to the beginning of the Maastrichtian, resulted in the formation of a thick limestone complex. The

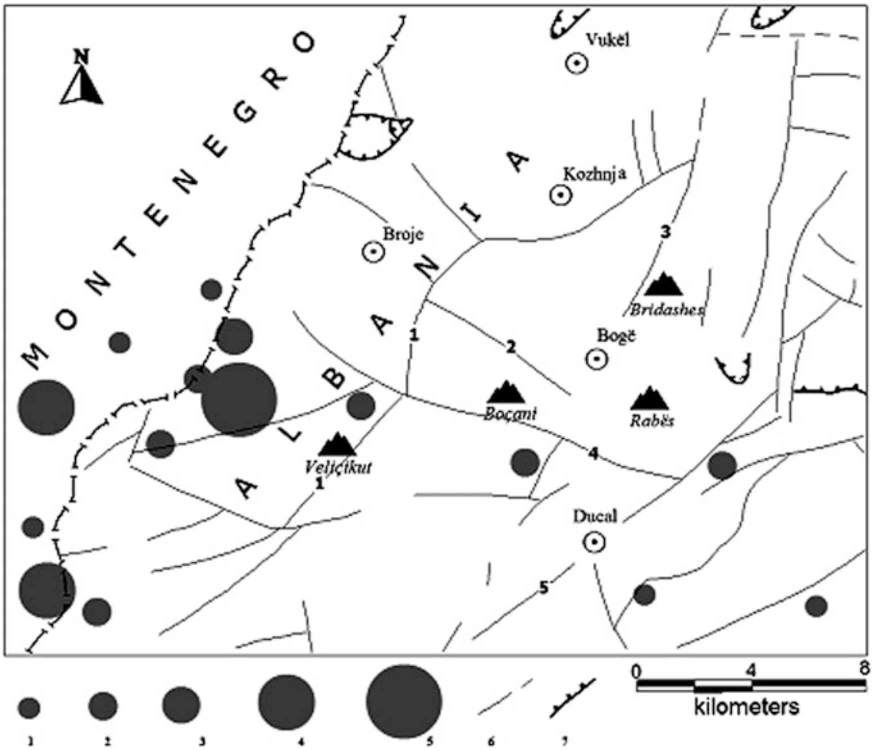

Fig. 2.24 Main fault structures and epicenters of recorded earthquakes for the period 1961–1988 in the studied area (Shanov 1999—Reproduced by permission of *Geologica Balcanica*) Earthquake magnitudes: *1*—$M < 2.0$; *2*—$M = 2.1$–3.0; *3*—$M = 3.1$–4.0; *4*—$M = 4.1$–5.0; *5*—$M = 5.1$–6.0; Faults: *6*—normal faults; *7*—thrusts; More important regional faults: Pjetroshan-Veliçikut-Kozhnje; *2*—Dobromiri; *3*—Böge- Budace; *4*—Rapsh-Boçani; *5*—Ducal

following tectonic events during the Alpine tectonogenetic phases and especially the intense overthrusting of a part of the limestones complex to the South increased the thickness of the rock complex (Fig. 2.26).

The neotectonic uplift and denudation led to the contemporary complex relief, with altitudes exceeding 2,000 m. It could be supposed that the thickness of the carbonate rocks, now subjected to karstification, is more than 1,500 m. An argument for this supposition is the concentration of important karstic springs at altitude of some tens of meters over sea level and running out of impressive quantities of fresh water in Shkodra Lake and Adriatic Sea. The tectonic factor should be also taken into account—fault sets that facilitate the drainage of superficial water outflow by channels, which do not allow always the formation of accessible karstic cavities.

According to the Hydrogeological Map of PSR of Albania M 1:200 000 (1981), the fault marked by the line Pjetroshan-Velicikut-Kozhnje plays the role of main distributor of underground water outflow in the region localized west-northwest of Böge settlement. There are concentrations of karstic springs along the northwestern fault wall. Probably, an enormous underground water flow is drained by the same fault, coming out on the surface near the village of Pjetroshan by a well-developed karst spring system. One of the springs has a discharge up to 4 m^3/s.

At the same time, the southeastern fault wall, constituted by faulted blocks, offers all conditions needed for draining of huge superficial water quantities (most of all atmospheric) and their running toward the drainage zone. The investigated region is localized in joints-karstic type of water-bearing system having an effective infiltration ratio about 0.6–0.7. In these conditions, the atmospheric waters penetrate fast in the water-bearing system and flow toward their natural drainage level. In this way, no conditions stimulating the development of horizontal

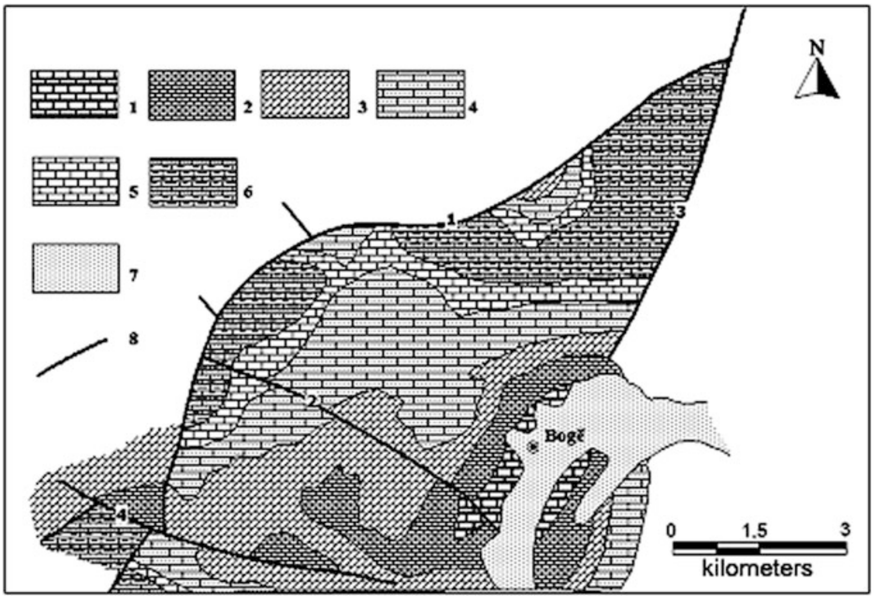

Fig. 2.25 Geological scheme of the investigated territory NW of the Böge settlement (North Albania), carried out on the base of Geological Map of Albania in scale 1:200 000 (1981) (Shanov 1999—Reproduced by permission of *Geologica Balcanica*) *1*—Upper Triassic limestones and dolomites; *2*—Lower Jurassic limestones and dolomites; *3*—Middle–Upper Jurassic undivided limestones and dolomites; *4*—Upper Jurassic limestones and clayey sands; *5*—Tithonian limestones; *6*—Lower Cretaceous limestones, carbonate limestones, clayey sands; *7*—Quaternary sediments in superimposed depressions; *8*—faults: *1*—Pjetroshan-Velicikut-Kozhnje; *2*—Dobromiri; *3*—Böge—Budace; *4*—Rapsh–Boçani

karst system could practically exist. The conditions for vertical channels precipices are much better. Several expeditions of the Bulgarian Speleological Federation just prove the mass development of precipices reaching depths from tens to 500 m (Fig. 2.27).

The speleological as well as the geological structural investigations in the karstic massif to the northwest of Böge settlement (Fig. 2.23) clarified additionally some problems and showed a strong significance of the fault tectonics as a factor for precipices and caverns formation in the most fragmented by young displacements zones.

The measurements of the space elements of joint systems and tectonic striations on different surfaces of outcrops have been carried out only at 16 points (Fig. 2.28) because of relief complexity, its difficult access and the limited time for field observations. The information turned to be sufficient for reconstruction of the main tectonic deformation phases after Early Jurassic times up to present days, which determine the main relief characteristics as well as the superficial and underground karst features.

2.3.1.3 Investigation Methods

Three basic methods were used for reconstruction of the principal axes of the tectonic stress field. Detailed analysis of the final results from each observation point allowed to distinguish the different deformation phases imprinted in the structure of the joint systems of the karstic massif and controlling the basic characteristics of the karstic processes and to determine their age.

Fault-Plane Solutions from Earthquakes

Only one fault-plane solution was available for the purposes of the investigation, i.e., an earthquake with magnitude $M = 5.1$ (f November 3, 1968) and epicenter localized to the southwest of the studied region (N 42.10, E 19.35°). The data are taken from the paper of Muço (1994).

Tectonic Stress Field Reconstruction from Striations on Slickensides

These investigations occupy the most significant place in the collected information because, in 11 points of

Fig. 2.26 Highly deformed and fractured limestones forming the borders of the valley of Böge

structural studies, indicators of displacements on the joint and fault surfaces have been found—exceptionally well-preserved tectonic striations covering in some cases surfaces of several square meters.

Reconstruction of the Tectonic Stress Fields Using Tectonic Shear Joints

This study has been carried out following the method of Nikolaev (1977), which has been already commented. In the region studied, mass measurements of joints have been carried out in four outcrops.

2.3.1.4 Results

Structural investigations applied for rock formations of different age (but within the Jurassic Period) allow to differentiate the reconstructed tectonic stresses in time. Table 2.2 shows diagrams of the reconstructed tectonic stress fields for the sites of performed measurements, which are related to a certain tectonic phase of a global scale. This turned out to be the most logical scheme when interpreting and comparing reconstructions for the sequence of Jurassic limestones of different age.

Fig. 2.27 Typical sub-vertical karst precipice in Albanian Dinarides

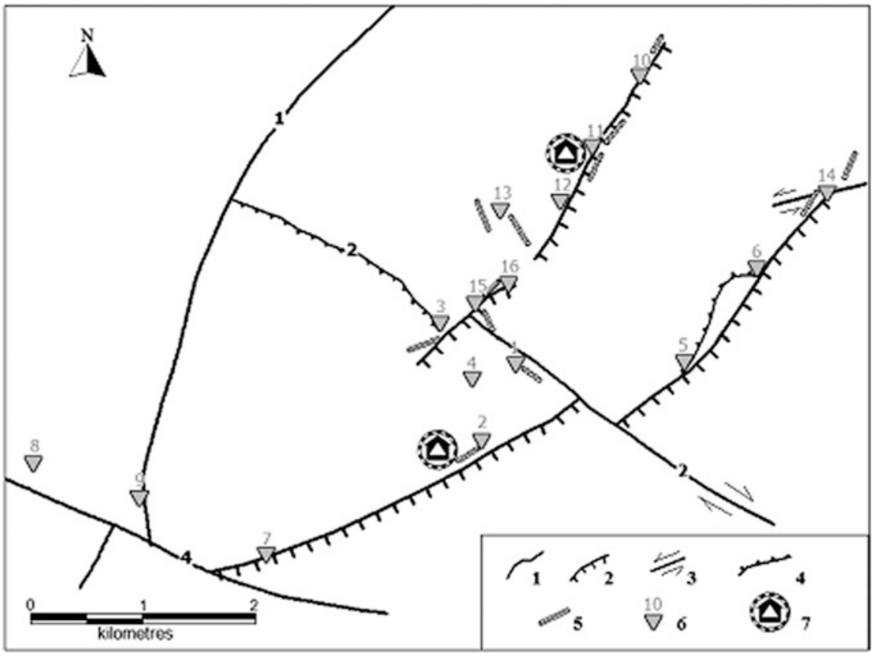

Fig. 2.28 Scheme of fault ruptures in the region investigated in 1994, sites of structural measurements and base karst forms orientations in plan view *1*—fault with undetermined type of displacements; *2*—normal fault; *3*—strike-slip fault; *4*—thrust; *5*—sites of structural measurements; *6*—speleological camps. Fault numbers follow these in Fig. 2.25: *1*—Pjetroshan-Velicikut-Kozhnjc; *2*—Dobromiri; *4*—Rapsh–Boçani

The youngest (Quaternary and recent) tectonic stress field is defined by the fault-plane solution of the only available earthquake focus near the territory studied. Its features (NW–SE compression and NE–SW extension) could be found in the reconstructions for sites 13, 14, and 9. The tectonic stress field is characterized by changed stress axes as compared to those of the Neotectonic (post-Miocene)

Table 2.2 Reconstructed time sequence of the tectonic stress fields for the studied area of Albanian Dinarides (Shanov 1999—Reproduced by permission of *Geologica Balcanica*)

Origin	Site №	TECTONIC PHASES: Late Cimmerian	Laramian	Pyrenean	Neotectonic	Recent	Method
Earthquake 03.11.1968 M=5.1 N 42.10^0 E 19.25^0							Fault-plane solution
J_3 - Limestones	5			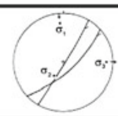			Striations on slickensides
	6				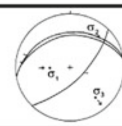		
	10				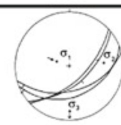		
J_3 - Limestones	12				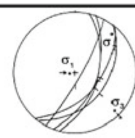		
	13		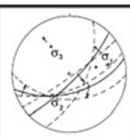	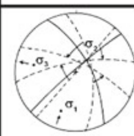	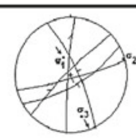	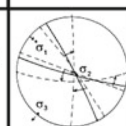	Striations & Shear joints
	14		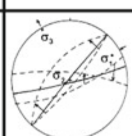			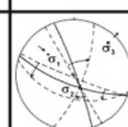	Shear joints
	15		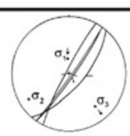				Striations on slickensides
	16		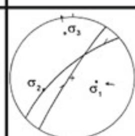				

(continued)

Table 2.2 (continued)

$J_{2\text{-}3}$ - Limestones	4	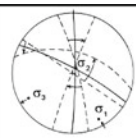		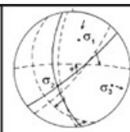			Shear joints
	7				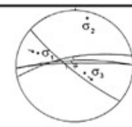		Striations on slickensides
	9					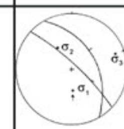	
J_2 - Limestones	2	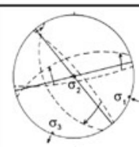	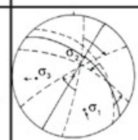				Shear joints
	8	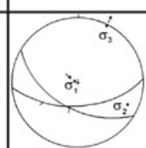					Striations on slickensides

stage, where the minimum tectonic stress σ_3 of NW–SE to E–W trend generated formation of neotectonic superimposed depressions generally elongated NE-SW (see Fig. 2.23). The compression was subvertical (uplifting) and it is well expressed by the striations on the tectonic slickenside at sites 6, 10, 12, and 13.

The most intense deformations can be referred to the Pyrenean phase (end Eocene). Then, under the conditions of strong pressure of almost N–S direction (see sites 5, 13, and 4), a southward thrusting of the Albanian Dinarides onto the Krasta-Çukali zone occurred. After the Middle Jurassic, Late Cimmerian, and after that, Laramian tectonic deformations affected the massif of limestones and dolomites. Reconstructions in sites 13, 14, 15, 16, and 2 are a clear evidence of this. The Laramian Phase is characterized by a strong subhorizontal northwest-southeast trending minimum principal stress σ_3.

The Late Cimmerian Phase shows features, which are very similar to the contemporary tectonic stress field. Taking into consideration that during the Pyrenean Phase the whole massif has been displaced to the south, presumably with some rotation, both most ancient phases posse an element of relativity in reconstructed directions of their principal tectonic stress axes.

2.3.1.5 Relations Between Karst Formation and Concrete Tectonic Conditions

The first step for determination of tectonic factors, influencing karst formation, is the analysis of the principal stresses that have led to the now observed structural ruptures in the discussed rock massif. The karst formation has started most likely at the end of the Eocene-Oligocene stage. By this time, the displacements of the limestone massif to the south had calmed down, and its intense uplifting started.

The detailed observations carried out in the sites of reconstruction of the tectonic stress field have resulted in some changes of the ideas concerning the fault network of the area. On the one hand, the normal faults are complicated by strike-slip displacements, being of the youngest age, and they correspond to the youngest (contemporary) tectonic stress field (Table 2.2). The well-expressed thrust structures (sites 3, 5, and 6) appear as relicts of the Laramian tectonic phase deformations. In the zones of shearing and mylonitization, there are conditions for formation (mainly because of mechanical export of particles by the water) of small horizontal cavities, which seldom reach more than several tens of meters (for example at sites 5 and 6). Their orientation is along the slip surface.

During the Pyrenean Phase, strong normal faulting along the ruptures of NE-SW direction and opening of joints systems into the same direction occurred. Most investigated vertical precipice caves developed on these joints. It is worth to emphasize that they all belong to zones with well- manifested faults.

Precipices near sites 10, 11, 12, and 16 are located along morphologically well-manifested fault still not shown on official maps. All these precipices are located in brecciated zones with clear tectonic slickensides and striations on them.

During the Pyrenean phase, tensile stresses varied locally from NW–SE to NE–SW direction, and the compression was oriented N–S or sub-vertically (uplifting of the massif). The subvertical compression lasted also during the Neotectonic stage when the orientation of the minimum stress σ_3 favored both the existence of earlier formed open cracks of NW–SE direction (sites 13 and 15—open karren and precipices; in case of site 1—widely open karren up to several meters). Some evidence of strike-slip displacements can be seen on site 14. The controlling role of the faults for the process of massif karstification is best observed in areas of Upper Jurassic clay sandstone, where caves could not exist without the influence of the tectonic factor. Strong faulting and crack opening favor mechanical export of debris and the formation of typical karstic precipices.

The contemporary displacements are not so active but in case of NW–SE orientation of σ_1 they have led to some clear strike-slip displacements along the Dobromiri Fault. Besides that, the erosion rate obviously becomes dominating over the uplifting process, and this results in sealing of many of the superficial karstic forms with deluvial materials. Thus, in spite of the high permeability for atmospheric waters into the karstic massif, the vertical type of open karstic systems are conserved only within fault zones, where, nevertheless, the young tectonic displacements do not allow their fast colmatation with materials from the rock weathering.

The sharp-shaped relief is a result not only of tectonic displacements, but also of chemical destruction of limestones and dolomites by rains and snow. The long lasting snow cover at this altitude (between 1,000 and 1,500 m) is a factor for chemical erosion durability through the year. Special analyses in the region for atmospheric waters aggression potential, as well as of the snow covering melting waters have not been done. Such an investigation would deepen the analysis of the reasons for the strong superficial and underground karstic processes in Albanian Dinarides.

2.3.2 Bulgaria: Tectonic Stress Fields Studies in Karst Systems

Bulgaria covers an area of 111,000 km^2. About 23 % of this area consists of carbonate rocks (i.e., pure limestone or dolomite) that host over 5,000 caves. Carbonate rocks, in which the majority of karst is developed, were formed during the Triassic, Jurassic, Cretaceous, and Tertiary periods. Less extensive karst with minor significance with respect to cave and karst development exists in Proterozoic marbles of Rila-Rhodopes area (Fig. 2.29).

Geomorphologically, there is an expressed distinction between the four principal regions (Popov 1982): (I) Danube Plain (Moesian Platform) in the northern part of Bulgaria; (II) Stara Planina (Balkan) Zone; (III) Intermediate Zone occupying the central parts of the country; (IV) Rila-Rhodopes Zone in the south (Fig. 2.29). The boundaries between the regions are roughly coinciding with faults and fault segments activated during the Neotectonic stage, some of them active till now and controlling the contemporary terrain morphology (USGS 2004). Only some of the active faults are recognized by the method of Paleoseismology (Meyer et al. 2007; Vanneste et al. Vanneste et al. 2006), the others are plotted on the base of published data (Cadet and Funiciello 2004; Georgiev et al. 2007; Kastelic et al. 2011; Radulov et al. 2006, 2011, 2012; Tzankov et al. 1998; Vapcarov et al. 1974; Vrablianski 1974), or verified during field works for different projects.

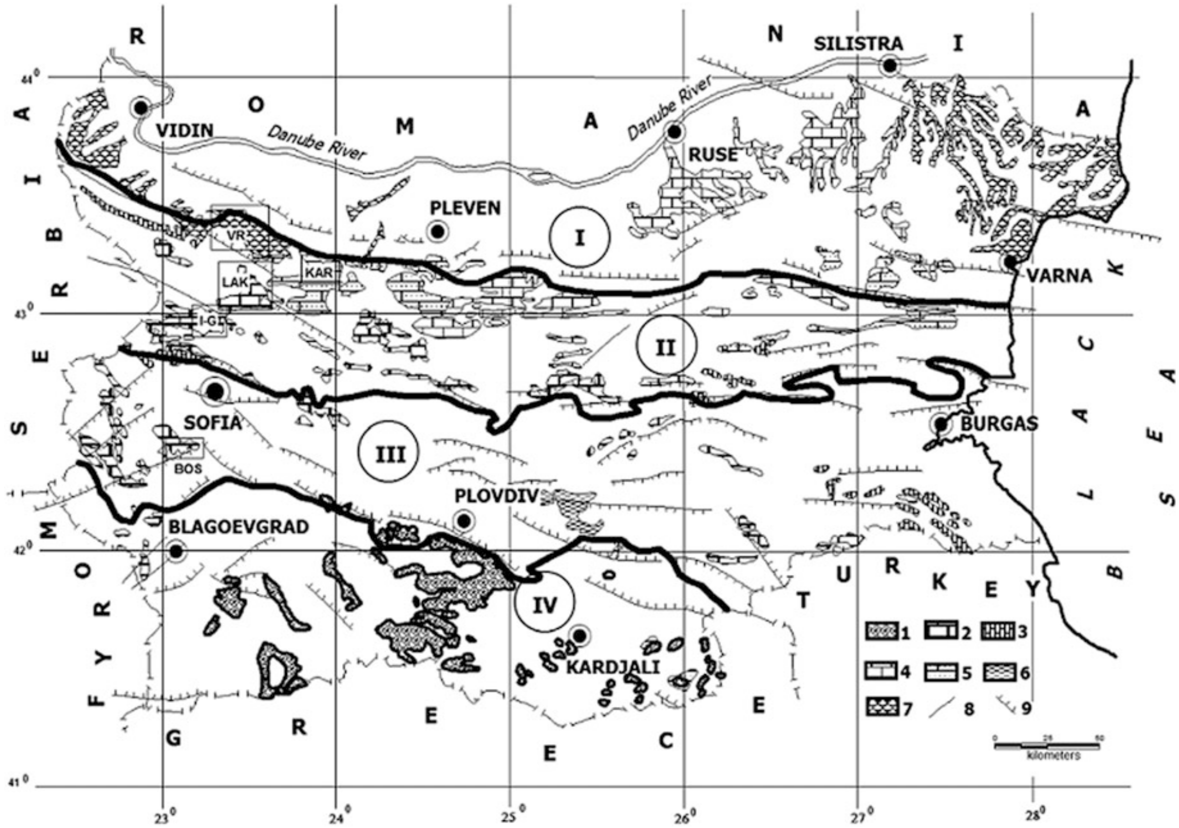

Fig. 2.29 Outcrops of karstified rocks on the territory of Bulgaria and principal karst zones, according to Popov (1982) Main regions: *I*—Danube Plain (Moesian platform); *II*—Stara Planina (Balkan) Zone; *III*—Intermediate Zone; *IV*—Rila-Rhodopes Zone Karstified rocks: *1*—Proterozoic marbles; *2*—Triassic limestones; *3*—Jurassic limestones; *4*—Upper Cretaceous limestones; *5*—Maastrichtian limestones; *6*—Paleogene limestones; *7*—Sarmatian limestones; Faults: *8*—strike-slip or undetermined type of movement; *9*—normal

The regions differ with respect to their cave and karst development, and on these grounds each of them was further subdivided into several karst districts. The Danube Plain has been discussed in Sect. 2.2 by the study of the area of Orlova Chuka Cave amd examples from the other regions are also presented .

2.3.2.1 Western Balkan Mountain

Western Balkan Mountain (Western Bulgaria), part of Stara Planina Zone, is known with important karst systems draining significant quantities of fresh water. This is an expressed mountainous area. The altitudes of the main ridge vary between 1,000 and 2,000 m, and the lowest part in Iskar River gorge is at 300–400 m. From hydrogeological view, six independent karst regions are distinguished in Western Balkan Mountain (Benderev et al. 2005). Case studies will be presented for three of them: VR—Vratsa karst region; LAK—Lakatnik karst region; I-G—Iskrets-Gubesh karst region. Their relative position is marked in Fig. 2.29.

Vratza Karst Region (VR)

Vratsa Karst Region, situated in the northern part of Western Balkan Mountain, is formed in deformed limestone layers of Jurassic and Lower Cretaceous age. The faults have been of important role for the development and evolution of the karst system. Studies on the tectonic stress fields (Fig. 2.30) were performed principally on Vratsa Block during speleological expeditions in 1985 and 1986 (analyses of the fracturing) and the preliminary results were published later (Chanov 1988). New data were included in this study, based on studies of striations on slickensides, electrical anisotropy, as well as reference on fault-plane solution from an earthquake in the

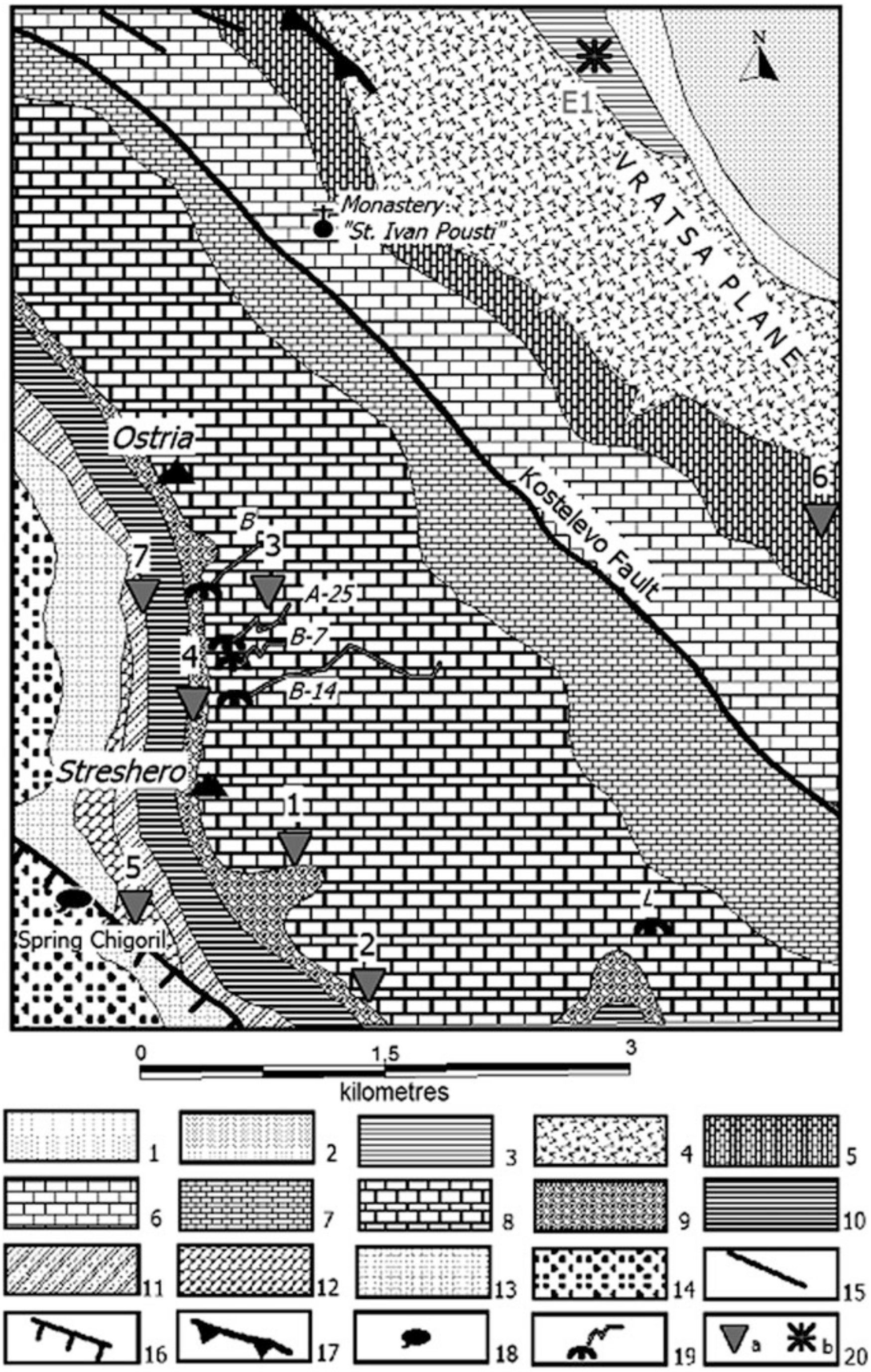

Fig. 2.30 Geological map of the area of Vratsa Block based on the Geological Map of Bulgaria, scale 1:100 000, sheet Berkovitsa (Haudutov and Dimitrova 1992) and Tronkov (1965) with the sites of reconstructions of the tectonic stress field and the principal caves. *1*—aQh: alluvial deposits; *2*—prQ_{p-h}: proluvial deposits; *3*—aQp: alluvial deposits of the older terraces; *4*—dQp: deluvial-proluvial sediments; *5*—lK_1^{ap}: limestones, marles and carbonate sandstones (Lyutibrod formation); *6*—$čK_1^{ap}$: Urgonian limestones (Cherepish formation); *7*—$slJ_2^t - K_1^v$: limestones of Slivnitsa formation; *8*—$XXJ_2^c - K_1^{bs}$: micritic limestones of Yavorets formation; *9*—pJ_2^{bj-b}: bioclastic limestones (Polaten formation); *10*—e/stJ_2^{a-bj}: black argillites of Stefanets Member; *11*—XIV $J_1^h - J_2^a$: sandy bioclastic limestones of Kostenets formation; *12*—XII $T_2^1 - T_2^k$: dolomites, marls and argillites from Beli Izvor formation; *13*—PeT_1: Petrohan Terrigenous formation; *14*—vr P_1: Permian breccias and conglomerates of Vrana formation; *15*—fault; *16*—normal fault; *17*—overthrust; *18*—spring; *19*—caves with horizontal projection of the main galleries: *L*—Ledenika Cave; *B-14*—Barki 14; *B-7*—Barki 7; *A-25*—Academic 25; *B*—Beliar; *20*—**a** site of study of the fracturing; **b** site of study of the electrical anisotropy

Fig. 2.31 View on the eastern boundary of Vratsa Block, Bulgaria

Moesian Platform, reflecting the contemporary tendencies of the tectonic processes near the studied area (Georgiev and Shanov 1991).

Vratsa Block is an integral part of the large Berkovitsa Block-Anticlinorium structure (after Tronkov 1965). The northern border of the block is a remarkable flexure, built of sediments of Triassic, Jurassic and Early Cretaceous age (Fig. 2.31). The flexure is discussed as the ductile effect of the movements along a large fault, located northwards of the flexure, and covered now by younger sediments. An important role during the tectonic evolution of Vratsa Block has been attributed to the longitudinal and transversal faults. According to Tronkov (1965), the analyses of all tectonic structures of Vratsa Block show their genetic relationship to the lateral strain acting with direction NNE–SSW (N30–40—N210–220°). This is the direction of the short deformation axis, the long axis being directed N120–130°. The faults in this situation appear as shear structures.

Hydrogeological Characteristics

From hydrogeological view, the regional geological, tectonic, physical, and geographical conditions predestined the presence of a totally drained monoclynal slope dipping toward north with two principal karst aquifers—Triassic and Middle Jurassic. A relatively thin terrigenous rock complex (Lower and Middle Jurassic) is dividing the two aquifers. The common regional water basis is formed by Lower Triassic sandstones. These rocks are relatively highly elevated with respect to the local erosion basis. The northern basis of erosion is the Vratsa Plane, separated from the studied karst area by the Kostelevo Fault (Fig. 2.30).

There is now sufficient data for the Lower Triassic aquifer. It is represented by a few outcrops in the northern and eastern peripheries of the basin. The rocks are weekly karstified. The aquifer receives its water from the atmospheric precipitation, as well as by infiltration from the lying on top karstic aquifer. A few springs are draining it; the biggest of them is Chigoril with discharge rate of 7–11 l/s (Antonov and Danchev 1980). But the more constant and independent from the atmospheric conditions discharge of the spring Chigoril is indicating the control of the water by the fault of Chigoril. The vertical rate of displacement was evaluated to be more than 300 m (Chanov 1988).

The principal aquifer (Upper Jurassic—Lower Cretaceous) is totally exposed on the surface. This fact predestines the high level of karstification related to the possibility of intensive feeding from the atmospheric precipitation. According to Spasov et al. (1998), more than 54 % of the atmospheric precipitation (in average 1,000 mm/m^2 per year) is feeding the underground waters. Part of the water forms temporal streams on the surface, but the water is quickly drained in the dolines. The karst springs situated in the northern part of Vratsa Mountain are draining the aquifer. Most of them are of ascending type.

Characteristics of the Karst of Vratsa Karst Region

The rainfalls are one of the most important factors determining the active development of the karst processes in the region. The classic type of karst is represented in the upper part of the mountain (Scorpil and Scorpil 1895, 1898; Radev 1915; Mishev and Popov 1958: Markowicz et al. 1972; Kostov 1997). Its formation is also controlled by tectonic factors, as well as by the geomorphological evolution of the area (Ilieva et al. 1981; Angelova et al. 1995, 1999).

Vratsa Karst Region represents a plateau with steep, even vertical slopes, except the narrow band from the south connecting it with the adjacent karst basin. It is built by a north-northeast dipping monoclyne of limestone layers of Late Jurassic and Early Cretaceous age (Fig. 2.30). They are separated from the underlying Iskar Carbonate Formation by a thin layer of non-karstified rocks of Early Middle Cretaceous age. The principal erosion basis is in the northeastern part of the plateau. The principal karst springs appear at that place. But, as a general rule for the entire area, the boundary between the karstified and non-karstified rocks is above the level of the local river network.

The principal part of the basin is characterized by outcropping on the surface karst with abundant karst forms. Some of the dolines are with dimensions 1–2 km^2, the biggest one reaching 2–2.2 km^2. The underground karst forms are predominant. More than 70 caves and precipices are known in this area, most of them in the limestones of Late Jurassic-Early Cretaceous age. Some zoning can be traced from southwest to northeast. The southwestern part contains relatively little horizontal caves. Above them, near the peaks Streshero and Ostria, there are considerable and complicated as morphology precipices. Here are the deepest Bulgarian caves Barkite 14, the caves Beliar, Barkite 8, Mijishnitsa. All of them begin from dolines and continue as a system of steps or dipping generally toward northwest segments, following the upper boundary of the underlying karst resisting rocks. Little water streams exist in every one of the caves, their discharges are depending directly from the atmospheric precipitation. The horizontal projections of these caves on the surface are shown in Fig. 2.30.

Typical precipices of different depths characterize the zone along the northeastern border of the plateau. The deeper one is Haydoushka Precipice, near the Ivan Pousti Monastery. Its entrance begins with a 108 m deep well. Horizontal caves are also known, some of them with springs. These ones are grouped near the Saint Ivan Pousti Monastery, the longest cave being of 546 m, and with a water stream inside. The tectonic control of karst along the border of the plateau is well expressed near Ivan Pousti Monastery (Fig. 2.32).

The seven longest caves of the region include 75 % of the total length of the galleries. The ratio between total vertical to total horizontal lengths shows the domination of the vertical karstification over the horizontal.

The karst formation began during the Early Miocene and continued during Pontian and Pliocene time. When Popov (1964) studied the genesis of Ledenika Cave, he showed that its formation dates from the beginning of the Dacian time, and it is related to the Pontian level of denudation. The same period of formation can be attributed to the caves and the precipices in the high parts of the plateau.

Results from the Tectonic Stress Fields Reconstructions

The reconstruction of the tectonic stress fields was the first step of the study. The second one was to adjust the received solutions in a tectonically logic scheme for the time of manifestation of a given tectonic strain. This scheme (Table 2.3) reflects the possible temporal evolution of the tectonic stress axes orientation for the area of Vratsa Block.

Looking at the performed reconstructions of the tectonic stress fields, the most coinciding with the described above tectonic deformations in macro scale are these from the method using the shear joints.

The oldest deformations are detected on site No 5 where the Triassic limestones retain the "memory" for two impacts. The first one is related to the Early Cimmerian Tectonic Phase (at the end of Upper Triassic time), and the second—to the Late Cimmerian Tectonic Phase (the second half of Upper Jurassic time). The limestones of Polaten Formation (site No 4) were also deformed during the Late Cimmerian Tectonic Phase. A second tectonic stress field is reflected in the fracturing, and it was reconstructed on sites No 1, 2, 3, and 6.

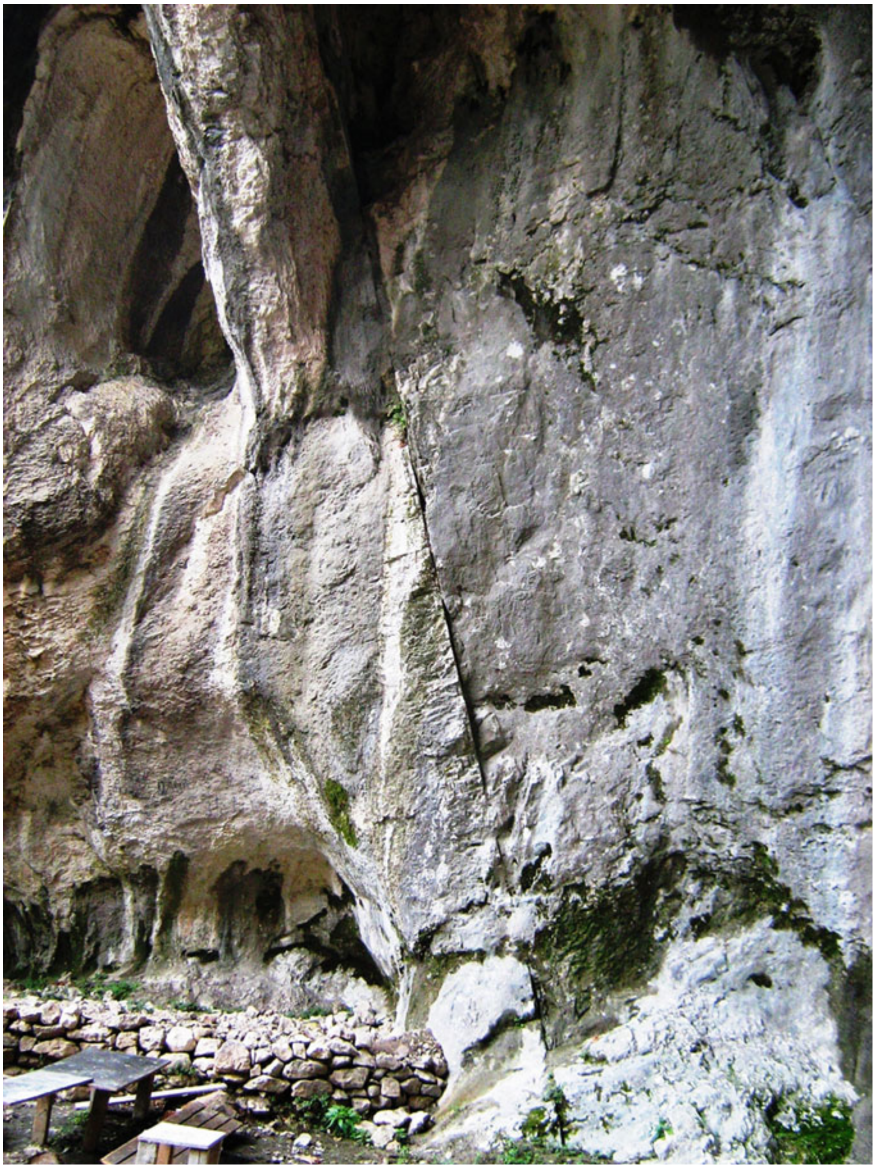

Fig. 2.32 Expressive tectonic control on the karst along the southern boundary of Vratsa Block near Ivan Pousti Monastery, Bulgaria

We suppose that this tectonic stress field is related to the Sub-Hercinian Tectonic Phase (at the end of the Turonian). On these three sites, a second group of clearly expressed joint systems exists, assumed to be a result of the Pyrenean Tectonic Phase (end of the Eocene). The importance of the deformations from the Sub-Hercinian Tectonic Phase is reflected also as well expressed orientation of the ellipse of anisotropy of the Lower Cretaceous limestones (Vertical Electrical Sounding at the site E1). Less expressed is the anisotropy ellipse for the upper part of the electrical profile. The long axis of the ellipse could be accepted as an indication of younger deformations, but arbitrary attributed to the Pyrenean Tectonic Phase.

Only one of the sites of the measurements (No 6) has shown deformations that could be related, with some level of probability, to the Neotectonic stage. The argument for this is the similarity of the reconstructed tectonic stress axes directions to the result of the fault-plane solution from the earthquake with magnitude $M = 3.6$ northwards of the studied area. But, all analyzed data do not show evidence for cardinal changes of the principal directions of tectonic strain after the Pyrenean Tectonic Phase.

Table 2.3 Reconstruction of the sequence of tectonic impact on the rocks of Vratsa Karst Region

Origin	Site №	TECTONIC PHASES: Early Cimmerian	Late Cimmerian	Sub-Hercinian	Pyrenean	Neotectonic and recent	Method
Earthquake 23.03.1987 M=3.6 N 43.88^0 E 23.56^0						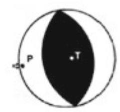	Fault-plane solution
Q + K_1 El	(VES)			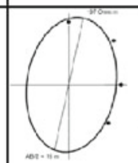	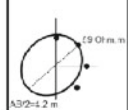		Electrical anisotropy
K_1 Limestones	6			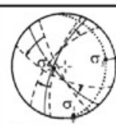	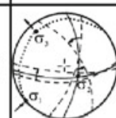	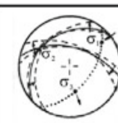	Shear joints
J_3 - Limestones	1			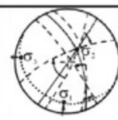	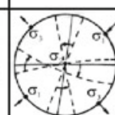		Shear joints
	2			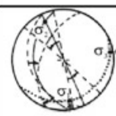	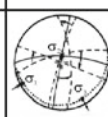		
	3			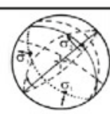	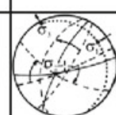		
J_2 Limestones	4		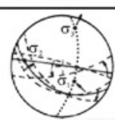	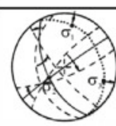			Shear joints
J_1 Sandstones	7				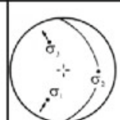		Striations on slickensides
T_2 Limestones	5	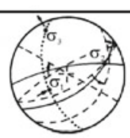	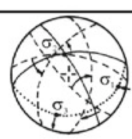				Shear joints

Fig. 2.33 Karst spring "Jitoliub", Milanovo Karst Basin, Lakatnik Karst Region, Bulgaria

This fact is reflected in the general NE–SW orientation of the karst galleries in the region. Analyzing the changes of principal stress axes from the Sub-Hercinian to the Pyrenean Phase, it is possible to deduce left rotation of the structures. For the most recent processes such a deformation was not established. The karst systems of the area are of precipice type, actually active, and draining the superficial and underground waters toward northeast. The contemporary configuration of the karst systems is possible only when the minimum tectonic stress axis σ_3 is nearly vertical.

Lakatnik Karst Region (LAK)

The Lakatnik karst spring "Jitoliub" is discharging waters drained from the southeastern part of the relatively higher karstified zone (LAK in Fig. 2.29) at the source neighborhood (Fig. 2.33)—Milanovo Basin. One of the biggest caves in Bulgaria—Temnata Dupka (more than 5 km long) is integrating the old karst levels, as well as the present active galleries and their natural water outflow—the spring "Jitoliub".

The necessity to use this water leads to ecological problems of the water qualities. One of the most important problems in the area is the correct recognition of the sites of the potential pollutant of the karst waters. A study on this problem in the context of the tectonic control of the underground cave galleries was published (Benderev et al. 2001).

Geological and Hydrogeological Background

Milanovo Basin (Fig. 2.34) with a surface of 101 km^2 is one of the biggest karst basins in Western Balkan Mountain (Benderev et al. 1987). Plakalnitsa Fault separates the basin on the northeast from the karst basins of Vratsa Karst Region. The rate of total vertical displacement along the fault is 500 m, and it disturbs the hydrological discontinuity of the karstified complexes of aquifers. The other borders are the abrupt slopes from south and southeast toward Iskar River, from southwest toward Proboynitza River, and Varshets and Ozirovo valleys from northwest. A flat plateau with average altitude of about 1,200 m is the highest part of Milanovo Basin, dominating the Iskar River valley (altitude 300–350 m).

Milanovo Karst Basin is build of Mesozoic rocks, overlying different in age Paleozoic basement (dominating granodiorite—granite complex) and Lower Triassic sediments of Petrohan Terrigenous Group. The lithological features of the Upper Triassic rocks determine the existence of one thick complex able to be karstified (Fig. 2.35), separated partially by the carbonate-terrigenous materials of Babino Formation

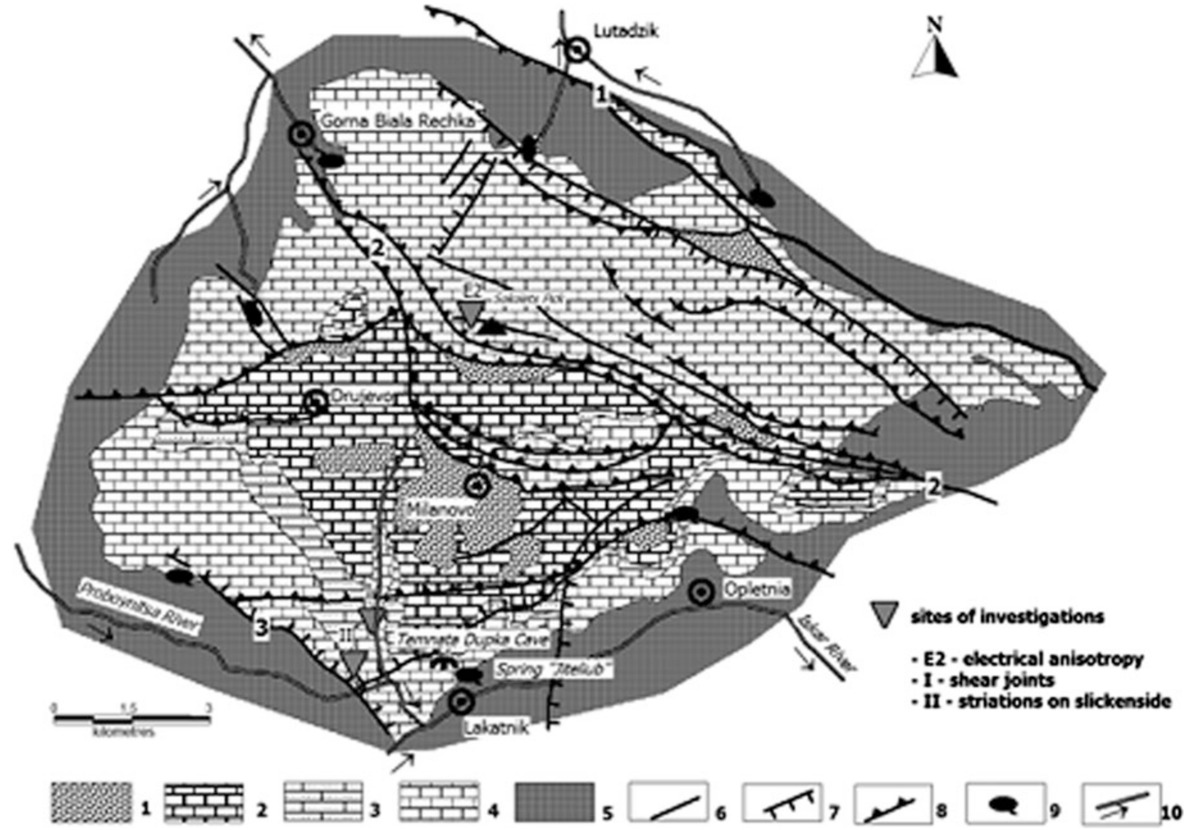

Fig. 2.34 General geological scheme of Milanovo Karst Basin (after Benderev et al. 2001) *1*—Terrigenous and carbonate-terrigenous rocks of Komshtitsa formation and Kostina formation; *2*—*Upper part* of Triassic carbonate complex (Rusinovdel formation); *3*—Intermediate Triassic carbonate-terrigenous layer (Babino formation); *4*—*Lower part* of Triassic carbonate complex (Svidol and Mogila formations); *5*—Paleozoic rock basement (granite complex) and Petrohan Terrigenous Group; *6*—fault of unknown type of movement; *7*—normal fault; *8*—thrust; *9*—Karst springs; *10*—Rivers; Main faults: (*1*) Plakalnitsa, (*2*) Pop-Sokolets, and (*3*) Proboynitsa

in two sub-complexes of limestones and dolomites (Mogila Formation with thickness of 150–350 m composed of Opletnia and Lakatnik Members, and Milanovo and Rusinovdel Formation—mainly dolomites). The lowest part of the sequence is most susceptible toward karstification processes.

The upper part of the Triassic rocks profile is composed of various terrigenous and carbonate-terrigenous rocks of Komshtitsa Formation and partially by the locally presented Jurassic terrigenous rocks of Kostina Formation.

Milanovo Karst Basin contains 103 caves and precipices, the horizontal or inclined caves being predominant. The ratio of the total altitude change to the length of the karst galleries is 0.07, and it presents the domination of the horizontal karstification. The velocity of the underground karst hydrological system hollowing is lower than the erosion on the surface and the entrenchment of Iskar River. For this reason, the lowest point of water discharging of Milanovo Karst Basin, the spring "Jitoliub" near Lakatnik Railway Station, is 10 m above the level of Iskar River. Milanovo Basin is receiving its water from the atmospheric precipitation, as well from the local rivers. Water losses were detected at the riverbed of Proboynitza River and some of its tributaries. The average total discharge of the basin springs is 1,341 l/s, or presented as a module of the groundwater flow—13.3 l/s.km^2. The minimum discharge is 197.5 l/s. The important part of the natural resources belongs to the spring of "Jitoliub" draining Lakatnik Karst Region. Some quantity of this water is used for supply of potable water.

The area near the railway station of Lakatnik is known with the largest quantity of underground karst

Fig. 2.35 View of the lithostratigraphic sequence above the spring "Jitoliub", Milanovo Karst Basin (Bulgaria)

forms—62 % of the caves of Milanovo Karst Basin. Most of the caves are not very long, but the largest cave is the only active one in the area—Temnata Dupka Cave with more than 5 km of galleries. This cave is situated at about 40 m just above the spring of "Jitoliub." The cave is a complicated labyrinth type system with underground river running out its waters trough the spring "Jitoliub." The spring water is a mixture between the underground flow from Proboynitza River and the atmospheric precipitation drained by Temnata Dupka Cave from the whole catchment zone. Analyses show, that when the spring discharge is low, the rate of feeding from Proboynitza River is less than 50 %, and it decreases with increasing spring discharge.

Tectonic Stress Fields and Preferential Directions of the Karst Galleries

Three methodologies were used for reconstruction of the tectonic stress axes (Benderev et al. 2001). The first one is based on the analysis of conjugated shear joints systems (Nikolaev 1977) and the direction of dispersion of their maximums. The measurements performed at site I in Fig. 2.34 (*I a and I b* diagrams on Table 2.4) have been analyzed. The second methodology is based on the kinematics characteristics of the movements on the rock block bounding surfaces—striations on slickensides. Clear traces of movements were found at the two sites (I and II, Fig. 2.34), and the analyses showed practically the same solution for the tectonic stress field characteristics. The summarized solution is plotted in Table 2.4 (diagram *II*).

Electrical anisotropy studies were performed near Sokolets Peak (site *E*2—Fig. 2.34). The ellipses of anisotropy were constructed using two arrays—$AB/2 = 12.5$ m and $AB/2 = 80.0$ m. The short array gives information for the first 10 m, the long array—for a depth of about 50 m below the surface. There is a clear coincidence of the long axes of the electrical anisotropy with the horizontal projections of the σ_1 axes of the two reconstructed tectonic stress fields (Table 2.4, diagrams *E*2 *a* and *E*2 *b*). The limestones are from the Triassic Carbonate Complex (T_2) and as a whole they are mostly affected by the Late Cimmerian Tectonic Phase. The main tectonic faults of the area strike NW–SE, likewise the axis of the anisotropy for array $AB/2 = 80.0$ m.

Table 2.4 Reconstruction of the sequence of tectonic impact on the rocks of Lakatnik Karst Region

Origin	Site №	Late Cimmerian	Pyrenean	Neotectonic and recent	Method
T_2 **limestones**	E2 (azimuthal measurements)	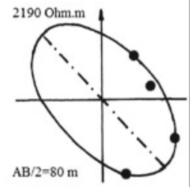 a	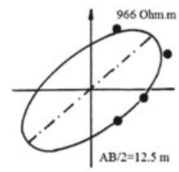 b		Electrical anisotropy
T_2 **limestones**	I	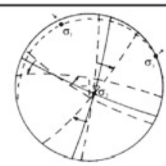 a	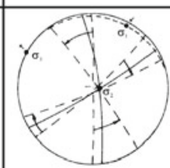 b		Shear joints
T_2 **Limestones**	II		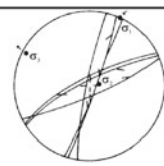		Striations on slickensides
T_2 **limestones** Temnata Dupka Cave	N 43.0895⁰ E 23.3831⁰			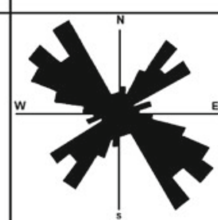	Cumulative length of the cave galleries

Better expressed is the eccentricity of the ellipse of electrical anisotropy near the surface. At site No. *E*2, the most intensive karstification is determined for the first 10–15 m. It is well seen, that the long axis of the anisotropy for $AB/2 = 12.5$ m is oriented NE–SW and it can be interpreted as reflection of the compression during the Pyrenean Tectonic Phase, realized through a number of thrusts (see Fig. 2.34), and creating conditions for opening of fractures along the same direction, and consequently their erosion and karst formation.

The conclusions about the reconstructed stress fields and the origin of the karst system are:

1. The first tectonic deformation of the whole Triassic carbonate rock complex is probably related to forces causing the overthrusting movements along the longitudinal faults of Milanovo Karst Basin (diagram *Ia* on Table 2.4). Following the studies of Tronkov (1965) it can be accepted that the deformations were a result of the Late Cimmerian Tectonic Phase at the end of the Jurassic period. It coincides with the tectonic stress field of the same age, reconstructed northward in Vratsa Karst Region (see Table 2.3, site No. 5). Conditions for opening of NW oriented fractures were created. But this is not related to the initial time of draining

of the ground waters and the formation of the NW-SE branch of the karst galleries of Temnata Dupka Cave (Table 2.4). This direction is even contemporary active and this fact suggests a coincidence of today stress axes orientations with these at the end of the Jurassic.

The inferred age of initiation of the karst formation process is 4.5 MA, i.e., from the beginning of the Pliocene (Angelova et al. 1999), and it was probably facilitated by the fractures created or reactivated during the next stage of deformations.

2. The second stage of deformation created a new system of shear joints (diagram I *b* on Table 2.4), but some of the older joint surfaces were also translators of the block movements. The striations on the slickensides confirm the existence of this tectonic stress field (diagram II on Table 2.4). This stress field favored the opening of the northeastwards striking shear joints of the older deformation stage (see diagram I *a* on Table 2.4) and their transformation in fissures. The regional studies (Chanov 1988) have given reasons for the impact of the Pyrenean Tectonic Phase on this process, as it was discussed above for the specific features of Vratsa Karst Region. It can be accepted that the same regional tectonic stress conditions had remained from the Oligocene to the Pliocene Epoch, when the process of karst formation started. The northeast–southwest directed galleries of the Temnata Dupka Cave reflect exactly this situation (Table 2.4).

Iskrets-Gubesh Karst Region (I-G)

Iskrets-Gubesh Karst Region (I-G) is the third area of Western Balkan Mountain where the geodynamic processes have a direct impact on the evolution of the karst system (Fig. 2.29). The studies, related to the karst tectonics of the area (Paskalev et al. 1992) and to the impact of the blasts from the local quarries on the discharge of Iskrets karst springs (Shanov et al. 2001; Shanov and Benderev 2005) supplied the necessary data for understanding the close relationship between the local tectonics, the tectonic stress fields and the karst features of the region.

During the twentieth century, the springs dried up several times. After Vranchea Earthquake from 1977 ($M = 7.2$) at a distance of about 400 km from the site, the discharge rate dropped down from 5.5 to 0.5 m^3/s during 7.5 h (Paskalev et al. 1992). Later, the discharge rate raised abruptly to 13.5 m^3/s, and began to decrease gradually (Fig. 2.36). Similar event happened during the local Svoge Earthquake of 1979, as well as on the April 11, 1982, when any significant earthquake was not recorded at the localities, nor in the whole Balkan Region.

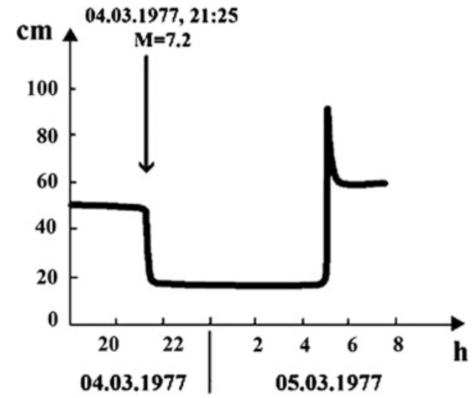

Fig. 2.36 Changes of the discharge rate of Iskrets Karst Springs after Vrancea Earthquake of 04.03.1977, M = 7.2 (Paskalev et al. 1992—Reproduced by permission of *Bulletin of Bulgarian Geological Society*)

The question for the seismic impact is of importance for the local authorities because of the significance of the springs as a major source of fresh water for the municipality of the town of Svoge. The normally used quantities are of the rate of 150 l/s. The impact from the blasts in the quarries has not the potential to disturb the normal discharge of the springs (Shanov et al. 2001; Shanov and Benderev 2005). The only factor for such disturbances can be the local tectonics and the dynamics of the processes inside the karst system.

Iskrets Karst Springs have a very variable discharge—from 280 to more than 50,000 l/s (Benderev 1989). They drained more than 80 % of the territory of Ponor Mountain (a part of Western Balkan Mountain). The springs are related to the karst system of the upper part of the Triassic Aquifer of Iskar Carbonate Group. The atmospheric precipitations on the feeding area of the springs (about 140 km^2) provide the principal quantities of water—62 % of the average annual discharge of the springs. Geological, tectonic and geomorphological conditions predestine the existence of water saturated zone north of the springs. The underground lake surface inside the neighboring Dushnika Cave has a level at 2 m above the springs' level (Fig. 2.37). The level of the

Fig. 2.37 View of the entrance of Dushnika Cave

underground lake can rise abruptly even to 13 m after intensive atmospheric precipitations and snow melting. In this case, a river appears from the lower entrance of the cave.

Geological Background

Triassic and Jurassic autochthonous sediments crop out in the area of Iskrets Karst Springs (Fig. 2.38). These rocks represent a part of the northern limb of Izdremets-Gubesh syncline. To the north of the village of Breze, it is cut by a number of E–W oriented faults. An important tectonic role is attributed to the N–S trending Ejdan-Breze normal fault (Fig. 2.38). Practically, the structures in the autochthonous sediments are controlling the underground water streams.

Svoge Allochtone is a structure built of the two regional Breze and Iskrets overthrusts. In the area of Iskrets Karst Spring, the Breze overthrust covers the sediments of the autochthone. The overthrust represents a complicated structure, including a number of overthrusted imbrications (Fig. 2.38). The plane of thrusting is almost sub-horizontal, and only its frontal part is inclined southward. The overthrust is composed of Triassic and Jurassic sediments.

Iskrets Overthrust is the most important allochthonous structure in the area. It covers and is younger than Breze Overthrust. It is built of Ordovician rocks. Folds and faults were formed in its frontal part.

The most important faults are (Fig. 2.38):

Topilia Faults. They are two subparallel faults situated northwards of the village of Breze, strike N 100–110°. The southern one is well seen in the morphology, the northern one is displacing Quaternary blockages, and this could be a reason to suppose their recent activity.

Sulio Fault is a normal fault striking N 130–140°. It continues to the east, outside the studied area. The southern block is subsided.

Ejdan-Breze Fault is a normal fault with right-lateral component of the movements. The horizontal displacement is evaluated at 250 m, while the vertical one is 40–55 m. The western block is subsided. The interpretation is (according to Paskalev et al. 1992) that the right-lateral movements appeared first and lately, during the Illyrian Tectonic Phase, the vertical displacement occurred. The fault is not displacing Topilia Faults and other northwards located faults, but it disturbs the structures of the overthrusted imbrications.

Tchernovodene Fault is one of the important tectonic structures near Iskrets Karst Springs. Its northern block is built of Babino Formation (Upper Anisian), Milanovo Formation (Ladinian) and Rusinovdel Formation (Ladinian—Middle Carnian), and the southern block is composed of the sediments of Opletnia Member (Lower-Upper Anisian). The performed

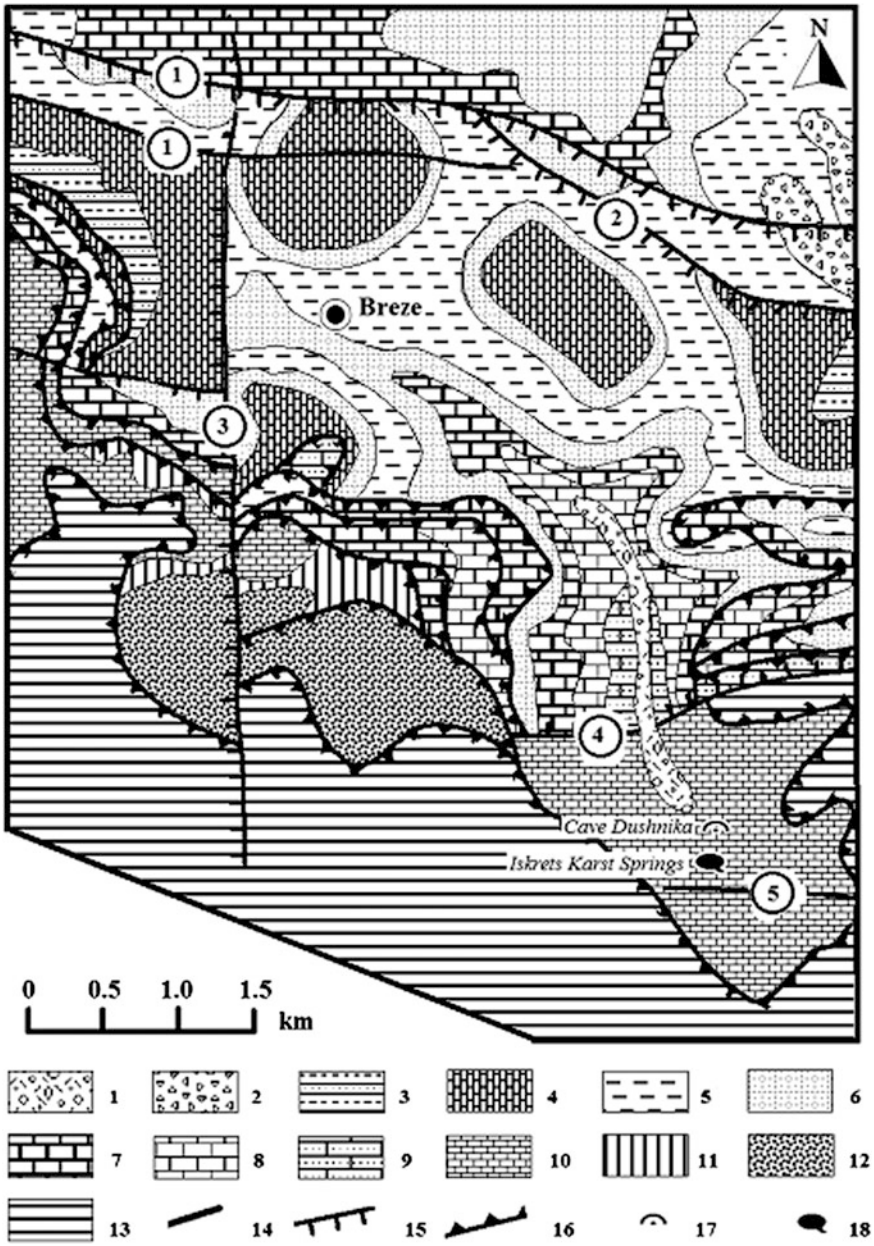

Fig. 2.38 Geological map of the area of Iskrets Karst Springs (according to Paskalev et al. 1992—Reproduced by permission of *Bulletin of Bulgarian Geological Society*) *1*—Quaternary alluvium (gravel and sands); *2*—Quaternary colluvium (rubbles); *3*—Lower Cretaceous (Salash formation); *4*—Tithonian-Berriasian (Glojene formation); *5*—Lower-Middle Bajocian (Etropole Formation); *6*—Sinemurian (Ozirovo formation); *7*—Hettangian (Kostino formation); *8*—Ladinian (Milanovo formation); *9*—*Upper* Anisian (Babino Formation); *10*—Anisian (Lakatnik Member); *11* —*Middle* Anisian (Opletnia Member); *12*—*Lower* Triassic (Petrohan Terrigenous Group); *13*—Ordovician (Grohoten formation); *14*—fault with unknown movements of the blocks; *15*—normal fault; *16*—overthrust; *17*—Cave Dushnika; *18*—Iskrets Karst springs; Faults: (*1*) Topilia faults; (2) Sulio fault; (*3*) Ejdan-Breze fault; (*4*) Tchernovodene fault; (*5*) Dushnika fault

geophysical studies have shown that the northern block subsided (Paskalev et al. 1992).

Dushnika Fault. It cuts the sediments of Opletnia Member, to the south of Iskrets Karst Springs. The advance of Iskrets Overthrust toward north created conditions for activation of the fault as inverse structure, and probably it created conditions for barraging the underground water flow and the formation of the springs.

Tectonic Stress Fields Reconstructions and Directions of the Karst Galleries

Two methods were applied for the analysis of the tectonic stress fields—Nikolaev's Method (Nikolaev 1977) based on the dispersion of the shear joints density and studies of the electrical anisotropy.

The shear joints analyses are based on data from three sites in the vicinity of the karst springs and Dushnika Cave (Fig. 2.39). The reconstructions gave

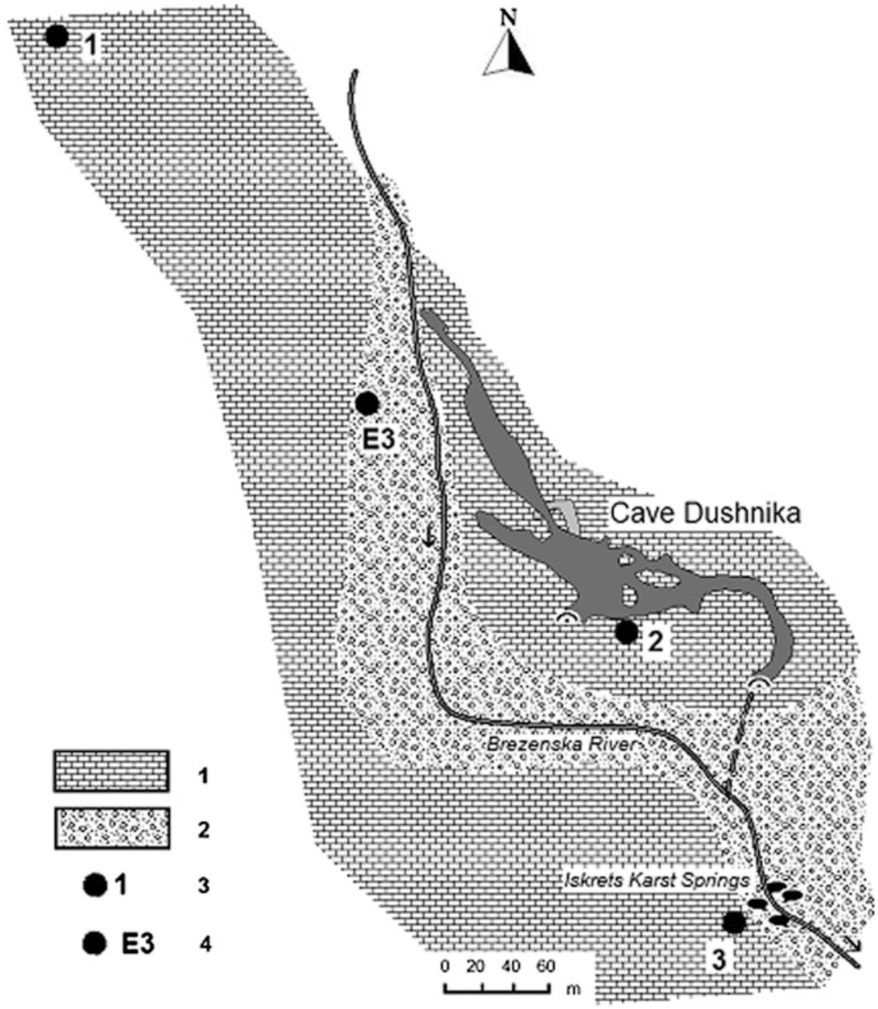

Fig. 2.39 Situation at the vicinity of Dushnika Cave with a scheme of the cave and the sites of performed studies *1*—Limestones of Opletnia Member (*Lower–Upper* Anisian); *2*—Quaternary sediments (mainly alluvial); *3*—Site of measurements of shear joints; *4*—Site of performed electrical anisotropy studies

similar solutions for all sites. The summarized diagrams using 110 measurements from the sites represent the statistically most stable solution. Two distinct tectonic impacts have been inferred that created two preferential directions of open fractures in the limestones of Opletnia Member. These two directions have the same orientations as shown for Vratsa and Lakatnik karst regions—NW–SE and NE–SW (Table 2.5). The first one is controlling these galleries of Dushnika Cave that are now active, the second is more or less coinciding with the orientation of the entrance part of the cave.

If so, the first tectonic deformation is the same that impacted the Triassic carbonate rocks in Western Balkan Mountain, and it is accepted to be a result of the Late Cimmerian Tectonic Phase at the end of the Jurassic period. Conditions for opening of NW fractures were created. These fractures obviously control the NW-SE branch of the karst galleries (Table 2.5).

The second reconstructed stress field favored the opening of the northeastwards striking fissures. The regional studies and the presented above interpretations for Vratsa and Lakatnik karst regions have demonstrated that the resulting deformations, most probably, reflect the impact of the Pyrenean Tectonic Phase, and that the same regional tectonic stress conditions had remained from the Oligocene to the Pliocene. The NE–SW oriented galleries of Dushnika Cave reflect one more time this situation (Table 2.5). The ellipse of the electrical anisotropy for the first 15 m from the surface ($AB/2 = 30$) has its long axis oriented exactly in this direction. The fault-plane solution for the nearest earthquake of 09.03.1980,

Table 2.5 Reconstruction of the sequence of tectonic impact on the rocks of Iskrets-Gubesh Karst Region

Origin	Site №	Late Cimmerian	Sub-Hercinian	Pyrenean	Neotectonic and recent	Method
Earthquake 09.03.1980 M=4.4 N 42.95^0 E 23.35^0					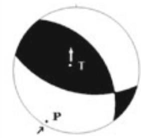	Fault - plane solution
T_2 limestones	E3 (azimuthal measurements)		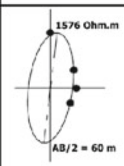 a	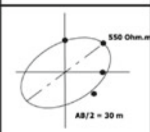 b		Electrical anisotropy
T_2 limestones	1, 2 and 3	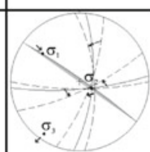 a		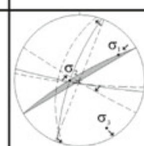 b		Shear joints
T_2 limestones Dushnika Cave	N 43.0895^0 E 23.2356^0				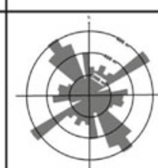	Cumulative length of the cave galleries

$M = 4.4$ (Table 2.5) gives also reason to postulate that the general orientation of the tectonic stress field has been not changed drastically since the deformational processes during the Pyrenean Tectonic Phase till now.

The orientation of the long axis of the electrical anisotropy at N 5° for depths of about 30 m ($AB/2 = 60$ m) has not any response on the diagram of the karst galleries (Table 2.5). But for Vratsa Karst Region the same orientation was detected in the Lower Cretaceous limestones and it was attributed to the Sub-Hercinian Tectonic Phase (end of Turonian time). In the studied area in the vicinity of Dushnika Cave we can only suppose that this orientation is due to the satellite fractures related to the well expressed N–S striking *Ejdan-Breze Fault*, reflected also in the morphology of the terrain as factor for the local N–S orientation of the valley of Breze River.

The cause for interruption of the underground water flow during strong seismic events is probably related to tectonic deformation or rock collapses with temporary formation of barrages inside the unknown parts of the Cave Dushnika northward of the Iskrets Karst Springs, especially in the area of Chernovodene Fault (Fig. 2.38). The existence of unknown large underground spaces has been proved by geophysical studies to the north of the known parts of the cave (Paskalev et al. 1992).

2.3.2.2 Central Balkan Area: Karlukovo Karst Region

One of the most spectacular karst areas on the territory of Bulgaria is Karlukovo Karst Region (KAR). It is located in the Central Balkan, in the morphological structure named Central Fore Balkan (Fig. 2.29). It is known especially for the cave with the spectacular

Fig. 2.40 Remote view to the entrance of Prohodna Cave, Karlukovo Karst Region, Central Balkan, Bulgaria

highest cave entrance in Bulgaria (42.5 m) of Prohodna Cave (Fig. 2.40), as well as for the multiple vertical and horizontal caves in the area.

Geological Background

Karlukovo Karst Region is situated in Lukovit Syncline. This is a well-expressed asymmetric structure in the northern part of the Fore Balkan, affecting carbonate sediments of Campanian, Maastrichtian and Paleocene age, and complicated by fold and faults (Karagjuleva 1971). The area of direct interest is situated northwards of the village of Karlukovo (Fig. 2.41). Dominant sediments are the limestones of Kailaka Formation—Late Maastrichtian; they build the westernmost part of Lukovit Syncline. Aptian and Albian sediments of Roman Formation (sands and marls) occur southward.

Maastrichtian limestones are highly fractured and karstified. This fact and the canyon type erosional incisions suggest relatively young tectonic activity, closely related to the karst processes. The faults, crossing the area of interest, are not well recognized geologically. The geophysical works during 1985–1986 (electrical profiling and WLF profiling—personal unpublished data of S. Shanov) discovered the existence of a covered fault, controlling the karst in the area.

The most significant results from the performed geophysical works were:

- It was proven that a significant fault exists, named Karlukovo Fault, striking NW–SE. The fault is natural westwards prolongation of the regional Brestnik-Preslav Flexure (Fig. 2.41);
- The fault is dividing the less karstified limestones to the north from intensively karstified limestones of the southern block. All important karst caves are located directly south of the fault;
- Karlukovo Fault offers an explanation of the hydrogeological features of the area, including the karst springs;
- New unknown karst cavities were predicted to the south of Karlukovo Fault and after a long period of exploration of Bankovitsa Cave, the speleologists discovered in 2008 new galleries with an underground river. These galleries coincide with the geophysical anomalies and their trend corresponds to the reconstructed preferred directions of the open fissures when analyzing the tectonic stress fields.

The scheme in Fig. 2.42 shows the main sites of the performed structural and geophysical studies, as well as the maps of the caves.

Tectonic Stress Fields Reconstructions

As in the above-discussed case studies, two methods were applied to analyze the tectonic stress fields—Nikolaev's Method (1977), based on the dispersion of shear joints density, and studies of the electrical anisotropy.

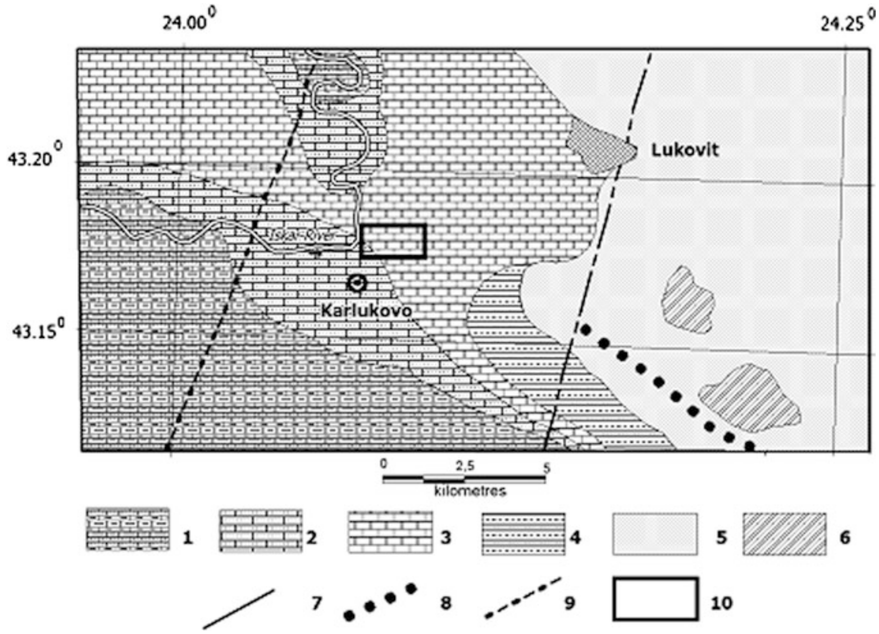

Fig. 2.41 Geological map of the region of Karlukovo Village. *1*—Roman formation rmK_1^{a-al} (sandstones and marls); *2*—Terrigenous-carbonate formation $14K_2^{cn-m}$; *3*—Kailaka formation kK_2^m (limestones); *4*—sandstones, siltstones, clays and marls $13Pg_2$; *5*—Ugarchin formation $ugPg_2$ (sandstones, clays, marls and siltstones); *6*—Opanets formation opN_1^b (clays and limestones); *7*—fault covered by younger sediments; *8*—flexure; *9*—fault line according to gravimetric data; *10*—studied territory

The summarized data on the shear joints from sites 1, 2, and 3 (302 measurements) were statistically processed and as a result two tectonic stress fields were reconstructed that had affected the Maastrichtian limestones (Fig. 2.42, diagrams *A* and *B*).

The first stress field is characterized by sub-horizontal maximum compression in NW–SE direction, while the minimum tectonic stress axis is also sub-horizontal and NE–SW oriented. This situation is favorable for opening of fissures dipping 75° northeastwards (strike N 115°). The strike is more or less coinciding with the general direction of Karlukovo Fault.

In the second stress field, σ_1 and σ_3 are also sub-horizontal, but the compression is NE–SW directed, whereas the minimum stress axis strikes NW–SE. In this case the fractures striking N 18° and dipping 80° are optimally oriented for opening and karstification.

These two fields have impacted the limestones during the Late Alpine Tectonic Phase when the main structures of the Balkan Montain were formed (45 Ma ago). The local tectonic stress conditions provoked the formation of Karlukovo Fault and the relative uplift of its southern block. The initial conditions for karst formation were created and they were more active in the southern block being exposed to more intensive denudation.

Later, probably during Neotectonic time, the general N–S compression created conditions for development of NNE–SSW fissures. The process was relatively fast and lead to the formation of canyon type valleys in the southern block, at some sites cutting the older karst forms. During Neotectonic time, the total uplift of the area is evaluated at about 300 m (Vrablianski 1974).

Studies of the electrical anisotropy were performed at three sites (Fig. 2.42) with array $AB/2 = 30$ m. Site KE 1 and KE 3 have similar solutions and the long axes of the electrical anisotropy ellipses are more or less corresponding to the strike of Karlukovo Fault, i.e., they reflect the first tectonic stress field. Site KE 2 is practically inside the fault zone, it has different orientation of the anisotropy axis, corresponding exactly to the second reconstructed stress field. The possible interpretation is that it reflects superimposed deformations of the trend of Karlukovo Fault leading to its sinusoidal curvature.

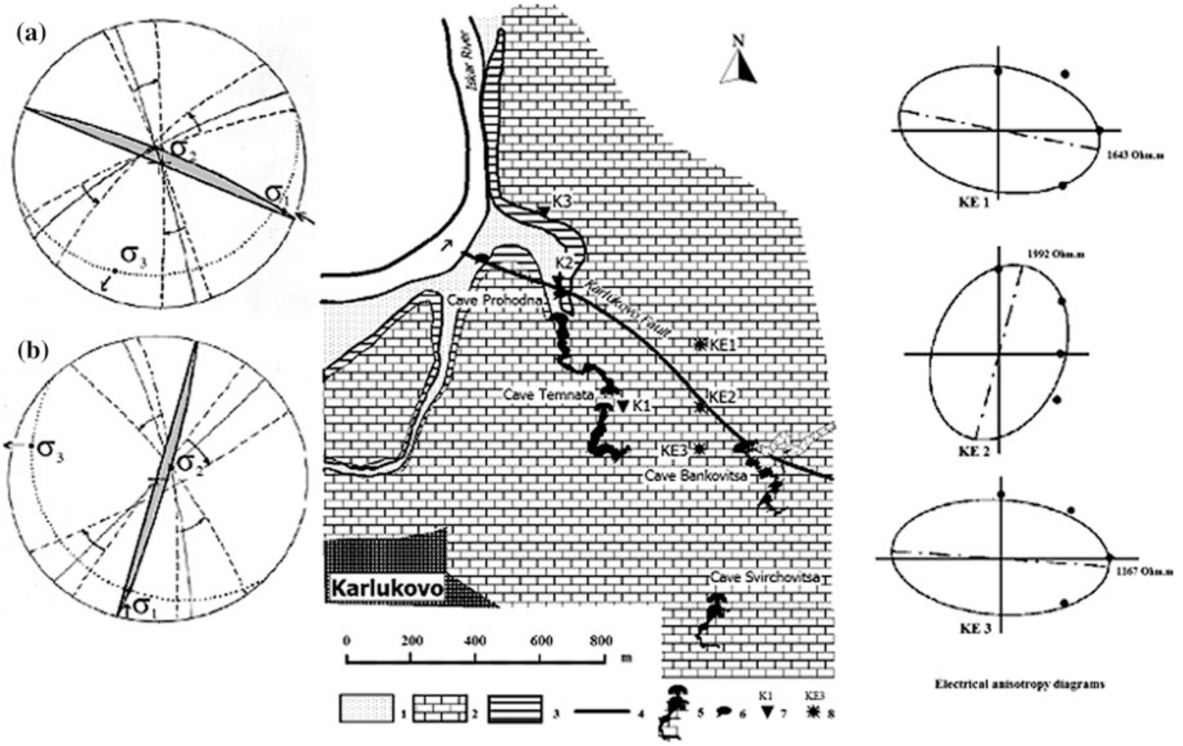

Fig. 2.42 Scheme of the studied territory NE of the village of Karlukovo with diagrams from the studied sites *1*—Quaternary deposits; *2*—Maastrichtian limestones; *3*—rock slope (canyon type); *4*—fault; *5*—cave entrance and horizontal projection of the galleries; *6*—karst springs; *7*—site of measuring of shear joints; *8*—site of study of the electrical anisotropy

Looking on the maps of the caves in the area (Fig. 2.42) it is clear, that the tendency of the cave galleries is to follow one of the preferential directions of open fractures, created by the principal tectonic impacts on the Maastrichtian limestones.

2.3.2.3 Intermediate Zone—Bosnek Karst Region

The karst system in Triassic limestones near the village of Bosnek (Southwestern Bulgaria) contains the longest Bulgarian cave - Duhlata (more than 17 km of total length of the galleries). Bosnek karst Region (BOS—Fig. 2.29), from tectonic point of view, belongs to Golo Burdo thrust unit (Jelev 1982; Gochev 1983; Zagorchev et al. 1994). Important structural and geophysical studies were done in this area for understanding the tectonic control on the karst formation and to explain better the hydrogeological features of the area (Benderev and Shanov, 1997; Shanov et al. 2001; Mihailova et al. 2006). Results from these studies will be analyzed and discussed below.

Geological Background

The karst-rock complex consists of Triassic carbonate rocks (Fig. 2.43). They overlie red sandstones, conglomerates and siltstones. The siltstones were transformed into quartzite at the contact zone of Vitosha pluton. The carbonate rocks cover an area of 23 km^2 and are about 200 m thick. Thick packages (about 50 m) of argillite and siltstone divide the carbonate rocks, playing the role of local aquicludes. The beds situated below these packages consist of limestone, and over them—of dolomite. Jurassic and Cretaceous rocks locally occur in the NE part of the area. A set of faults of different age of formation and activation has complicated the tectonic structure of the area, and in some cases, these faults control the relief, as well as the features of the karst system. The relief is typically mountainous—about 800 masl near the dam lake of Studena and up to 1,400 m in the NE part. The waters of Struma river principally, and also from other smaller rivers in the area, are the main factor for the karstification. The river loses its flow in the area of the contact between sandstone and carbonate rocks, as

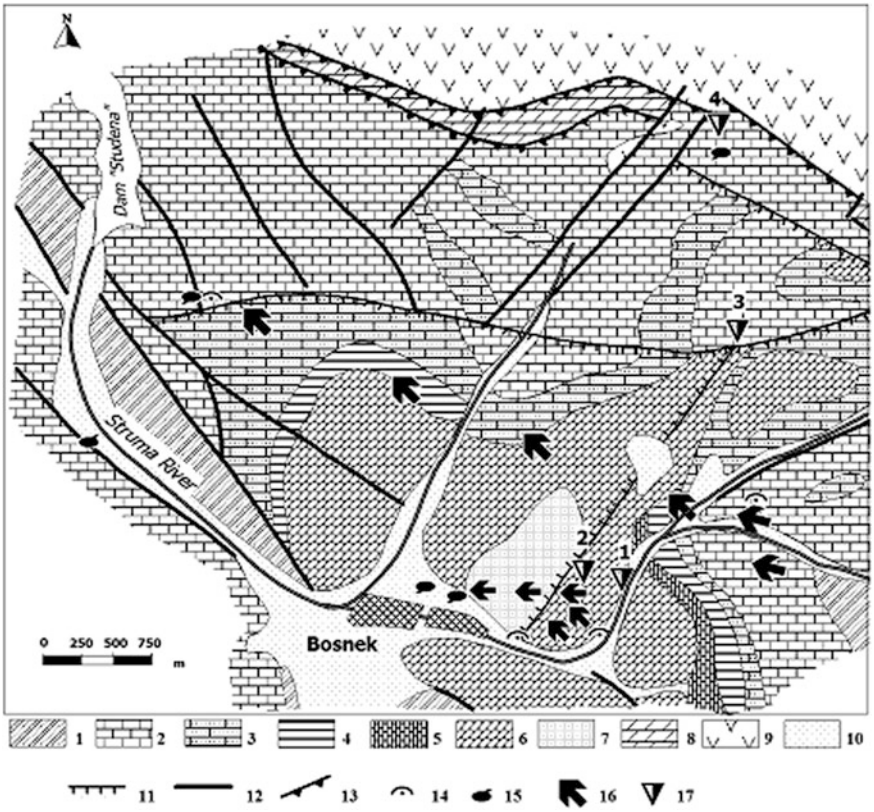

Fig. 2.43 Scheme of geological, tectonic and hydrogeological features of Bosnek Karst Region (after Benderev and Shanov 1997) *1*—Lower Triassic sandstones (T_1); *2*—Anisian limestones (T_2^a); *3*—Ladinian dolomites (T_2^l); *4*—Ladinian shales (T_2^l); *5*—Carnian limestones (T_3^k); *6*—Dolomites (Carnian-Norian—T_3^{k-n}); *7*—Limestones (Carnian-Norian—T_3^{k-n}); *8*—Siltstones and marls (Tithonian—J_3); *9*—Senonian volcanic rocks of Vitosha Mountain (K_2^s); *10*—Quaternary sediments; *11*—fault; *12*—normal fault; *13*—thrust; *14*—cave entrance; *15*—karst spring; *16*—principal direction of underground water flow; *17*—site of investigations of the rock fracturing

well as at the zones of the faults inter-crossing eastof the village of Bosnek. Two karst springs, situated in the northern part of Bosnek, disgorge their water again into the river of Struma (Fig. 2.43).

Exactly between the places of water losses and the springs near the village of Bosnek, the longest cave in Bulgaria named Duhlata is situated, with total galleries length over 17 km. Our studies on the tectonic stress fields and their impact on the hydrogeological peculiarities of the area (Benderev and Shanov 1997) have shown that tectonic stress fields created during the geological history systems of fractures, controlling the underground waters in the processes of karst formation.

The boundaries of Triassic carbonate complexes, are commonly tectonic that is predestined by the structural position of the discussed area. Orogenic processes and the related karst evolution are controlled by Pernik Fault Zone (Bonchev 1961, 1971; Kostadinov 1965; Matova and Angelova 1994) during Quaternary. Most of the faults crossing the area are practically segments of this zone with general strike NW–SE. Tectonic processes caused macro- and micro-block differential movements and fracturing of the rocks, leading to the formation of the contemporary valley of Struma River, as well as dividing the underground catchment, basins and formation of cave systems (Benderev and Shanov 1997). The processes of present day tectonic activity continue, and this is reflected by the swarm of seismic activity at 20 km northwestwards of the region during 2012 (Radulov et al. 2012), the strongest earthquake being of magnitude $M = 5.4$.

Karst Evolution

The investigated area was a part of Pernik basin during the Paleogene and was filled with sediments of

Middle Oligocene—Lower Miocene age. Probably, the Jurassic and Triassic sediments were overthrusted over Vitosha Pluton during Post-Oligocene time. Conditions were created for typical allogenous karst formation in a complex geologic-tectonic setting.

During the Pliocene-Pleistocene, as a result of the activation of orogenic processes, the morphological units around Bosnek Karst Region were shaped (Matova and Angelova 1994). The initial tectonic impulse was not so strong and for that reason the Struma River keeps its outflow direction toward west. Both the relicts of this old river valley and the accompanying them alluvial deposits could be seen SE of Bosnek Village.

The Quaternary stage begins with a change in the intensity of tectonic processes. As a result of repeated movements and subsequent vertical tectonic deformations, the rock complexes affected by karstification were exposed on the surface and the formation of an underground karst complex started. The valley and karst complex development are considered as related to the changes of the character of the tectonic movements, phases of the glacial epoch, lithostructural features and Quaternary tectonic activity. During the Upper Pleistocene, segments of Pernik Fault Zone were activated. The NW-SE trending faults of Bosnek Karst region belong to this fault zone. As a result of this process, two separate areas are formed in Bosnek Karst Region. The tendency of regional uplift and river incision continued after the Middle Pleistocene. The karst processes from the Pleistocene up to now are determined by Struma River, being simultaneously a rivershed and a drainage system (Benderev and Angelova 1999). The faster block uplifting of Vitosha Mountain led to the formation of a steep slope of Struma River valley and consequently the river water begun to flow underground in the zones of carbonate rocks.

The alternation of active uplift and relatively low tectonic activity led to formation of different levels of galleries, some of them even under the contemporary river valley. As a fact proving the presence of different stages in the karst development, mainly the structure of Duhlata Cave system should be considered where the cave galleries are much longer and where seven horizontal levels could be clearly delimited. These levels and their number correlate closely with river terrace fragments found on the valley slopes (Benderev and Angelova 1999). The oldest and hypsometrically highest galleries could be considered as the most upper and oldest way of underground water flow that corresponds to the planation during the Pliocene-Pleistocene time. Thus, the age of that process could be accepted as a beginning of a more intensive karstification of the whole Bosnek Karst Region. As a result, a complex multi-leveled labyrinth cave with a basic underground stream and a few small tributaries has been created. The process of the cave morphogenesis continues up to present days.

Tectonic Stress Fields Reconstructions

The reconstructions of the tectonic stress fields were made using the statistical approach for analyzing the conjugated shear joint systems, the kinematics of the deformations along faults discovered in Duhlata Cave (well-preserved striations on slickensides), and the fault-plane solutions for some local earthquakes. The studied sites are outcrops of limestones, as well as inside the Duhlata Cave (Fig. 2.44). Initially, two expressed tectonic stress fields have been reconstructed (Table 2.6).

The older stress field is determined to be from Post-Oligocene time (Benderev and Shanov 1997). This stress field reflects the tectonic phase of trusting of the Mesozoic rock complexes over the volcanic rocks of Cretaceous age of Vitosha Pluton. The studies in the cave discovered one older tectonic stress field. The orientation of the minimum tectonic stress axis σ_3 is subvertical whereas the maximum tectonic stress axis is sub-horizontal, and this is a clear indication for trusting regime of the deformations.

The inferred second tectonic stress field is of Pliocene-Quaternary age. The tectonic compression was directed NW–SE and the active sub-horizontal NE–SW tectonic extension created possibilities for opening of the NW–SE fractures and their karstification. The logical consequence was that the karst galleries and the way of the underground waters have the same general direction (Fig. 2.43). Namely this deformation is reflected in the movements along fault No. 2 in Fig. 2.44 and the formation of slickensides on the fault surface.

During the works in the cave Duhlata we discovered also the second generation of tectonic striations. They are well preserved in the cave and are probably very young because the clay is remaining on the striations (Fig. 2.45). The solution practically confirms the Pliocene-Quaternary orientation of the

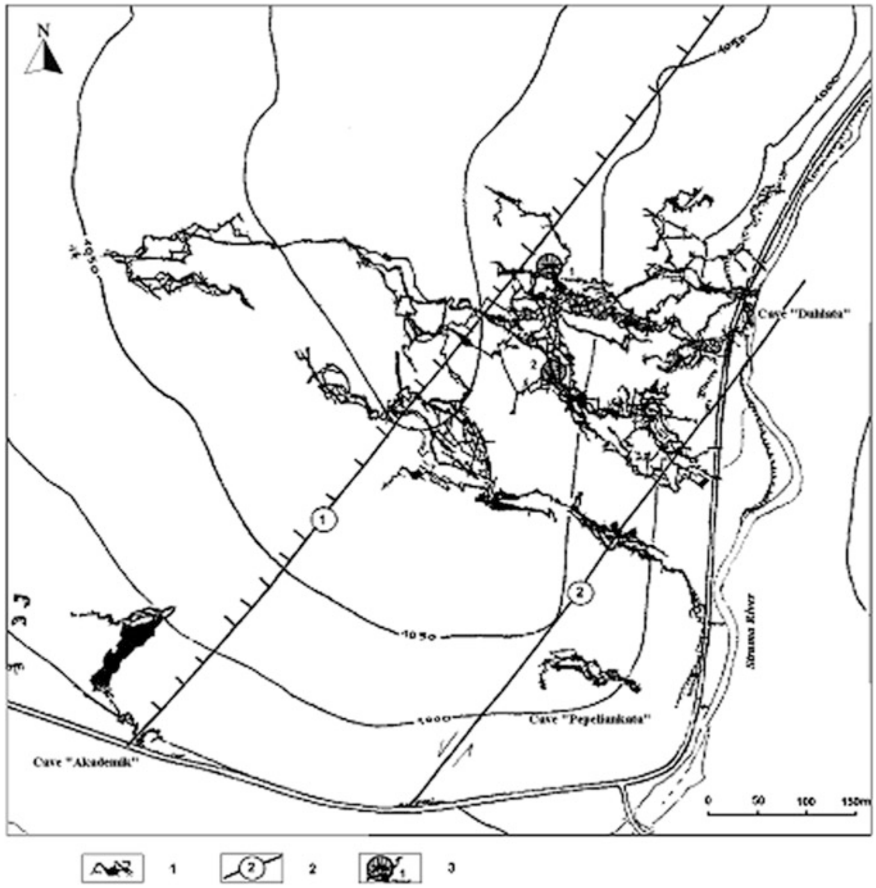

Fig. 2.44 Scheme of the caves in Bosnek Karst Region in the vicinity of Cave Duhlata (based on the scheme from Benderev and Angelova 1999) *1—horizontal projections* of the karst galleries; *2*—fault; *3*—site of investigations inside the Cave Duhlata, Bosnek Karst Region, Bulgaria

Fig. 2.45 Preserved tectonic striations in Cave Duhlata, Bosnek Karst Region, Bulgaria

Table 2.6 Reconstruction of the sequence of tectonic impact on the rocks of Bosnek Karst Region

Origin	Site №	Post-Oligocene	Pliocene-Quaternary	Contemporary	Method
Earthquake 22.05.2012 $M_w = 5.6$ N 43.65^0 E 23.00^0				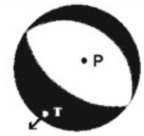	Fault-plane solution
T^{k-n}_3 **dolomites**	1 and 2	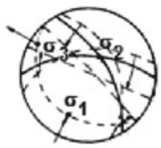			Shear joints
T^{k-n}_3 **dolomites**	1 and 2	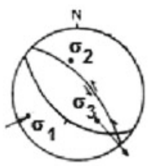	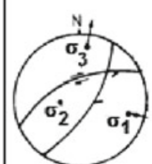		Striations on slickensides
T^a_2 **limestones**	3				Shear joints
T^a_2 **limestones**	4		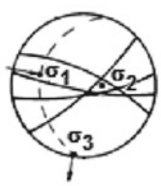		Shear joints and striations on slickensides

tectonic stress axes—sub-horizontal E–W compression and N–S extension.

Due to the fact that some of the older karst forms were cut and displaced, and because of the position of the studied area between two very active seismic zones in this part of the Balkans, we think that the detected traces of young movements can be related to a past seismic event (or events). The nearest reconstructed fault-plane solution from 2012 Pernik Earthquake is supporting the opening of the NW–SE oriented fractures (Table 2.6), which is the general trend of the karst galleries of the caves.

The age of the left-lateral movement along fault No. 2 (Fig. 2.44) is not clear. This fault was known from the geological mapping in scale 1:25,000 only northeastwards from the karstified area. It displaces sediments of Jurassic age. We discovered its extension toward SW and a slickenside with striations, showing also left-lateral displacement. The entrance of Cave Duhlata lies exactly on this fault. The fault is expressed in the relief, it stops the galleries of Pepeliankata Cave, but its impact on the karst systems is not very well expressed.

Clearer control on the karst processes can be found along fault No. 1 (Fig. 2.44). Namely, a subsidence of the NW block is noted in the area inside the cave of Duhlata. In this block the density of the karst galleries is lower and the mapped galleries are active. This fault is also controlling the morphology of the Akademik Cave (Fig. 2.44). One possible reason for the expressed impact of this fault on the karst system could be paleo-earthquake activity. The sudden subsidence of the NW block adjacent to the fault could juxtapose its old galleries to the active ones of the SE block. The younger galleries of the NW block have been filled with clay or other sediments, or are inside the phreatic zone. This assumption is supported by the fresh striations on the fault surface in the cave of Duhlata. There are a lot of broken or inclined stalagmites, but the caves of the region are frequently visited by a number of people and thorough studies have to be made for filtering the naturally from the artificially broken stalagmites.

2.3.3 Cuba: Structural and Geophysical Study of the Karst System of Guaso Plateau (Eastern Cuba)

2.3.3.1 Regional Characteristics

Guaso Plateau is situated 1,000 km southeast of the City of Havana (Republic of Cuba), in the district of Guantanamo, Province Sierra Oriente (Fig. 2.46). The studied region by the Bulgarian-Cuban expedition in 1988 covered a territory of 230 km^2, occupied by tropical forests.

The altitude is between 100 m and 800 m above sea level and the plateau is cut by canyon-like, narrow valleys. This difference in the altitudes creates a situation, where the average annual temperature changes from 20 to 23 °C in the upper part of the plateau to 24–27 °C at its foot. The plateau is a barrier for the humid air from the North, from the Atlantic Ocean. The abundant rains, even during the dry season, form significant surface and underground water flows toward North and only a part of the water runs toward South as underground current inside the 500 m thick layer of Eocene limestones (Formation Charko Redondo). Due to the geographical location of the plateau in the subtropical zone, a seasonal dynamics of the rainfall exists, with 70–76 % of the rains during the humid season (May–October). The water balance, calculated by Cuban hydrogeologists has proved that considerable part of the water is drained to the South, toward the Caribbean Sea, using unknown underground ways. This water is extremely needed for the normal water supply and development of the town of Guantanamo and its vicinities. The main problem of the expedition was the detection of the underground way of the water and to improve the possibility to exploit sufficient quantity of potable water from the karst system. The base for the studies were the topographic maps in scale 1:50,000, the geological map in scale 1:50,000 drown by Hungarian and Cuban geologists, as well as the aerial photos of the region. The results were only partially published (Andreychuk and Benderev 1991; Chanov and Benderev, 1993).

2.3.3.2 Geological and Hydrogeological Background

The rock massif of Guaso Plateau is built mainly of carbonate rocks. The geological sketch of the studied area is shown in Fig. 2.47. The following stratigraphic units are present:

- BUCUEY (BUC)—$K_{1-2}^{\mathrm{al-t}}$—magmatic, metamorphic and volcanic rocks with total thickness more than 500 m. The outcrops are located predominantly in the northern part of the plateau. On some of these sites, a thick weathered soil *(terra rossa)* was formed, containing manganese-iron concretions. On the upper part of the plateau, over the sedimentary rocks, remnants of an allochtonous serpentinite overthrust can be found.
- PICOTA (PIC)—$K_2^{\mathrm{cp}-m}$—conglomerates and breccias with thickness varying between 100 and 150 m.
- CHARCO REDONDO (CHR)—P_2^2—Eocene limestones with thickness from 200 to 500 m. In these rocks intensive processes of karstification formed numerous caves, hollows, abysses, underground rivers and lakes. This formation was the principal target for exploration from the Bulgarian-Cuban expedition during 2 months. The total length of the mapped karst galleries was about 20 km, 8,382 m of them being active galleries with underground river in the longest cave El Campanario. Unfortunately, in

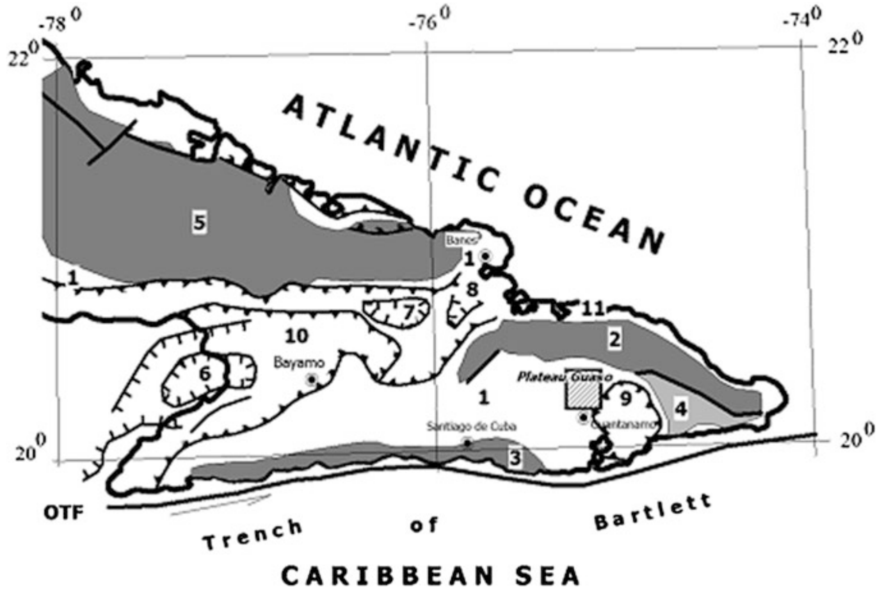

Fig. 2.46 Schema of the principal tectonic units of Eastern Cuba. The studied territory is hatched. *OTF*—North Caribbean (Oriente) Transform Fault *1*—Synclinorium of East Cuba; *2*—Anticlinorium Mayeri-Baracoa; *3*—Anticlinorium of Sierra Maestra; *4*—Horst structure of Sierra del Purlal; *5*—Anticlinorium of Camagüey; *6*—Depression of Guacanayabo; *7*—Depression of Cacocum; *8*—Depression of Nippe; *9*—Depression of Guantanamo; *10*—Depression of Cauto; *11*—Depression of Bahia de Nippe

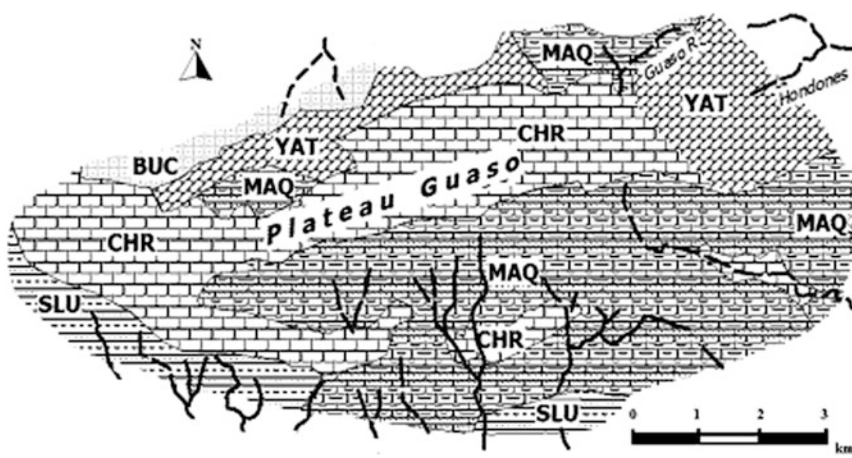

Fig. 2.47 Generalized scheme of lithostratigraphic units in the vicinity of Guaso Plateau (Eastern Cuba) and main temporary and permanent rivers. *Formations*: BUCUEY (*BUC*)—K_{1-2}^{al-t}; CHARCO REDONDO (*CHR*)—P_2^2; SAN LUIS (*SLU*)—P_2^{2-3}; MAQUEY (*MAQ*)—P_3^3—N_1^1; YATERAS (*YAT*)—N_1^{1-2}

the last day of the expedition, all drown maps were confiscated by Cuban military representatives.

- SAN LUIS (SLU)—P_2^{2-3}—Sedimentary formation of clays, marls and thin clayey sand layers. The total thickness of this formation is about 350 m. It covers the plane southwards from Plateau Guaso, overlying the limestones of Charco Redondo Formation.
- MAQUEY (MAQ)—P_3^3—N_1^1—Molasse formation represented by 200 m thick beds of marls, clayey limestones or marls containing thin limestone layers. Everywhere, on the top of the plateau, it covers the limestones of Charco Redondo Formation and its sediments fill up the negative forms of the paleo-relief.

- YATERAS (YAT)—N_1^{1-2}—Organogenic, coral-reef limestones with a thickness not exceeding 50 m. Exotic blocks of this formation can be found in the sediments of Maquey Formation. It is supposed that some surface rivers at the top of Guaso Plateau have lost their waters when reaching the rocks of YAT Formation.
- Quaternary (Q)—Soils with thickness from some centimeters to several meters. At the top of the plateau, there are negative forms with 25 m thick clay layer with rock debris.

The tectonic background (Fig. 2.46) is assumed to be a result of the geodynamic evolution of the Cuban micro-plate at the contact with the oceanic plate—the trench of Bartlett (Lilienberg 1983; Cobeilla 1984; Rojas-Agramonte et al. 2003). This trench predetermines the existence of Oriente fault system (N 80–90°) with expressed sinistral strike-slip movement. It has affected the southern Sierra Maestra mountain range, SE Cuba, and portrays the dynamics and tectonic evolution of the southern Cuban coast in the boundary zone between the Caribbean and North American plates (Rojas-Agramonte et al. 2003). The region has been affected by historical and recent earthquakes. The fault-plane solutions from earthquakes along the trench are in agreement with the dominant ENE-WSW compression established onshore (Rojas-Agramonte et al. 2003). As a result, the faults of the Oriente system have been cut and displaced by a younger system of faults striking N 40–60°.

The hydrometrical studies during the expedition have shown that 1.2 m^3/s of water is drained by the karst system of Guaso Plateau (Chanov and Benderev 1993). The feeding of the karst waters is from infiltration of surface waters, especially in the areas where Charco Redondo and Yateras formations outcrop. Guaso River disappears in a sink-hole near the cave of Sumitero with a discharge of 300 dm^3/s (middle of January, 1988), and reappears as a river from the cave El Campanario with a discharge of 500 dm^3/s (Andreychuk and Benderev 1991). The modulus of the underground stream is approximately 8 dm^3/s km^2. Taking into account the season of the recording, the quantity is the minimal one. After rains the quantity of the water rises considerably because the high permeability of the karst system. As an example, the discharge rate of the river from the cave El Campanario raised to 15–20 m^3/s during 36 h after strong rainfall in January, 1988. Practically, at that time, these considerable quantities of water were not exploited, except these from the Spring Bataldo, used for water supply of local plant for production of sugar, and the river from the cave El Campanario, used by a hydro-electrical power plant.

The performed geological and geophysical investigations have proved that the karst system can be subdivided into two hydrological units. The western part is characterized by a clearly expressed zone of water saturation entirely inside the karst cavities of Charco Redondo Formation. The reason of its formation is the existence of a fault barrier at the foot of Guaso Plateau, where the karstified rocks of CHR contact the clays of SLU Formation. Along this E-W trending border spillways exist, being at the same altitude and with the same chemical composition of the water. According to geophysical data, a karstified layer can be expected southwards of this line, representing a confined aquifer.

The geological conditions in the eastern part of Guaso Plateau are more complicated. MAC Formation is of wide occurrence and is resistant to karstification. The existing large karst negative forms on the surface are filled up with *terra rossa*. These traits and the tectonic faults contribute to the formation of local barriers for the water. Two rivers on the surface gather the waters from the plateau—Guaso and Hondoness Rivers. Hondoness River appears in the northeastern part of the plateau, but at the contact with the limestones of CHR Formation it is flowing down inside the subsurface karst system. Downwards it appears as several springs at the contact between the limestones and the Quaternary sediments.

Guaso River is formed by a number of karst springs on the top of the plateau and after some kilometers disappears in Somitero of Guaso, forming a spectacular underground river, successfully traced by the speleological studies in the caves El Campanario and Somitero. The karst system there has considerable water permeability—more than 100 m^3/s.

The performed geophysical works in 1988, using electrical methods (vertical and azimuthal electrical soundings), permitted detection of karst forms with considerable dimensions, discovered and mapped later by the speleologists. The dimensions of the galleries are 20 m and more in diameter and their tops are only 10–20 m below the surface. These significant dimensions of karst galleries, formed inside relatively

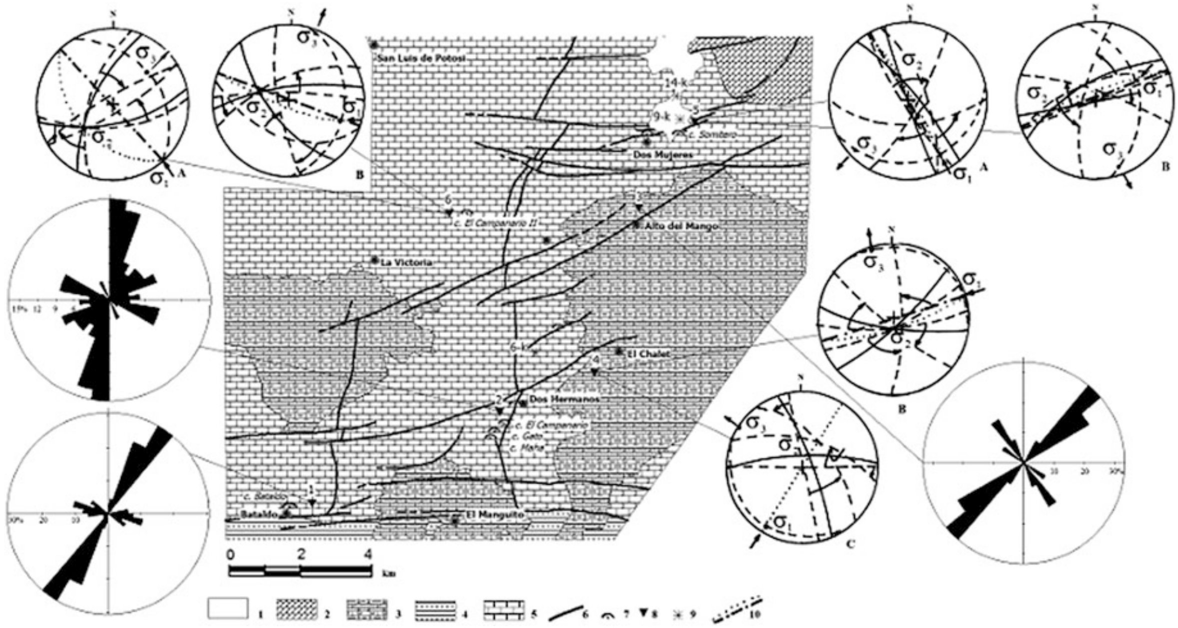

Fig. 2.48 Detailed geological map of the studied territory on Plateau Guaso (Eastern Cuba) and reconstructions of the tectonic stress fields based on measurements of joints (on the base of the map elaborated by K. Bonev) *1*—Quaternary sediments—*Q*; *2*—Formation YAT; *3*—Formation MAQ; *4*—Formation SLU; *5*—Formation CHR; *6*—fault; *7*—cave entrance; *8*—site of structural measurements; *9*—site of studies of the electrical anisotropy; *10*—most probable position of the open fractures on the stereograms

young rocks, are due to the tropical conditions of karst formation and evolution.

2.3.3.3 Tectonic Stress Fields and Their Control on the Karst System

Two methods were applied for the analysis of the tectonic stress fields—Nikolaev's Method (Nikolaev 1977), based on the dispersion of the shear joints density and studies of the electrical anisotropy. Additionally, at three sites only, the directions of few fractures have been measured (number from 10 to 20) and rose-diagrams were plotted in Fig. 2.48—sites 1, 2 and 3. These rose-diagrams reflect normally the strike of the adjacent lineaments and they are not sufficiently informative for reliable geological conclusions.

Quite different, as quality, is the information from the sites of mass measurements of shear joints. It permitted the reconstruction of the tectonic stress fields and the analysis concerning their impact on the karst formation and evolution (Fig. 2.48—sites 4, 5 and 6). The tectonic interpretation of the diagrams of the electrical anisotropy has been made also in the context of the tectonic stress field reconstructions and the scheme of the fault systems drown on the base of remote photos and field verifications (Fig. 2.48).

Sites 5 and 6 characterize fracturing of the limestones of CHR Formation. Two tectonic stress fields are detected in this formation. The first one (*A*) and maybe the oldest for this formation has provoked the opening of fractures with NW–SE direction. The second one (*B*), being of great importance for the recent tectonic situation in the region, determines the existence of sub-equatorial fractures and faults, controlling the step-like subsidence of CHR Formation to the south. This tectonic stress field acted after the consolidation of the sedimentation of MAQ Formation, because it was also reconstructed using the joint set in the marls of this formation (Site 4). The variations in the directions from N 80° to 110° correlate well with the regional faults near the sites of measurement. The sub-equatorial faults are in some places barrier for the karst processes and re-distributor of the water. The commented tectonic stress field coincides with deformation phase *D*1 of N–S extension, exemplified mainly by karst-filled extensional veins and normal faults (Rojas-Agramonte et al. 2003). These authors correlated this deformation with the regional kinematics in the Caribbean realm, imposed by the opening of the Cayman trough and the disruption between Cuba and Hispaniola.

The youngest tectonic stress field was reconstructed only in the marls of MAQ Formation (Site 4—*C*). This tectonic stress field determines the opening of a sub-vertical system of fractures with general direction N 30°. This is also the general direction of the galleries of the largest cave system in the region—El Campanario. It is reflected also by the rose-diagram from Site 3 (Fig. 2.48). At the entrance of El Campanario Cave the rose-diagram of the fracture orientation is mostly coinciding with the strike of the system of faults with orientation favorable for opening under the conditions of stress field C. A number of cave entrances are situated along these faults. Rojas-Agramonte et al. (2003) reconstructed deformation phases *D*2 and *D*3 comprising NE–SW to nearly N–S directed compression.

Sites 6-k, 9-k and 14-k in Fig. 2.48 are the places of azimuthal vertical electrical sounding. The corresponding graphs are plotted on Table 2.7.

The graphs show the general tendencies of the electrical anisotropy on the site of measurements. Sites 6-k and 14-k are informative for the limestones of CHR Formation, while site 9-k is on a large negative karst structure with a tick filling of young, mostly Quaternary sediments.

The ellipses of anisotropy at point 6-k are for depths not exceeding 10 m and their general direction of the long axes N 95° reflects the controlling role on the fracturing of the nearest fault with the same direction. But the site was situated exactly over the known galleries of Campanario Cave and the abrupt changes of the direction of the anisotropy ellipse to azimuths between N 5° and 50° is reflecting the preferential direction of the cave galleries. The situation is similar for point 9-k where a clear coincidence exists between the long axes of the electrical anisotropy ellipses (N 50°) and the detected lineaments with SW-NE direction. The young age of this direction was discussed above and probably it controls the recent karstification. It can be also assumed that this is the direction of a satellite fault to the well expressed regional fault zone of E–W direction.

The E-W direction is well reflected in the ellipses of anisotropy from point 14-k. Even to depth more than 100 m, the direction N 90–95° is so stable that it clearly illustrates the controlling role of the sub-equatorial fault on the karst structures near the falling of Guaso River into the underground karst system.

2.3.4 France: Tectonic Stresses and Their Control on the Karst Formation in Plateau of Vaucluse (Alps Maritimes, France)

Plateau of Vaucluse, framed by Mont Ventoux (1,912 m) from northwest, by the Mountain of Lure (1,826 m) from northeast, and by the geological structure, named Syncline of Apt from the south (Fig. 2.49), is worldwide known with its karst phenomena. Spring Fontaine de Vaucluse is the most impressive karst manifestation in this region (vauclusian type of spring). The 308 m deep abyss is draining the underground waters from the plateau. The coloring test of waters from different places on the plateau or in the caves has shown a relation between the caves and the Spring of Vaucluse (Mudry and Puig 1991). Among a number of publications concerning the karst of this area, a study on the relationship between karst formation and recent tectonics in the context of the tectonic stress fields has been published (Shanov and Cousset 1993). More detailed analyses, including reference on geodetic records, completed these studies (Shanov and Georgiev 2001). The presented analyses follow the principal results from these two publications.

Southeastern France is also an area of earthquake activity and this fact allows for a more complete evaluation of the contemporary tectonic stress field and the related processes in the karst.

2.3.4.1 Geological Background

Plateau of Vaucluse is formed by limestones and marl-limestones of Lower Cretaceous-Hauterivian, Barremian and Bedoulian age, as well as by rocks of the Urgonian reef facies (after Fage 1981). The Provencal tectonic phase at the end of the Eocene has marked the uplift of Plateau of Vaucluse and the beginning of the karst processes in the limestones. The contemporary morphological features were formed during the Post-Pontian tectonic phase, expressed by the overthrusts of Mont Ventoux and of Lure Mountain, when the Provencal tectonic block

Table 2.7 Graphs from the azimuthal studies of the parameters of the electrical resistivity on Plateau Guaso (Cuba)

Site №	Azimuth [N ⁰]	Electrical anisotropy	Eccentricity	Electrical resistivity [Ohm.m]
6-k	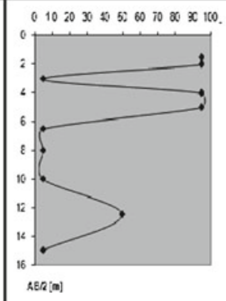	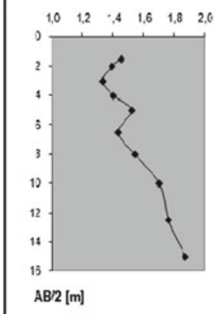	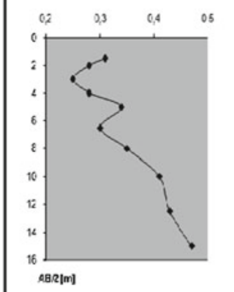	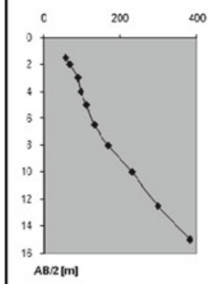
9-k	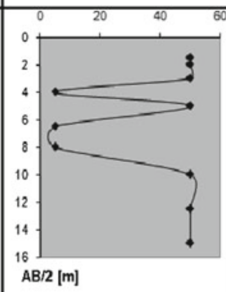	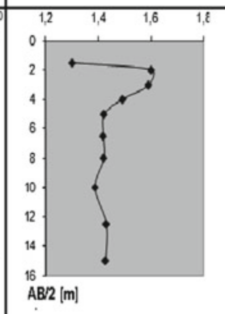	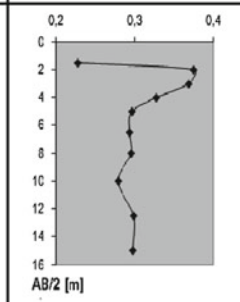	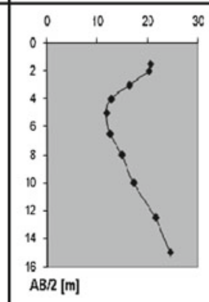
14-k	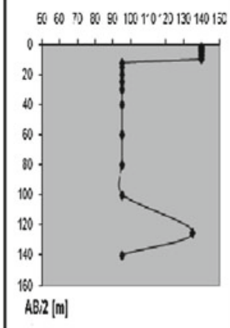	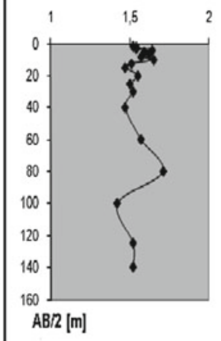	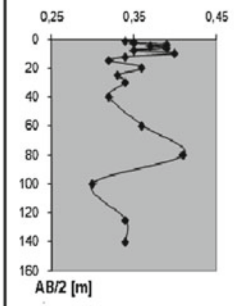	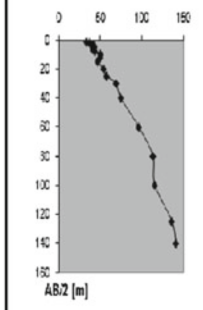

moved toward north. During this period, the NW–SE strike-slip faults formed (Fig. 2.49). The better expressed Post-Burdiganian (end of Oligocene) phase should be noted, when NE–SW striking faults were formed, controlling to a great extend the recent karst evolution in the rock massif.

Analyzing the genesis of Plateau of Vaucluse on the base of the principal forms of surface karst, Depambour and Guedon (2004) discovered recently deformed paleo-surfaces, but they have originated on a regional scale since Post-Miocene time. All intermediate surfaces (alt. 850 m) cut the Miocene deposits (Burdigalien) of Aurel—Sault Depression. This reveals a major phase of Post-Miocene denudation. These surfaces of karstic flattening are assumed to be related to the vast po1jes of the sectors of Saint Christol and Sault. Their genesis, dependent on dysfunctions of the endokarstic drainage, could be related

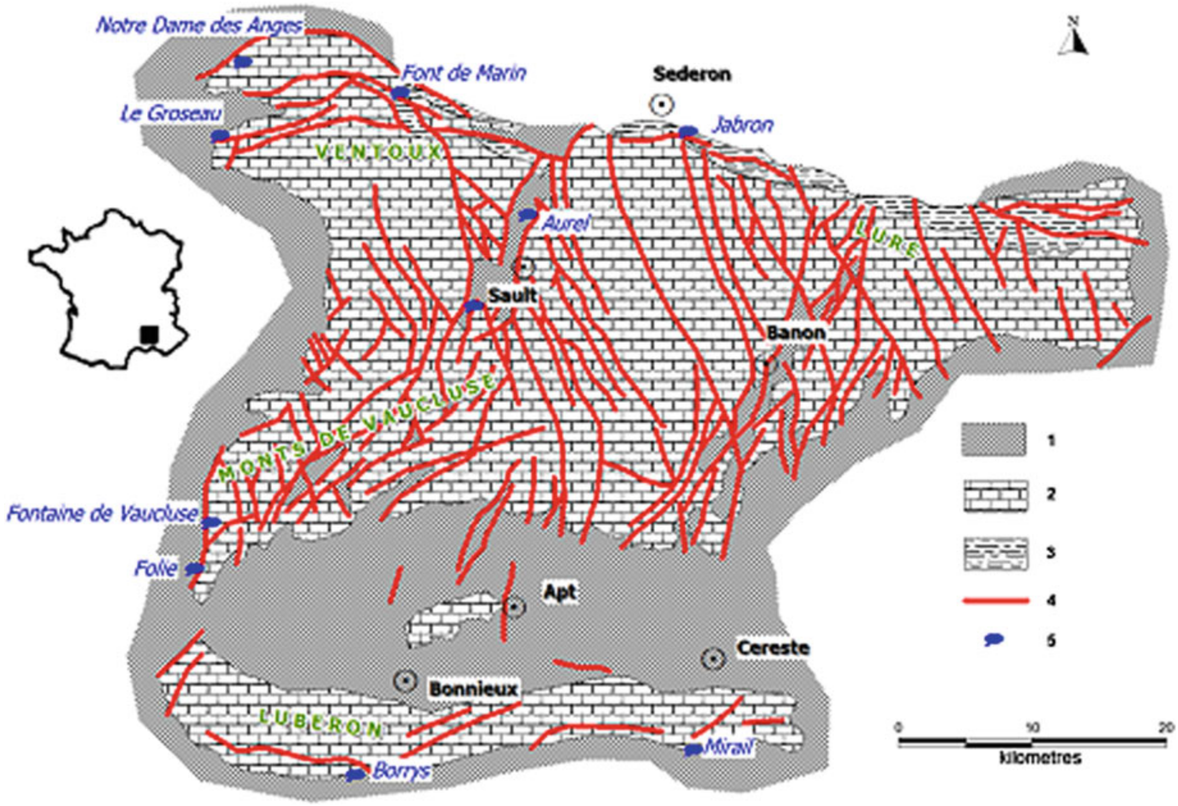

Fig. 2.49 Geological scheme of the region of Vaucluse (after Mudry and Puig 1991) *1*—Bedoulien terrain; *2*—Lower Cretaceous limestones; *3*—Neocomian marls; *4*—fault; 5—spring

to the Pliocene transgression (Depambour and Guedon 2004).

From hydrogeological point of view, the role of the spring of Vaucluse (Fig. 2.50) for the draining of underground waters is well studied (Murdy and Puig 1991). It is necessary to note also that the hydrogeological unit Luberon-Vaucluse continues below the syncline of Cavaillon (Gouvernet et al. 1971) and this was confirmed by the borehole near Chene, 5 km westwards from the town of Apt.

2.3.4.2 Methods of Study

Fracturing

Mass measurements of the space elements of joints (dip direction and dip angle) in different outcrops of the rock massif were done and they provide the basic data for applying the method of Nikolaev (1977) for reconstruction of the main axes of the tectonic stress fields. As shown above, when presenting the different case studies, most convenient for the development of the karst process are these fractures that are perpendicular to the minimum tectonic stress axis (tectonic extension). These fractures (tensional fractures) are the least resistant to the water current and they are most effectively widened when dissolution of the limestones is going on (Dreybrodt 1988).

Karst Galleries Orientation

The diagrams of the orientation of the karst galleries could be useful for indication of the main preferred ways of the underground waters. Mostly, this is the direction of the open fractures and the practice has shown that this type of fractures in the recent active karst systems is normally connected with the youngest tectonic stress field.

Earthquakes

The most appropriate method for determining the main directions of the contemporary tectonic stress

Fig. 2.50 Principal hole of Spring of Vaucluse in summer season (low water level)

field are the fault-plane solutions from earthquakes (ex.: Mattauer and Mercier 1980). Every fault-plane solution for a given earthquake focus is closely related to the local tectonic conditions. They often show a remarkable coherence for large areas. The concentration or the alignment of epicenters of weak earthquakes in some territories helps to detect the contemporary active tectonic zones.

Satellite Laser Ranging Geodetic Solutions

The Grasse laser tracking station velocity (SE France) is derived from the analysis of 977,000 normal points of the geodynamic satellite Lageos-1 covered the data span of 16 years—from January 1984 till December 1999 (Shanov and Georgiev 2001). The data reduction and analysis procedure were performed by the SLRP 3.2 software for dynamic orbital analysis and least-square parameter estimation (Georgiev and Kotzev 1995) using the recent dynamicmodels and fundamental constants (McCarthy 1996).

2.3.4.3 Tectonic Stress Fields and Analyses of Their Control on the Karst System

Data on shear joints analysis from the limestones of the plateau have been collected from five outcrops (Fig. 2.51). The elements of 100 joints at least were measured on every site. After mathematical processing and the corresponding interpretation, two tectonic stress fields have been reconstructed, both having remarkable coherence in directions of maximum and minimum tectonic stress axes for the different sites. The characteristic feature of both stress fields is the sub-horizontal position of the maximum and minimum stress axes. The problem was to determine the relative age of every one of the tectonic stress fields.

The elaboration of rose-diagrams, indicating the preferential directions of the horizontal galleries, has been made using the maps of the cave galleries in the region (Fage, 1981). It is evident (Fig. 2.51) that, in general, the NE–SW direction is preferential and there is a close relationship between the open fractures, indicated on Table 2.8 as product of the Post-Burdiganian Phase, and the karst galleries. This direction is also well marked by the general strike of the youngest faults.

The scheme of these faults is elaborated on the base of two principal sources of information—The Map of Remote Sensing Lineaments of France in a scale 1:1 000 000 (Scanvic and Weecksteen 1984) and the Seismotectonic Map of France (Voght and Godefroy 1981). The lineaments from satellite images could be accepted under some conditions as traces of reactivated faults or faults formed during the neotectonic stage and active up to now. The faults from the Seismotectonic Map are interpreted as structures,

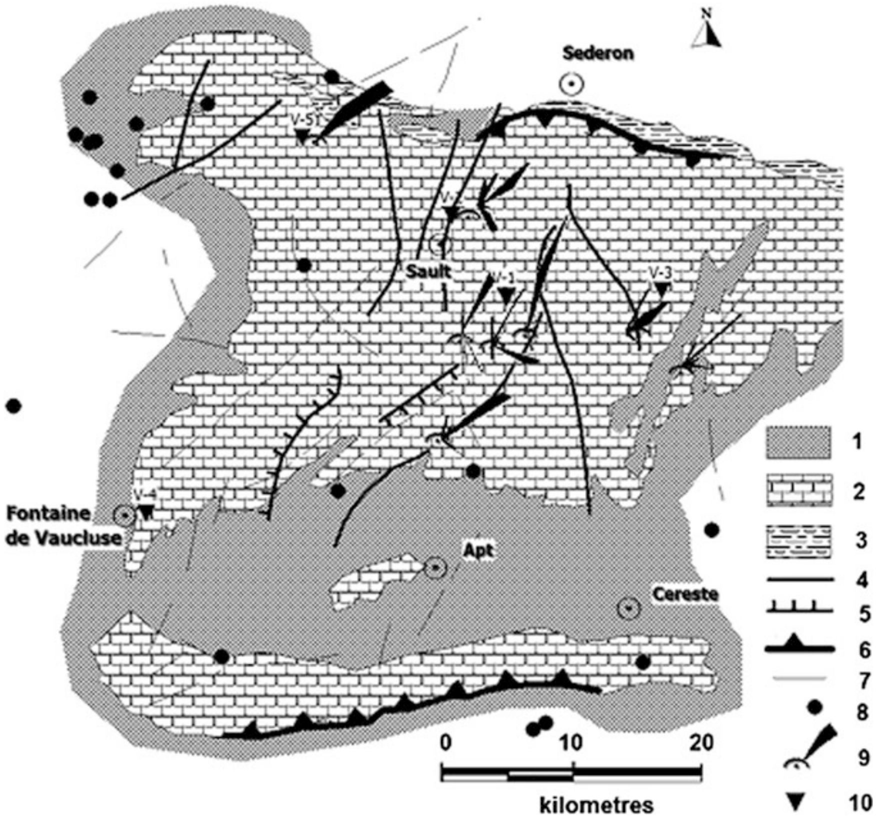

Fig. 2.51 Geological scheme of Plateau of Vaucluse with elements of geodynamics (after Shanov and Cousset 1993; Shanov and Georgiev 2001) *1*—Bedoulien terrain; *2*—Lower Cretaceous limestones; *3*—Neocomian marls; *4*—fault; *5*—normal fault; *6*—front of thrusting; *7*—remote sensing lineaments; *8*—earthquake epicenters (magnitudes $M_L = 1.0$–3.0 and time interval from 1982 to September 2013); *9*—cave location with rose-diagram of the karst galleries; *10*—point of mass measurements of joints

connected directly to the present day tectonic processes. They could be distributors of the seismic energy or generators of this energy. For the monts of Vaucluse and Ventoux a clear coincidence exists between the main strike of these faults (NE–SW) and the preferred direction of karst processes, in spite of the well-developed fault system with general trend NW–SE (see Fig. 2.49). Such a result has been discussed for the whole region (Mudry and Puig 1991). The NW–SE fault direction is probably a result of the oldest tectonic stress field that has deformed the limestones during the earlier stage of their diagenesis. This is reflected in the reconstructed direction of compression using the stylolite indentation (Shanov and Cousset 1993).

Processes of formation of young NE–SW striking faults are also reflected by the chain arrangement of earthquake epicenters to the northwest of Mont Ventoux (Fig. 2.51). The earthquakes are of low magnitudes (less than $M_L = 3.0$). But, the most important confirmation for the existence of contemporary compressive NE–SW directed strain for this region is the result of the fault-plane solutions from the earthquakes (Shanov and Georgiev 2001). The fault-plane solutions from earthquakes northeast of the studied region show, as a general rule, orientation of the maximum strain compatible to the maximum stress axis of the youngest tectonic stress field, reflected by the joint systems of the limestones (see Table 2.8).

The absolute velocity vectors for the site GRASSE displacement, the nearest Laser Tracking Site, according to the NOVEL1A model and to the Satelite Laser Ranging global geodetic solution, demonstrate practically the same orientation and the velocity range of about 25 mm/year toward northeast and this is the general trend for the western part of the Eurasian Plate (Table 2.8). There is a small residual motion with respect to Eurasia of about 4–5 mm/year in southeastern direction (Shanov and Georgiev 2001). The absolute site motion is in good agreement with the general direction of the *P*-axes from the earthquake fault-plane solutions, and this could be interpreted as an evidence for the direct relationship

Table 2.8 Reconstructed time sequence of the tectonic stress fields for the studied area of Alps Maritimes

<table>
<tr><th>Origin</th><th>Site №</th><th>Post-Eocene (?)</th><th>Provencal</th><th>Post-Burdiganien</th><th>Recent</th><th>Method</th></tr>
<tr><td colspan="2">Earthquake
19.06.1972
M=3.8
N 44.38^0
E 6.35^0</td><td></td><td></td><td></td><td></td><td>Fault-plane solution</td></tr>
<tr><td colspan="2">Laser site
GRASSE
N 43.754464
E 6.921947</td><td></td><td></td><td></td><td>
</td><td>Determination of plate motion</td></tr>
<tr><td colspan="2">1</td><td>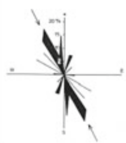</td><td></td><td></td><td></td><td>Stylolite's indentation</td></tr>
<tr><td rowspan="5">K_1 – Lower Cretaceous limestones</td><td>1</td><td>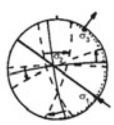</td><td>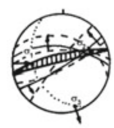</td><td></td><td></td><td rowspan="5">Shear joints</td></tr>
<tr><td>2</td><td></td><td>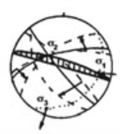</td><td>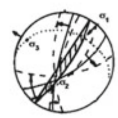</td><td></td></tr>
<tr><td>3</td><td></td><td>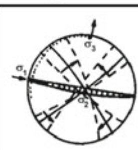</td><td>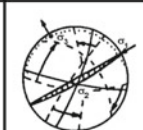</td><td></td></tr>
<tr><td>4</td><td></td><td></td><td></td><td>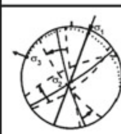</td></tr>
<tr><td>5</td><td></td><td>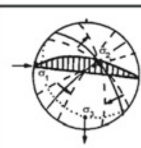</td><td>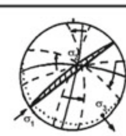</td><td></td></tr>
</table>

between the continental motion and the induced compressive strain in the Earth's crust. The rock fracturing under the induced stress, for the case study, opens the way for the underground waters, and the consecutive formation of the karst galleries, the youngest of them following the direction of the maximum tectonic stress axis.

References

Amadei B (1983) Rock anisotropy and the theory of stress measurement. Springer, Berlin, p 478

Andreychuk VN, Benderev AD (1991) Regional peculiarities of the anthropogenic impact on the karst of mountain countries. Informational materials, Ural Branch of Academy of Sciences of USSR, Kongur, p 133 (in Rissian)

Angelier J (1994) Fault slip analysis and paleostress reconstruction. In: Hancock PL (ed) Continental deformation. University of Bristol, Pergamon Press, Oxford, pp 53–100

Angelier J, Mechler P (1977) Sur une méthode graphique de recherche des contraintes principales également utilisable en tectonique et en séismologie: la méthode des dièdres droits. Bull Soc Geol Fr 7:1309–1318

Angelova D, Benderev A, Baltakov G, Ilieva I, Nenov T (1995) On the evolution of the karst in Stara Planina Gorge. J Bulg Geol Soc 3:111–124 (in Bulgarian)

Angelova D, Benderev A, Kostov K (1999) On the age of the caves in the Stara Planina Iskar gorge, NW Bulgaria. In: European Conference "Karst 99", 10–15 Sept 1999, Grands Causses–Vercors, pp 25–35

Antonov H, Danchev D (1980) Ground waters in Bulgaria. Tehnika, Sofia, p 360 (in Bulgarian)

Aubouin J, Brousse R, Lehman JP (1988) Précis de géologie. Tectonique, tectonophysique, 4th edn. Dunod Université, Paris, p 519

Benderev A (1989) Karst and karst waters of Ponor Mountain. PhD Thesis, NIPI-KG, p 157 (in Bulgarian)

Benderev A, Angelova D (1999) Evolution of karst in the southern part of Vitosha Mountain, Bulgaria. Thereotical and applied karstology 11–12(1998–1999):75–82

Benderev A, Shanov S (1997). Karst waters from the region of Bosnek (West Bulgaria): Characteristics and conditions of formation. 12th International Congress of Speleology, La Chaux-de-Fonds. In: Proceedings, v.2, 6 Conference of Limestone Hydrology and Fissured Media, pp 255–258

Benderev A, Shanov S, Ilieva I (1987) Peculiarities of formation of the karst of Western Stara Planina Mountain. In: Proceedings of the conference "The problems of the complex study of the karst of the mountain territories", Tbilisi-Tzhaltubo-Suhumi, 5.12.1987, 5–12.10.1987, pp 94–97 (in Russian)

Benderev A, Shanov S, Ilieva I (2001) Evaluation of the environmental threats affecting the Lakatnik karst region (Western Balkan mountains, Bulgaria). In: Proceedings of the 7th conference on limestone hydrology and fissured media, Besançon, France, 20–22 Sept 2001, pp 31–35

Benderev A, Spassov V, Shanov S, Mihaylova B (2005) Hydrogeological karst features of the Western Balkan (Bulgaria) and the anthropogenous impact. In: Proceedings of the international conference "Water Resources and Environmental Problems in Karst—CVIJIC 2005", Belgrade & Kotor, 13–22 Sept 2005, pp 37–42

Biçoku T, Aliaj Sh (1973a) Historical Tectonic Regionalisation of Albania. In: Proceedings of the Seminar on the Seismotectonic Map of the Balkan Region, UNESCO, Dubrovnik. Appendix: Maps, No.l

Biçoku T, Aliaj Sh (1973b) Neotectonic Map of the Balkan Region, UNESCO. Appendix: Maps, No. 6

Biçoku T, Papa A, Shelu R (1978) Dinarides: Albania. In: Tectonics of Europe and the adjacent territories. Nauka, Moscow, pp 468–472 (in Russian)

Bielenstein HU, Barron K (1971) In situ stress. A summary of presentations and discussions given in Theme I at the Conference of Structural Geology to Rock Mechanics Problems. Department of Energy, Mines and Resources, Mines Branch, Ottawa

Bonchev E (1961) Notes on main faults in Bulgaria. Stud Geol Bulgaria Stratigr tect 2:5–29 (in Bulgarian)

Bonchev E (1971) Problems of Bulgarian geotectonics. Technica, Sofia, p 204 (in Bulgarian)

Brace WF (1960) An extension of the Griffith theory of fracture to rocks. J Geophys Res 65:3477–3480

Cadet JP, Funiciello R (2004) Geodynamic map of the Mediterranean. Commission of the Geological map of the World, 2 sheets

Caputo R (1989) FAULT. A programme for structural analysis. Manual. Department of Earth Sciences, University of Florence, Firenze, p 55

Caputo M, Caputo R (1988) Structural analysis: new analytical approach and applications. Ann Tectonicae II(2):84–89

Caputo M, Caputo R (1989) Estimate of the regional stress field using joint systems. Bull Geol Soc Greece XXIII(1):101–108

Chanov S (1988) Conditions géologiques et tectoniques de la formation des cavités karstiques dans la région de "Barkité" et de "Béliar", montagne de Stara Planina près de Vratza (Bulgarie). Dans: "Récit d'une amitié", Saint Herblain: 12–14

Chanov S, Benderev A (1993) Structural, geophysical and hydrogeological explorations on the karst system of Plateau Guaso (Cuba). In: International symposium on water resources in karst with special emphasis in arid and semi-arid zones, 23–26 Oct, Shiraz, Iran, pp 595–611

Cobiella J (1984) Sobra et origen del extremo oriental de la fosa de Bartlett. Editorial Oriente, Santiago de Cuba, p 43

Cox A, Hart R (1989) Plates Tectonics. Mir, Moscow, p 428 (in Russian)

Depambour Ch, Guendon J-L (2004) Eléments de rèflexion sur la morphogenèse des plateaux de Vaucluse (France): les apports du karst superficiel. Karstologia n° 42

Dilek Y, Koçiu S (2004) Neotectonics, seismology and the mode of Late Cenozoic crustal deformation in the Albanides, Balkan Peninsula. Denver Annual Meeting, 7–10 Nov, paper No 19–14, Abstract

Dreybrodt W (1988) Processes in Karst Systems. Physics, Chemistry and Geology. Springer, Berlin, p 288

Drumia AV, Shebalin NV (1985) Earthquake: where, when, why? Shtiintsa, Kishinev, p 196 (in Russian)
Dunne WM, Hancock PL (1994) Paleostress analysis of small-scale brittle structures. In: Continental deformation. Pergamon Press, Oxford, pp 101–120
Dupin JM, Sassi W, Angelier J (1983) Homogeneous stress hypothesis and actual fault slip: a distinct element analysis. J Struct Geol 15:1033–1043
Engelder T (1994) Brittle crack propagation. In: Continental deformation. Pergamon Press, Oxford, pp 43–52
Evlogiev J, Karachorov P, Todorov M, Hristov D (1997) Study on the genesis of the fractures in Orlova Chuka Cave, Rouse District. Eng Geol Hydrogeol 24(BAS):33–39 (in Bulgarian)
Fage L-H (1981) Spéléo sportive. Edisud, Dans les monts de Vaucluse, p 96
Filipov L (ed) (1992) Geological Map of Bulgaria 1:100 000, Sheet "Byala"
Gamond JF (1983) Displacement features associated with fault zones: a comparison between observed examples and experimental models. J Struct Geol 5:33–45
Georgiev I, Kotzev V (1995) Tectonic plate motion from satellite laser ranging to Lageos 1. In: Proceedings of the I-st international symposium on deformations, 5–9 Sept, Istanbul, Turkey, pp 454–472
Georgiev Tz, Shanov S (1991) Contemporary geodynamics of the western part of the Moesian Platform (Lom Depression). Bulg Geoph J LXVII(3):3–9 (in Bulgarian)
Georgiev I, Dimitrov D, Belijashki T, Pashova L, Shanov S, Nikolov G (2007) Geodetic constraints on kinematics of southwestern Bulgaria from GPS and leveling data. Geological Society, London, Special Publications 01/2007; 291(1):143–157. doi:10.1144/SP291.7
Gephard J, Forsyth D (1984) An improved method for determining the regional stress tensor using earthquake focal mechanism data. J Geophys Res 89:9305–9320
Gochev P (1983) Subhercynian Allochthon in West Srednogorie. Geotect Tectonophys Geodyn Geol Inst BAS 15:3–17 (in Bulgarian)
Gouvernet C, Guieu G, Rousset C (1971) Provence. Guides géologiques régionaux, Masson et Cie, Paris, p 230
Griffith AA (1924) Theory of rupture. In: Proceedings of first international congress for applied mechanics, Delft, pp 55–63
Harta Geologjike RPS Te Shquiperise M 1:200 000 (Geological Map of Albania) (1981) Tirana, Ministria e Industrise dhe e Minerave
Haydutov I, Dimitrova R (ed) (1992) Geological map of Bulgaria 1:100 000, Sheet "Berkovitsa"
Hmelevskoy VK (1984) Electrical prospecting. University of Moscow, Moscow, p 422 (in Russian)
Hunt L, Reynolds S, Hadley S, Downton J, Chopra S (2011) Causal fracture prediction: curvature, stress and geomechanics. Leading Edge SEG 30(11):1274–1286
Hydrogeological Map of PSR of Albania M 1:200 000 (1981) Tirana
Ilieva I, Zdravkov I, Benderev A (1981) The role of the tectonic movements for the development of the karst at the area or Cherepish Railway Station. Proceedings "Scientific and Practical Conference on Tourism, Alpinism, Caving and Environment Protection", Rousse, 4–6 May 1979, pp 207–214 (in Bulgarian)
Jaeger J (1975) Rock mechanics and engineering. Mir, Moscow, p 256 (in Russian)
Jelev V (1982) Characteristics and development of Vitosha central magmathogenetic structure. PhD Thesis, University of Mining and Geology, Sofia (in Bulgarian)
Karagjuleva J (1971) The northern boundary of Fore-Balkan. In: Tectonics of Fore-Balkan. BAS, Sofia, pp 66–107 (in Bulgarian)
Kastelic V, Radulov A, Glavanovic B (2011) Improving the resolution of seismic hazard estimates for critical facilities: the database of Eastern Europe crustal seismogenic sources in the frame of the SHARE project. In: Proceedings of the 30th meeting of the GNGDS (Gruppo Nazionale di geofisica della terra solida), pp 218–221
Kostadinov V (1965) The border between Kaishte and Srednogorie tectonic zones and stages of development. In: Proceedings CBGA, VII Congress, vol 1, pp 45–49 (in Russian)
Kostov K (1997) Karst morphology in Bazovski part of Vratsa mountain (Stara planina, NW Bulgaria). In: Proceedings of 12th International Congress of Speleology, La Chaux-de-Fonds (Newchatel, Switzerland), 10–17 Aug, vol 1, pp 409–412
Letouzey YJ (1986) Cenozoic paleo-stress pattern in the Alpine foreland and structural interpretation in a platform basin. Tectonophysics 132:215–231
Lilienberg DA (1983) Morphotectonics and recent geodynamics of the interaction region between Cuba microplate and Bartlett deepwater trench. In: Symposium of the morphotectonics Working Group IOU, Bulgaria, pp 204–232
Lundborg H (1968) Strength of rock-like materials. Int J Rock Mech Min Sci 5(5):427–454
Markowicz M, Popov V, Pulina M (1972) Coments of Karst denudation in Bulgaria.—Geogr. Polonica 23:118–139
Matova M, Angelova D (1994) Geological, seismotectonical and environmental problems of Pernik graben (Western Bulgaria). In: Proceedings of 7th Congress of the International Association of Engineering geology, Lisbon, Portugal, vol III, pp 2027–2032
Mattauer M, Mercier JL (1980) Microtectonique et grande tectonique. Livre Jubilaire de la Soc Géol Fr Mem h.-s. n° 10:141–161
McCarthy D (ed) (1996) IERS Technical note 21: IERS Convention, 95 p. Observatoire de Paris
McClintock FA, Walsh JB (1962) Friction on Griffith cracks in rocks under pressure. In: Proceedings of IV U.S. National congress of applied mechanics, Berkeley
Meyer B, Sébrier M, Dimitrov D (2007) Rare destructive earthquakes in Europe: The 1904 Bulgaria event case. Earth Planet Sci Lett 253:485–496
Michael AJ (1987) Use of focal mechanisms to determine stress—a control study. J Geoph Res 92:357–368
Mihailova B, Mitev A, Benderev A, Shanov S (2006) Hydrogeological and geophysical investigations for localization the river recharge of the ground waters of the Bosnek Karst Region. In: Proceedings National conference "Geosciences", 30 Nov–1 Dec 2006, Sofia, pp 403–406 (in Bulgarian)
Mishev D, Popov V (1958) The karst of Vratsa Mountain, Sofia. Nature 7:7–13 (in Bulgarian)
Mudry J, Puig JM (1991) Le karst de la Fontaine de Vaucluse. Karstologia 18:29–38

Muço B (1994) Focal mechanism solutions for Albanian earthquakes for the years 1964–1988. Tectonophysics 231:311–323

Nikolaev PN (1977) Methode of statistical analysis of joints and reconstruction of the tectonic stress fields. J High Schools Geol Prosp Moscow 12:103–115 (in Russian)

Nystuen (ed) JP (1989) Rules and recommendations for naming geological units in Norway by the Norwegian Commitee on Stratigraphy. Nor Geol Tidsskr 69(Supplement 2):111

Paskalev M, Benderev A, Shanov S (1992) Tectonic conditions of the region of the Iskrets Karst Springs (West Stara-Planina). Rev Bulg Geol Soc 53(part 2):69–81 (in Bulgarian)

Popov V (1964) Morphology and genesis of Ledenika Cave. Bull Geogr Inst BAS 8:77–87 (in Bulgarian)

Popov V (1982) Travel under the ground. Nauka i Izkustvo, Sofia, pp 152 (in Bulgarian)

Price NJ (1959) Mechanics of jointing in rocks. Geol Mag 96:149–167

Price NJ (1966) Fault and joint development in brittle and semi-brittle rock. Pergamon Press, Oxford

Radev J (1915) Karst forms in Western Stara Planina. Ann Sofia University, Hist Phil Fac 10–11:149 (in Bulgarian)

Radulov A (2002) Quaternary karst in the valley of Rusenski Lom River and its tributaries. PhD Thesis, Geological Institute, BAS (in Bulgarian)

Radulov A, Vanneste K, Verbeeck K, Yaneva M, Petermans T, Camelbeeck T, Shanov S (2006) Paleoearthquake correlation in three trenches along Orizovo—Chirpan active fault segment. National conference “Geosciences 2006”, Sofia, 30 Nov–1 Dec, Proceedings, pp 71–74

Radulov A, Dilov Tz, Yaneva M, Nikolov N, Kostov K, Nikolov V (2011) Earthquake faults in Sofia Basin. In: National conference “Geosciences 2011”, Sofia, Proceedings, pp 99–100 (in Bulgarian)

Radulov A,Yaneva M, Shanov S, Nikolov V, Kostov K, Nikolov N, Hristov V, Dobrev N, Mitev A (2012) Report on field survey after May 22, 2012 Pernik earthquake, June 6, 2012, Part 1: Coseismic geological effects related to May 22, 2012 Pernik earthquake, Western Bulgaria http://www.geology.bas.bg

Ramsay JG (1980) Shear zone geometry: a review. J Struct Geol 2:83–99

Reid HF (1911) The elastic rebound theory of earthquakes. Bull Dept Geol Univ California 6:413

Rojas-Agramonte Y, Neubauer F, Handler R, Garcia-Delgado DE, Friedl G, Delgado-Damas R (2003) Neogene-Quaternary tectonics along the North Caribbean transform fault, Cuba. EGS—AGU—EUG Joint Assembly, Abstracts from the meeting held in Nice, France, 6–11 Apr 2003, abstract #2830

Sassi W, Carey-Gailhardis E (1987) Interpretation mechanique du glissement sur les failles: introduction d’un critere de frottement. Ann Tectonicae I(2):139–154

Scanvic J-Y, Weecksteen G (1984) Carte des linéaments de la France. Echelle 1:1 000 000, BRGM

Scholz K (2002) The mechanics of earthquake faulting. Cambridge University Press, Cambridge, p 472

Scorpil H, Scorpil K (1895) O kraskych zjevech v Bulharsku. Rozpr Ceske Akad 4(2):1–35

Scorpil H, Scorpil K (1898) Sources et pertes des eaux en Bulgarie. Mem Soc speleol 15:99–139

Shanov S (1999) Tectonic conditions for the karst processes near Karlukovo Village (Fore-Balkan). In: Proceedings National scientific conference on the problems of Karst and Speleology, Sofia, pp 37–43 (in Bulgarian)

Shanov S (2005) Post-Cretaceous to recent stress fields in the SE Moesian Platform (Bulgaria), Tectonophysics, vol 410, Issues 1–4, The Carpathians-Pannonian Basin System—Natural Laboratory for Coupled Lithospheric-Surface Processes, 9 Dec 2005, pp 217–233

Shanov S, Benderev A (2005) Seismic impact from earthquakes and from grouped blasts in quarries on the discharge of karst springs. In: Proceedings of the international conference “Water Resources and Environmental Problems in Karst—CVIJIC 2005”, Belgrade & Kotor, 13–22 Sept 2005, pp 145–150

Shanov S, Cousset O (1993) Tectonic stress fields and Karst processes in the Plateau of Vaucluse (South-Eastern France). In: International symposium on water resources in Karst with special emphasis in arid and semi arid zones, 25–26 Oct, Shiraz, Iran, Proceedings, vol 2, pp 775–783

Shanov S, Georgiev I (2001) Tectonic stresses and their control on the karst formation in the Plateau of Vaucluse (South-East France). Riviera 2000—Tectonique active et géomorphologie. Villefranche-sur-Mer, Revue d’Analyse Spatiale, No spécial 2001:139–144

Shanov S, Georgiev T, Dimitrov B (1988) Contemporary tectonic stress field in North Eastern Bulgaria. J Bul Geol Soc 1:39–46 (in Bulgarian)

Shanov S, Stoyanov S (1986) On a method for treatment and dynamic interpretation of joints. Rew Bulg Geol Soc 57(part 1):64–73 (in Bulgarian with an Abstract in English)

Shanov S, Benderev A, Ilieva (2001) Traces of recent active tectonics in the cave of Duhlata (Southwestern Bulgaria). Riviera 2000—Tectonique active et géomorphologie. Villefranche-sur-Mer, Revue d’Analyse Spatiale, No spécial 2001:145–150

Sharma PV (1997) Environmental and engineering geophysics. Cambridge University Press, Cambridge, p 475

Sheriff RE (1984) Encyclopedic dictionary of exploration geophysics. Nedra, Moscow, p 352 (in Russian)

Spasov V, Benderev A, Gabeva D (1998) Perspectives for more effective using of the underground karst waters of the region of the town of Vratsa. In: Proceedings of the National conference “Water resources—usage and preservation”, Sofia, 23–25 Sept 1998, pp 47–51 (in Bulgarian)

Spenser EU (1981) Introduction in Structural Geology. Nedra, Leningrad, p 368 (in Russian)

Stacey F (1972) Physics of the Earth. Mir, Moscow, p 342 (in Russian)

Stoyanov S (1970) Certain physical aspects of faulting in the Earth’s crust. Bull Geol Inst Ser Geotectonics BAS 19:127–140 (in Russian with abstract in English)

Trollop DH (1983) Criteria of failure of brittle rocks. In: Introduction in rock mechanics. Mir, Moscow, pp 96–113 (in Russian)

Tronkov D (1965) Tectonics and analysis of the structures in the Vratza Block of Western Stara Planina. Plastic deformations near the fault planes. Stud Geol Bulgaria Ser “Stratigraphy and Tectonics” 6:217–257 (in Bulgarian)

Tsankov Ts (ed) (1991) Geological map of Bulgaria 1:100 000, Sheet “Vratsa”

Tzankov T, Burchfiel C, Royden L (1998) Neotectonic (Quaternary) Map of Bulgaria. Scale 1:500 000. General Aspects on the Quaternary Tectonic Evolution of Bulgaria. Publishing House Grafika, Sofia

Uhov SB (1975) Rock basement of hydro-technical facilities. Energia, Moscow, p 264 (in Russian)

USGS (2004) Shuttle Radar Topography Mission, 3 Arc Second scenes N43E023 and N43E024, Unfilled Unfinished 2.0. Maryland, University of Maryland, College Park, Global Land Cover Facility, Feb 2000

Vanneste K, Radulov A, De Martini P, Nikolov G, Petermans T, Verbeeck K, Camelbeeck T, Pantosti D, Dimitrov D, Shanov S (2006) Paleoseismologic investigation of the fault rupture of the 14 April 1928 Chirpan earthquake (M 6.8), Southern Bulgaria. J Geophys Res 111:B01303. doi:10.1029/2005JB003814

Vapcarov I, Galabov J, Michev K, Georgiev M, Vrablianski I (1974) Neotectonic map of Bulgaria, Scale 1:000 000. In: Proceedings of the seminar on the seismotectonic map of the Balkan region, UNESCO, Skopje, App. Maps, No 11

Vergely P, Sassi W, Carey-Gailhardis E (1987) Analyse graphique des failles a l'aide des focalisations des stries. Bull Soc Geol de France 8, t. III, n° 2:395–402

Vogt J, Godefroy P (1981) Carte sismotectonique de la France. Présentation et mode d'emploi. Mem. du BRGM, No 111

Vrablianski B (1974) Main lines of tectonic activation of the Earth's crust in Bulgaria during the Antropogean. Compte Rend. de l'Acad Bulg des Sci 27(7):953–956

Yakubovskiy Y (1973) Electrical prospecting. Nedra, Moscow, p 299 (in Russian)

Zagorchev I, Marinova R, Tchounev D, Tchumachenko P, Sapunov Y, Yanev S (1994) Explonatory note to the Geological map of Bulgaria in scale 1:100000, Pernik map sheet Committee of Geoloy and Mineral Resources, Sofia, p 92 (in Bulgarian)

Springer

http://www.springer.com/978-3-662-43991-3

Dynamic Tectonics and Karst
Shanov, S.; Kostov, K.
2015, XI, 123 p. 119 illus., 25 illus. in color., Hardcover
ISBN: 978-3-662-43991-3